Growth dynamics and life history inferences in extant deer from histological analysis of bone tissues

Teresa Calderón Sánchez

Supervisor
Meike Köhler

UAB
Universitat Autònoma de Barcelona

ICP
Institut Català de Paleontologia
Miquel Crusafont

Growth dynamics and life history inferences in extant deer from histological analysis of bone tissues

Teresa Calderón Sánchez

Dissertation presented by Teresa Calderón Sánchez in fulfilment of the requirements for the degree of Doctor in the Universitat Autònoma de Barcelona, doctorate program in Biodiversity of the Departament de Biologia Animal, Biologia Vegetal i d'Ecologia. Under the supervision of:

- Dra. Meike Köhler, ICREA at Institut Català de Paleontologia Miquel Crusafont and teacher of the Departament de Biologia Animal, Biologia Vegetal i d'Ecologia at Universitat Autònoma de Barcelona.

Doctoral candidate
Teresa Calderón Sánchez

Supervisor
Dra. Meike Köhler

"I like the scientific spirit—the holding off, the being sure but not too sure, the willingness to surrender ideas when the evidence is against them: this is ultimately fine—it always keeps the way beyond open—always gives life, thought, affection, the whole man, a chance to try over again after a mistake—after a wrong guess."

—Walt Whitman

TABLE OF CONTENTS

LIST OF PUBLICATIONS

This thesis has led to the following publications:

1. **Teresa Calderón**, Daniel DeMiguel, Walter Arnold, Gabrielle Stalder and Meike Köhler. *Calibration of life history traits with epiphyseal closure, dental eruption and bone histology in captive and wild red deer*. <u>Journal of Anatomy</u> 235 (2019). Pages 205-216. doi: 10.1111/joa.13016.
   <u>Main contributions of this thesis's author:</u>
   Study planning and design, histological analysis, data analysis, writing and preparation of figures and tables.

2. **Teresa Calderón**, Walter Arnold, Gabrielle Stalder, Johanna Painer and Meike Köhler. *Labelling experiments in red deer provide a general model for bone growth dynamics in ruminants*. Scientific Reports 11 (2021). Pages 1-14. doi: 0.1038/s41598-021-93547-4.
   <u>Main contributions of this thesis's author:</u>
   Histological analysis, data analysis, writing and preparation of figures and tables.

CLARIFYING NOTE

In addition to the bone histological analysis presented in this thesis, an analysis of dental material from *Cervus elaphus* was performed. Thin sections of different molars were prepared at the ICP laboratory. These thin sections were subsequently analysed during a visit to the Hard Tissue Research Unit at the New York University College of Dentistry under the supervision of Timothy G. Bromage. Once the results were gathered, it was determined that they were inconclusive, and the analyses were to be repeated using a different microscopic technique. As this has not been possible due to the global health circumstances, it was decided that this dissertation will focus only on the bone histology analysis, which provides sufficient results for accomplishing the main objectives.

ACKNOWLEDGEMENTS

En primer lugar, me gustaría agradecer a la Dra. Meike Köhler y al Dr. Daniel DeMiguel por darme la oportunidad formar parte del departamento de Paleobiología evolutiva del Institut Català de Paleontologia Miquel Crusafont. A la Dra. Meike Köhler agradezco el haber comenzado a guiarme en el mundo de la paleohistología, del que tanto me queda aún por aprender, y al Dr. Daniel DeMiguel el haberlo hecho a través de la historia evolutiva de los cérvidos. También agradezco al Dr. Tim Bromage, por acogerme en su magnífico laboratorio de imagen en Nueva York así como al Dr. Walter Arnold, la Dra. Gabrielle Stalder y la Dra. Johanna Painer, investigadores del *Research Institute of Wildlife Veterinary* de Viena, con los que he tenido la suerte de colaborar.

Antes de proseguir, creo necesario retroceder un poco en el tiempo y dedicar un pequeño espacio para agradecer a las personas que impulsaron y guiaron mi pasión por el estudio de la biodiversidad, ya que la motivación que me contagió cada una de ellas es la responsable de que yo haya finalizado esta tesis. Rosalía fue la primera persona que me enseñó biología y paleontología. En el campo, me contagió toda la ilusión que a ella le producían pequeños hallazgos que pasarían desapercibidos ante ojos desatentos. Más tarde, el Dr. Salvador Peris, me hizo perder la cabeza por la ecología y evolución de los vertebrados (lo imagino volando muy alto con los alcaudones). La Dra. Rosario Rivas me enseñó a investigar y, poco después, la Dra. Yolanda Melero me

sumergió de lleno en el mundo de la ecología y me animó a seguir el camino de la investigación.

A lo largo de estos años de tesis, yo también he crecido, como los huesos de los ciervos. Si tuviera que trazar la curva de mi crecimiento, asemejaría al recorrido del *Dragon Khan*: subidas de motivación vertiginosas, doble *loop* y alguna que otra bajada al inframundo. Sin embargo, he de señalar que durante esa compleja trayectoria no he estado sola, sino que han sido muchas las personas que han impulsado ese crecimiento y que han sido también precursoras de momentos inolvidables.

Para empezar, he tenido unos compañeros de departamento geniales, hoy en día grandes amigos, a los que tengo mucho que agradecer. A Guillem, por sacar siempre tiempo para aclararme tantísimas dudas, por comprenderme y apoyarme con la tesis. También por endulzar mis desayunos con dinosaurus, ayudarme a desconectar con las escapadas a la *Muntanya* y también al Kruger (bendita paciencia con la fotógrafa), por enseñarme catalán, codirigir el idioma wilmelaniano y por las otras muchas tonterías que me han hecho reír tantísimo. Agradezco también a Carmen, por compartir conmigo sus conocimientos de histología, por sus comentarios tan constructivos y su ayuda con la tesis. También por los ratitos de desconexión del trabajo y las risas en las calles de Madrid, París y Cape Town. A Manuelillo, agradecerle el transformar ciervos en estado cuestionable de descomposición en información sumamente valiosa bajo el microscopio, pero también por las charlas pajariles, las comilonas en su casa-paraíso (convivir con herrerillos capuchinos es un lujo innegable) y las excursiones. Gracias también a todo el equipo de ICPners por las risas, las cenas, las cervezas de viernes en la época pre-covid y al resto de integrantes del ICP por todo el tiempo compartido.

Fuera del ámbito del ICP, pero dentro de las inmediaciones Barcelonesas, agradezco a mi hermano del viento, Alfonso, que durante estos

años ha sido mi familia del oeste en el este. Gracias por las salidas *ornitofreaks* a los deltas, las rutas en bici y las canciones inventadas. También por hacerme de psicólogo tantas veces y apoyarme tanto con la tesis (y con lo que no era la tesis). A las integrantes de Pura Vida, por los desayunos hipercalóricos, las excursiones y los viajes. En especial a Eli y a Patri, por cuidarme tanto, quererme y entenderme tan bien. Y también por haberme hecho la vida un poquito más fácil cuando todo se venía abajo.

Quiero agradecer también a María, mi *twin*, por todo su apoyo y comprensión, por resolverme dudas gramaticales en inglés y catalán y por acogerme tantas veces y con tanto cariño en su hogar malagueño (gracias a ti también, Jorge). También a Coqui y a Albus a quienes he echado mucho de menos todo este tiempo, pero siempre han estado ahí y me han hecho llegar ABRAZOS singulares. A Raqui, por celebrar mis éxitos y dejarme celebrar los suyos, por motivarme siempre (hablar contigo un minuto proporciona un chute de motivación y alegría para un mes entero) y hacerme seguir confiando en la ciencia (*Science After All!*). A Iggy, por las interminables charlas sobre cérvidos, por compartir sus inquietudes conmigo y hacerme aprender siempre cosas nuevas. También por su apoyo incondicional y la confianza que tenía en que yo podía con esto (a veces estabas más convencido tú que yo misma). A Nuria, agradecerle la comprensión y el apoyo, sus maravillosas ideas de proyectos y también la motivación que me produce siempre el hablar con ella. A Carlos, por ayudarme a desconectar de la tesis haciéndome cambiar el microscopio por el teleobjetivo y el despacho por la naturaleza. A Estela le agradezco los paseos esclarecedores por la dehesa y el haberme escuchado en los momentos difíciles de la tesis a pesar de haber ignorado sus sinceras advertencias previas. Pero, sobre todo, por las risas que hemos compartido. A Sonia, Lucía, Mónica, Maripaz y Vero, por perdonar mis ausencias y por su atención acerca de cómo llevaba la tesis. A Israel, por aclararme mil dudas y animarme con la redacción, por hacerme reír ilustrando mis desgracias (y las

de los vampi-ciervos) y por nuestras conversaciones alternativas sobre literatura. A Jah, por ser mi familia al otro lado del Atlántico y a Joan y a sus charlas inspiradoras paseando por Manhattan. Me gustaría agradecer también a Dani por su confianza y positividad, por sus ánimos infinitos, por saber siempre cómo darle la vuelta a un mal día y por enseñarme que los límites son mentales (aunque de vez en cuando se me olvide).

A mis padres y a mi hermano, por ser mi refugio, por animarme siempre a hacer lo que de verdad me llena y por haber soportado mis estados de ánimo variables durante estos últimos meses. A mi abuela, por preocuparse siempre y sacarme una sonrisa cada vez que me dice que tengo que trabajar menos. A Mora, por estar literalmente a mi lado durante la escritura de gran parte de la tesis (aunque mucho tiempo haya sido panza arriba, roncando), y a Jara y a Zambra, por mantenerme un poco más asilvestrada de a lo que a mi madre le gustaría.

He de puntualizar que el desarrollo de esta tesis no hubiera sido lo mismo sin la poesía y la música de José Manuel Díez, que me han hecho bailar y volar cuando todos estábamos enjaulados; ni sin las maravillosas descripciones de Joaquín Araújo, que tanto me atalantan y que me han permitido disfrutar del campo cuando no me ha sido posible ser parte de él.

Finalmente me gustaría agradecer a Markus, Thinny, Ada, Otto, Niki, Saki, Diane y a todos los demás ciervos que han hecho esta tesis posible.

ABSTRACT

The study of life histories is fundamental for understanding the ecological and evolutionary processes of a species. The histological analysis of bone microstructure is the most promising method for reconstructing bone growth and inferring the life histories of extinct and extant vertebrates because it records the incremental growth of bone tissue. However, most histological studies have focused on fossil groups, and much work remains to be done on extant animals to better understand the dynamics and ontogenetic processes of their growth. This dissertation provides a histological analysis of the postcranial material of red deer (*Cervus elaphus* Linnaeus 1758), with the aim of shedding light on the bone growth dynamics of extant mammals.

Thin sections of limb bones (the femur and tibia) from individuals belonging to two different subspecies of red deer (*Cervus elaphus hispanicus* and *Cervus elaphus hippelaphus*) were analysed by transmitted and polarised light microscopy. The histological results were calibrated with known life history traits of *Cervus elaphus hippelaphus* individuals raised under semi-wild conditions. Additionally, six individuals of this population were labelled with fluorochromes to reconstruct their bone growth during early life stages. Afterwards, thin sections of the six labelled limb bones (the femur, tibia, metatarsus, humerus, radius and metacarpus) were analysed by transmitted, polarised and fluorescent light microscopy.

The histological analysis of ontogenetic series of red deer limb bones made it possible to describe in detail bone growth dynamics through ontogeny. One of the most significant transitions is the shift from the fibrolamellar complex to the lamellar bone (i.e. the external fundamental system) in the femora. This transition has been related to skeletal maturity, according to data

gathered on epiphyseal fusion and dental eruption patterns in red deer. Moreover, calibrating the number of cyclical growth marks with the known age of semi-wild individuals revealed that the femur is the best limb bone for calculating the age at maturity, while the tibia is an effective indicator of the age at death. In addition, fluorochrome labelling revealed the presence of non-cyclical growth marks recorded during early life, which suggests that these marks are associated with the animal's birth and weaning events. This approach also revealed how these single events disrupt growth rates and hence alter tissue deposition. Furthermore, two groups of calves (hand-raised and mother-reared individuals) expressed different histological features, revealing that individual nutritional regimes have an important impact on the effects of the weaning event on bone microstructure.

In summary, these findings contribute to a deeper understanding of bone growth dynamics through ontogeny. This thesis also provides insight into the impacts life history events have on bone growth and the environmental factors modulating them (e.g. nutrition). The results obtained from the histological analysis of red deer long bones will allow for more accurate interpretations of bone ontogeny in fossil taxa.

RESUMEN

El estudio de las historias de vida es fundamental para entender los procesos ecológicos y evolutivos de una especie. Uno de los mejores métodos para reconstruir el crecimiento óseo y hacer inferencias sobre la historia de vida de vertebrados tanto actuales como extintos es el análisis histológico de la microestructura, ya que recoge la información acerca de los procesos de crecimiento del tejido óseo. Sin embargo, la mayoría de los estudios histológicos están enfocados en grupos fósiles y aún queda mucho trabajo por hacer en grupos actuales para entender mejor las dinámicas y los procesos ontogenéticos del crecimiento. Esta tesis está enfocada en el análisis histológico de material postcraneal del ciervo rojo (*Cervus elaphus* Linnaeus, 1758) con el propósito de aportar información sobre las dinámicas de crecimiento en mamíferos actuales.

Se analizaron láminas delgadas obtenidas a partir de huesos largos (fémur y tibia) de ciervo rojo (*Cervus elaphus hispanicus* y *Cervus elaphus hippelaphus*) mediante microscopía de luz transmitida y polarizada. Los resultados obtenidos se calibraron con los parámetros de la historia vital conocidos de individuos de la subespecie *Cervus elaphus hippelaphus*, ya que los miembros de esta población fueron criados en condiciones de semilibertad. De manera adicional, seis individuos de la población en régimen de semilibertad fueron marcados con fluorocromos para reconstruir el crecimiento óseo durante sus primeros días de vida. Después, las láminas delgadas de seis huesos marcados (fémur, tibia, metatarso, húmero, radio y metacarpo) fueron analizadas bajo luz transmitida, polarizada y fluorescente.

El análisis histológico de huesos largos de diferentes estadios ontogenéticos del ciervo rojo hizo posible describir en detalle las dinámicas de

crecimiento a través de la ontogenia. Una de las transiciones más significativas es el cambio de tejido fibrolamelar a tejido lamelar (estructura conocida como EFS por sus siglas en inglés: *external fundamental system*) en el fémur, el cual ha sido relacionado con la madurez sexual de los individuos, según indican los datos recogidos acerca de la fusión de epífisis y patrón de erupción dental en el ciervo. Además, la calibración del número de marcas cíclicas con la edad conocida de los individuos en semilibertad reveló que el fémur es el mejor hueso largo para calcular la edad de madurez esquelética mientras que la tibia es un buen indicador de la edad de muerte del individuo. El marcaje con fluorocromos permitió atribuir la presencia de marcas no cíclicas grabadas durante los primeros estadios vitales a los eventos de nacimiento y destete. Este enfoque también reveló cómo estos eventos únicos causan alteraciones en las tasas de crecimiento y, por tanto, alteraciones en la deposición del tejido. Además, la diferente expresión de caracteres histológicos en dos grupos de cervatos (criados a mano y criados por su madre) reveló que el régimen nutricional es un factor importante que condiciona los efectos que el destete tiene en el hueso.

En resumen, todos estos resultados contribuyen a un mejor entendimiento de las dinámicas de crecimiento a través de la ontogenia. Esta tesis también contribuye a comprender los impactos que los eventos de la historia de vida ocasionan en el crecimiento óseo, así como de los factores que los modulan (como la nutrición). Además, los resultados obtenidos a partir de los análisis histológicos en ciervo rojo proporcionan una base firme para realizar mejores interpretaciones en grupos fósiles.

RESUM

L'estudi de les històries de vida és fonamental per entendre els processos ecològics i evolutius d'una espècie. Un dels millors mètodes per a reconstruir el creixement ossi i fer inferències sobre la història de vida de vertebrats tant actuals com extints és l'anàlisi histològica de la microestructura, ja que recull la informació sobre el creixement incremental del teixit ossi. No obstant això, la majoria dels estudis histològics s'han dedicat a grups fòssils i encara queda molta feina per fer en grups actuals per a entendre millor les dinàmiques i els processos ontogenètics del creixement. Aquesta tesi està enfocada en l'anàlisi histològica de material postcranial del cérvol vermell (*Cervus elaphus* Linnaeus, 1758) amb el propòsit d'aportar informació sobre les dinàmiques de creixement en mamífers actuals.

Es van analitzar làmines primes obtingudes a partir d'ossos llargs (fèmur i tíbia) mitjançant microscòpia de llum transmesa i polaritzada. Els resultats obtinguts es van calibrar amb els paràmetres de la història de vida coneguts d'individus de la subespècie *Cervus elaphus hippelaphus*, ja que els membres d'aquesta població van ser criats en condicions de semillibertat. De manera addicional, sis individus de la població en règim de semillibertat van ser marcats amb fluorocroms per a reconstruir el creixement ossi durant els seus primers dies de vida. Després, les làmines primes de sis ossos marcats (fèmur, tíbia, metatars, húmer, ràdio i metacarp), van ser analitzades sota llum transmesa, polaritzada i fluorescent.

L'anàlisi histològica d'ossos llargs de diferents estadis ontogenètics del cérvol vermell va fer possible descriure en detall les dinàmiques de creixement a través de l'ontogènia. Una de les transicions més significatives és el canvi de teixit fibro-lamel·lar a teixit lamel·lar (és a dir, el EFS per les sigles en anglés: *external fundamental system*) al fèmur, el qual ha estat relacionat amb l'arribada

a la maduresa sexual dels individus segons indiquen les dades recollides sobre la fusió d'epífisis i patró d'erupció dental en el cérvol. A més, el calibratge del nombre de marques cícliques amb l'edat coneguda dels individus en semillibertat va aclarir que el fèmur és el millor os llarg per a calcular l'edat de maduresa esquelètica mentre que la tíbia és un bon indicador de l'edat de mort de l'individu. El marcatge amb fluorocroms va permetre atribuir la presència de marques no cícliques gravades durant els primers estadis vitals als esdeveniments de naixement i deslletament. Aquest enfocament també va descobrir com aquests esdeveniments únics causen alteracions en les taxes de creixement i, per tant, alteracions en la deposició del teixit. A més, la diferent expressió de caràcters histològics en dos grups de cervatells (criats a mà i criats per la seva mare) va esbrinar que el règim nutricional és un factor important en els efectes que el deslletament tenen en l'os.

En resum, tots aquests resultats contribueixen a un millor enteniment de les dinàmiques de creixement a través de l'ontogènia. Aquesta tesi també contribueix a comprendre els impactes que els esdeveniments de la història de vida ocasionen en el creixement ossi, així com dels factors que els modulen (nutrició). A més, els resultats obtinguts de l'anàlisi histològica en cérvols proporcionen una base ferma per a realitzar millors interpretacions en grups fòssils.

CHAPTER 1. INTRODUCTION

1.1. Life history theory

In ecology, the term "life history" is understood as the set of developmental events that occur throughout the lifetime of an organism (i.e. from the moment of its birth until its death). In other words, the life history of an individual describes its particular growth patterns as well as its reproductive, maturation and survival strategies under specific ecological conditions (Braendle et al., 2011; Roff, 2002; Stearns, 1992). These events are shaped by life history traits: demographic parameters associated with time (e.g. age at sexual maturity, longevity, gestation period, calving interval) and size (e.g. size at birth, size at maturity, litter size) (Stearns, 1992). The expression of these traits is regulated by developmental, genetic, and phylogenetic factors, and, especially, by environmental conditions (Braendle et al., 2011; Roff, 1992). The combination of these factors determines individual fitness, expressed as reproductive success (i.e. the product of survival and fecundity) (Braendle et al., 2011; Roff, 2002; Stearns, 1992).

As resources (i.e. time and energy) that affect an individual's growth, reproduction and maintenance processes are limited, life history traits are modulated by constraining interactions called trade-offs (Braendle et al., 2011; Cody, 1966; Stearns, 1992). Trade-offs (e.g. reproduction vs. survival, current vs. future reproduction, reproduction vs. growth) represent the allocation of limited resources to one biological process over another (Braendle et al., 2011; Rockwood, 2006; Roff, 1992; Stearns, 1992, 1989). Darwin, citing Goethe and St. Hilaire, addressed this issue in the nineteenth century: "The budget of nature is fixed; but she is free to dispose of particular sums by an appropriation that

may please her. In order to spend on one side, she is forced to economize on the other side" (Rauw, 2008).

The distribution of this "budget" (i.e. energy) is modulated by extrinsic factors. The widely known *r/K* theory developed in the 1960s and 70s (MacArthur and Wilson, 1967; Pianka, 1970) considered the degree of density-dependence as the main selective pressure between populations. Fluctuating environments favour density-independent mortality, which leads to a periodic increase in resources and results in a large increase in population growth rate (i.e. the *r* parameter). Thus, *r*-selected populations usually inhabit unstable environments with changing levels of resources and present traits such as small body size, early maturity, high fecundity, high reproductive effort and, in some cases, semelparity (Pianka, 1970; Reznick et al., 2002). This strategy enhances the population growth rate. On the other hand, populations living in stable environments near carrying capacity (i.e. the *K* parameter) experience density-dependence, leading to a decrease in available resources and intense intra-specific competition. In *K*-strategist populations, natural selection favours traits that enhance persistence of individuals: large body size, delayed maturity, low reproductive effort, increased iteroparity and longer life spans (Pianka, 1970; Reznick et al., 2002). However, while this theory greatly contributed to the understanding of life history evolution, in the following decades, it was increasingly seen as an oversimplification and was replaced with demographic models (Gadgil and Bossert, 1970; Reznick et al., 2002; Stearns, 1992, 1989). These models were based on the notion that age-specific extrinsic mortality (i.e. predation) is the main driver behind resource allocation decisions (Roff, 1992; Stearns, 1992). Following this hypothesis, in environments with high extrinsic mortality, individuals show early maturity since resources are allocated to enhance early reproduction, thus shortening the juvenile period. On the contrary, in conditions with low extrinsic mortality,

individuals experience delayed maturity, as resources are channelled to growth and maintenance functions, resulting in long juvenile periods.

Resource allocation processes contribute to a great variety of life history traits, which have led to the diverse life history strategies that exist between individuals, populations, species and environments (Stearns, 1992). Life history theory explains the diversity of life history strategies by analysing how natural selection shapes the life history of an individual and adjusts its fitness depending on the environment (Roff, 2002; Stearns, 1992). Based on their variations, life history strategies can be placed along a slow-fast continuum (Stearns, 1983). A slow pace of life is characterised by initial costs and delayed benefits (e.g. delayed maturity, long lifespan, slow development, high parental investment), whereas initial benefits and delayed costs (e.g. fast development, early maturity, short lifespan, low parental investment) characterise a fast pace of life (Stearns, 1983).

Life history evolution is an essential part of evolutionary ecology (Stearns, 2000), and consequently, an increasingly large number of studies have focused on the mechanisms that shape life histories (e.g. Nussey et al., 2008; Hamel et al., 2010; Hou, 2013; Ibler, 2017). Moreover, life history theory has become the focus of interest in other disciplines, such as palaeontology, that seek to shed light on past life history strategies (Bromage et al., 2002; Chinsamy et al., 2020; Dirks et al., 2012; Hayashi et al., 2020; Köhler, 2010; Köhler and Moyà-Solà, 2009; Marín-Moratalla et al., 2011; Miszkiewicz et al., 2019; Moncunill-Solé et al., 2016; Nacarino-Meneses and Orlandi-Oliveras, 2019; Orlandi-Oliveras et al., 2016, 2018; Raia et al., 2003; Turvey and Holdaway, 2005).

1.2. Hard tissue analysis as a tool for life history inferences

Vertebrate hard tissue structures usually constitute the only evidence from past organisms and populations. Moreover, examining these structures is also sometimes the only way to study living vertebrates since the monitoring, capture, management and subsequent release of wild animals require an enormous amount of time, effort and resources. In these cases, analysing skeletal elements from both living and fossil organisms is vital for obtaining information about their life histories. The developmental stages of cranial and postcranial elements allow researchers to estimate age stages and obtain information on key developmental milestones (e.g. skeletal maturity and weaning; section 1.2.1.). In addition, hard tissues (i.e. bone, enamel, dentine and cementum) contain microstructural growth records. Thus, the histological analysis of their microstructures represents a powerful tool for inferring the life history and growth patterns of extinct and living taxa (section 1.2.2.).

1.2.1. The development of cranial and postcranial elements

The mammalian skeleton is a dynamic structure that undergoes modifications during animal growth to accommodate the increasing size of the animal. It is therefore possible to estimate the developmental stage of a given animal by analysing its skeletal elements (Hillson, 2005). Two of the main techniques for estimating a mammal's age at death are based on the axial skeleton and dental pattern.

The axial skeleton (i.e. limb bones) is composed of endochondral bone. Bone is formed from cartilage by a process of substitution that takes place during the individual's juvenile stage. As the bone forms, it is possible to distinguish three distinct parts: the diaphysis in the central part of the bone, the epiphysis in the distal parts and the metaphysis in the intermediate region

between them. Cartilage proliferation in the epiphysis causes bones to elongate. Bone begins to replace cartilage in the diaphysis and then continues towards the epiphysis (Fig. 1.1). When longitudinal growth ceases, the epiphysis is fused to the diaphysis, forming a single element, a phenomenon linked to skeletal maturity.
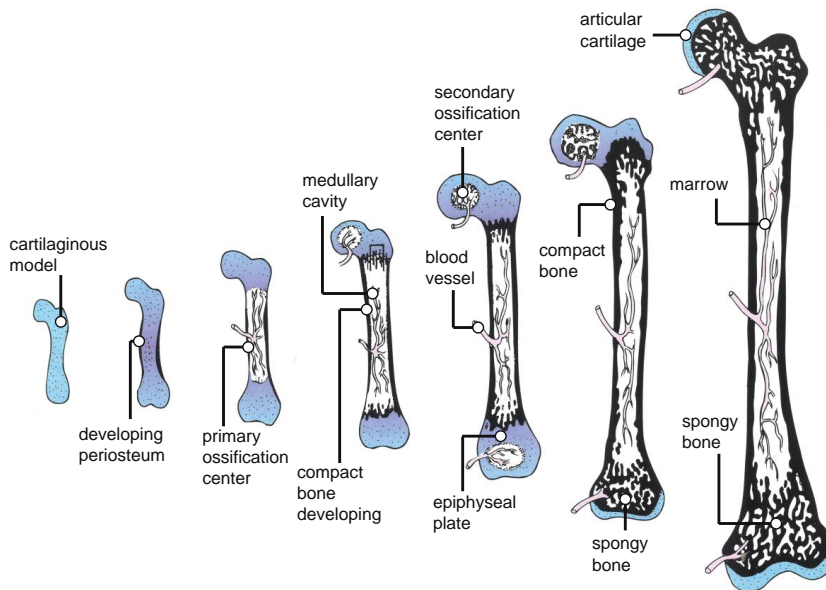
Figure 1.1. Endochondral ossification of a limb bone. Successive development stages from cartilaginous model (left) to bone fully formed (right). Modified from Kardong (2006).

In most mammals, an unfused epiphysis indicates a sub-adult age (exceptions include some micromammals, such as rats, and some large and late-maturing mammals, such as elephants) and therefore suggests that the animal is in an active growing stage (Morris, 1972; O'Connor, 2000). However, epiphyseal closure does not occur simultaneously in every bone of the skeleton but is conditioned by the developmental rates of the different bones (Morris, 1972). The epiphyseal fusion sequence can be predicted for a particular species (O'Connor, 2000). Based on this concept, Lesbre (1897) estimated the age of epiphyseal fusion for different bones of domestic animals. Since then, several

studies have continued to estimate the fusion sequence in different domestic and wild mammalian species (e.g. guinea pigs (Zuck, 1938), badgers (Ahnlund, 1976), white-tailed deer (Purdue, 1983), gazelle (Munro et al., 2009), sheep (Popkin et al., 2012)).

Most mammals are diphyodonts, meaning they possess two sets of teeth (Fig. 1.2). During the individual's development, the first set of deciduous or milk teeth (an immature attribute) is gradually replaced by the second set of permanent teeth (a mature attribute) (Hillson, 2005). Each tooth erupts following a species-specific eruption sequence. Variations of eruption sequences among species are determined by phylogeny (see for instance Veitschegger & Sánchez-Villagra (2015) for ungulates), although environmental factors can influence the time of eruption and cause variations at the intra-specific level (Loe et al., 2004). The study of the eruption pattern sheds light on the pace of life (Smith, 2000) as well as the occurrence of certain life history events (Anders et al., 2011). For instance, it has been demonstrated that the emergence of the first molar is strongly related to the weaning event (Dirks and Bowman, 2007; Smith, 1991) while the eruption of the third molar is related to the attainment of maturity (Engström et al., 1983). Some studies on domestic (Andrews, 1973; Lesbre, 1897; Reiland, 1978) and wild species (e.g. Azorit et al., 2002; Munro et al., 2009; Kierdorf et al., 2012) have predicted the eruption times of permanent teeth, which provides an estimation of the individual's age at death, particularly if not all of the teeth have fully erupted (i.e. if the individual has not yet reached adulthood). Once permanent dentition is completed, the age at death can be still estimated by the degree of dental wear. Two approaches are used for measuring the degree of dental wear (Hillson, 2005): one measures the crown height (widely used in herbivores; Lowe, 1967) and the other is based on the occlusal pattern of the dentine and the exposed cement (Payne, 1973). Anders et al., (2011) presented a general pattern of mammalian dental stages based on tooth eruption and wear.
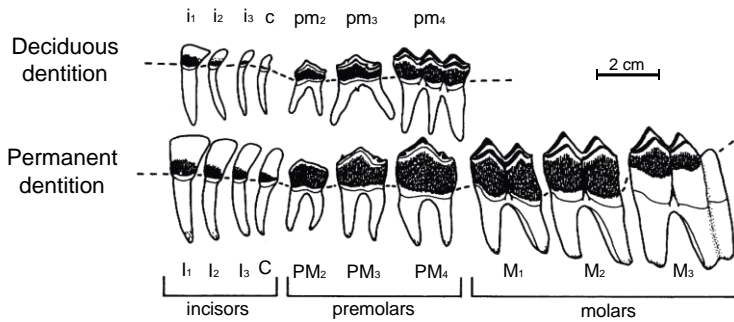
Figure 1.2. Set of lower deciduous and permanent teeth of red deer. Modified from Mitchell (1967).

1.2.2. Bone tissue as recording structures: a histological approach

In addition to the size-related adjustments that the bones of a growing animal undergo, the internal microstructure of the bones also experiences modifications. Due to the incremental growth of bone tissue, growth dynamics are recorded in the bone (Chinsamy-Turan, 2005; Klevezal, 1996), giving an accurate template that contains information about the growth process. Consequently, the histological analysis of bone microstructure is considered the most promising method for reconstructing bone growth and inferring life history (Castanet, 2006; Castanet et al., 1993; Chinsamy-Turan, 2005; Klevezal, 1996; Woodward et al., 2013).

The properties of the bone matrix and the presence of growth marks embedded within the tissue are the two main features that make inferring life history traits related to age or growth rates possible. Bone tissue is classified according to the internal arrangement of collagen and bone cells within the bone matrix (Amprino, 1947; Francillon-Vieillot et al., 1990). The organization of the matrix is influenced by the rate of bone deposition. A highly disorganised matrix arrangement, classified as woven tissue, has the fastest deposition rate. On the contrary, lamellar bone is characterised by a highly

organised matrix and is deposited at a slow rate. Between these two extremes, there are types of tissue that exhibit intermediate deposition rates (Chinsamy-Turan, 2005; de Margerie et al., 2002; Francillon-Vieillot et al., 1990; Huttenlocker et al., 2013; see methods). The correlation between the depositional rates and the arrangement of the matrix, known as Amprino's rule, allow histologists to infer growth rates from bone tissue (Amprino, 1947; Chinsamy-Turan, 2005; de Margerie et al., 2002; Huttenlocker et al., 2013). Moreover, the transition from one tissue type to another within a bone reflects changes in deposition rates that are often linked to life history events. For instance, in mammals, vertebrates with asymptotic growth, long bones begin to develop through the apposition of fast and disorganised tissue, which is the predominant tissue in the prenatal and juvenile periods (Fig 1.3). Later, when maturity is reached, the rate of tissue apposition slows down, and the tissue starts to exhibit a highly organised arrangement (Chinsamy-Turan, 2005; Klevezal, 1996; Woodward et al., 2013). Known as the external fundamental system (EFS), this slow-forming tissue, which is deposited after maturity, appears in the outer part of the cortex and represents the remaining life span of the individual (Fig 1.3). There has been much debate on whether the appearance of the EFS indicates that an individual's skeletal (Amson et al., 2015; Kolb et al., 2015a) or sexual maturity has been reached (Jordana et al., 2016; Marín-Moratalla et al., 2013b; Nacarino-Meneses et al., 2016a).

Bone growth marks constitute another histological feature to interpret growth and to infer age-related life history traits (Fig 1.3). The presence of these marks within bone tissue indicates a change in growth rates or the resorption of previously deposited bone tissue. A bone growth mark is classified as an annulus when it is composed of a thin band of slow-growing tissue, which indicates a decrease in growth rate. However, a thin dark line is considered a line of arrested growth (LAG). LAGs indicate a pause in tissue deposition of unknown duration. Bone growth marks can also be classified as non-cyclical

or cyclical growth marks according to their annual periodicity (Woodward et al., 2013). The counting of the cyclical marks, known as skeletochronology, allows histologists to infer the timing of life history traits, such as age at maturity and especially age at death, while the study of non-cyclical marks sheds light on single life history events (see Chapter 3).

On this basis, the histological approach has been developed for fossil groups (a discipline called paleohistology) with the purpose of obtaining information on bone development, biomechanics and life history-related parameters (e.g. growth rates), among others. In the second half of the 20th century, the exhaustive studies of Donald Enlow (Enlow, 1962a, 1962b; Enlow and Brown, 1958, 1957, 1956) and Armand de Ricqlés (Padian, 2013, 2011) contributed substantively to the histological study of fossil tetrapods and provided a solid basis for subsequent histological studies (Botha and Chinsamy, 2005; Chinsamy-Turan, 2005; Chinsamy, 1994; Erickson, 2005; Horner et al., 2000a, 1999; Huttenlocker and Botha-Brink, 2014; Padian et al., 2004, 2001; Ray et al., 2004, 2005; Sander, 2000). Although the mammalian group was little studied at the time (Klevezal, 1996), in recent decades, many studies have inferred life history traits by analysing bone tissues from fossil and extant mammals (Amson et al., 2015; García-Martínez et al., 2011; Jordana et al., 2016; Köhler, 2010; Köhler and Moyà-Solà, 2009; Kolb et al., 2015b; Marín-Moratalla et al., 2013b, 2014; Martinez-Maza et al., 2014; Moncunill-Solé et al., 2016; Nacarino-Meneses et al., 2016b, 2016a; Nacarino-Meneses and Orlandi-Oliveras, 2019; Orlandi-Oliveras et al., 2016, 2018).
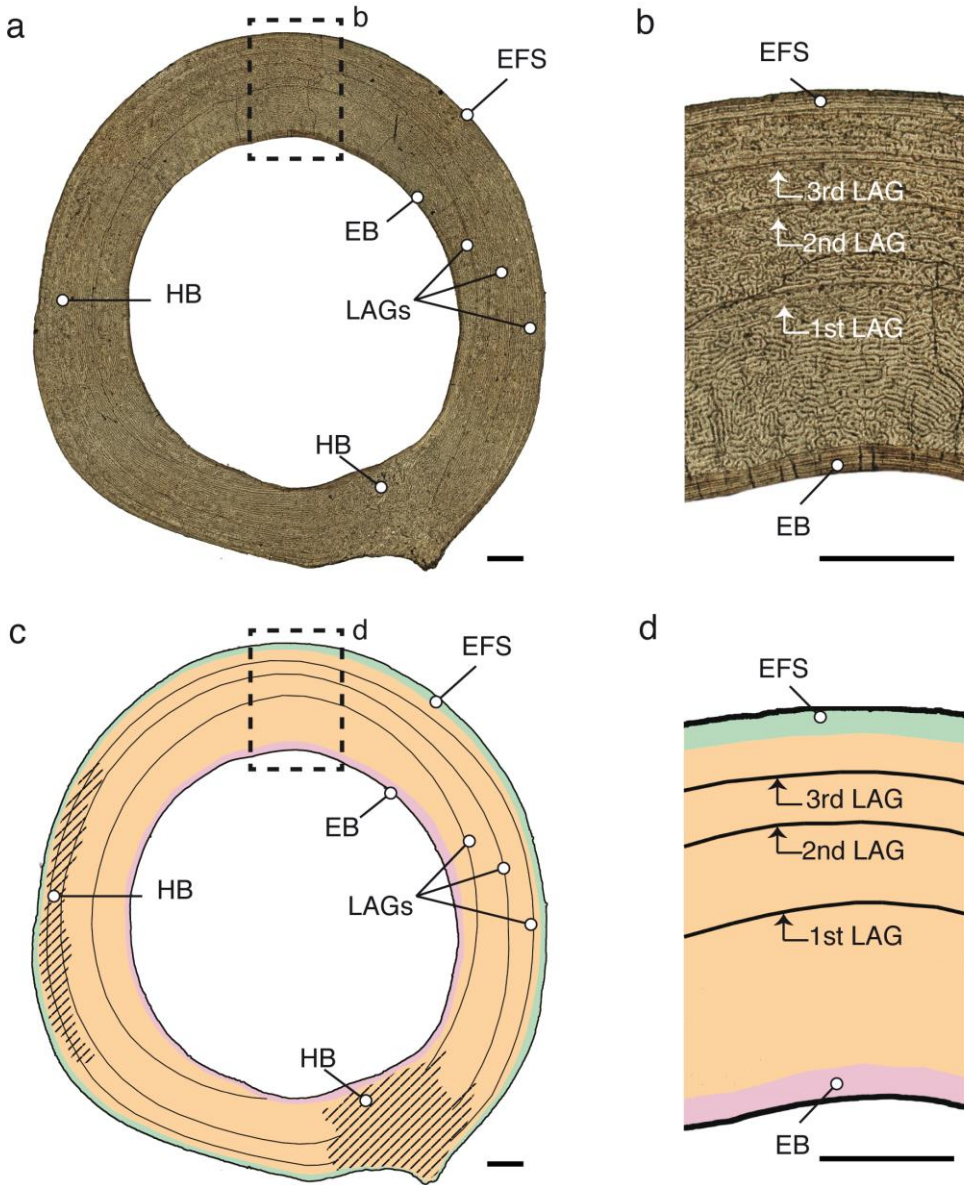
Figure 1.3. Histological and schematic detail of a femur cortex. (a,c) bone cortex obtained from the femur midshaft; (b,d) detail of the anterior part of the femur. EB: endosteal bone; HB: Haversian bone; LAG: Line of Arrested Growth. EFS: External Fundamental System. Orange colour: primary, fast-growing tissue (i.e. FLC). Blue colour: primary, slow-forming tissue (i.e. EFS). Pink colour: deposits of secondary bone (i.e. EB). Scale bar: 2mm

1.2.2.1. Fluorescent labelling as a tool for a quantitative approach

In vivo bone labelling with fluorochromes provides quantitative information on tissue deposition that cannot be obtained otherwise. By using this approach, some authors (Castanet et al., 2000; de Margerie et al., 2004, 2002) have statistically tested Amprino's rule (which states that the tissue type is determined by the rate of deposition) and estimated the growth rates of different bone tissues in birds. Fluorescent labelling has also been used to evaluate bone remodelling patterns in small mammals (Montoya-Sanhueza et al., 2021). Labels deposited within bone tissue can also act as a temporal reference point, allowing histologists to calibrate life history traits with age (Castanet et al., 2004, 1996). Furthermore, fluorescent labelling allows histologists to estimate the periodicity of bone deposition and its relationship with dental incremental structures (Bromage et al., 2009).

1.3. Deer

Deer (Cervidae) are the second most diverse group of ruminant artiodactyls (Grooves, 2007). Extant members of the suborder Ruminantia fall into six families: Bovidae, Cervidae, Antilocapridae, Giraffidae, Moschidae and Tragulidae (Gentry, 2000). With the exception of the Tragulidae family, all belong to the Pecora group. Despite the shared features with the rest of artiodactyls (i.e. long limb bones whose weight is mostly supported by the third and fourth digits and a double-pulley astragalus), ruminants possess tetra-selenodont teeth and a specialised digestive system with a compartmentalised stomach (Gentry, 2000). Microbial fermentation of the food occurs in the rumen; thereafter, food is regurgitated as cud that completes its digestion in the reticulum, omasum (absent in tragulids; Clauss & Rössner, 2014), abomasum and intestines. Furthermore, most of the living families have

cranial appendages: horns (Bovidae), antlers (Cervidae), pronghorns (Antilocapridae) and simple ossicones (Giraffidae) (DeMiguel et al., 2014; Gentry, 2000).

The family Cervidae is comprised of 51 species that inhabit areas from the Arctic to the Tropics. Cervids show a wide range of body sizes, from 10 kg (*Pudu*) to 800 kg (*Alces*) (Vaughan et al., 2013). They are characterised by apophyseal cranial appendages (a bony extension of the frontal bone) called antlers that are shed annually (see section 1.3.3.). Antlers are restricted to males, except in the genus *Rangifer*, in which females also bear antlers. In addition, most deer exhibit low-crowned (brachydont) dentition and specific cranial features, such as two lacrimal foramina, a lacrimal fossa and pre-orbital vacuity (Heckeberg, 2020). Cervids also have a closed distal metatarsal gully and a "cervid-type" canal for the common digital that runs through the middle of the metatarsus III-IV (Sánchez et al., 2010).

Brooke (1878) grouped members of the family Cervidae into two subfamilies according to the retained portion of their reduced second and fifth digits: Cervinae (plesiometacarpal: proximal portion retained), consisting of Muntiacini and Cervini tribes, and Capreolinae (telemetacarpal: distal portion retained), consisting of Alceini, Capreolini, Odocoileini and Rangiferini tribes. This classification has been corroborated by posterior phylogenetical analyses (Gilbert et al., 2006; Heckeberg, 2020; Pitra et al., 2004). Members of the genus *Cervus* belong to the Cervini together with *Axis*, *Dama*, *Elaphorus*, *Rucervus* and *Rusa*.

1.3.1. Evolutionary history

Ruminants emerged from the radiation of selenodont artiodactyls that took place during the middle-late Eocene (≈ 40my; Webb and Taylor, 1980). The

clade Pecora appeared in the Eocene-Oligocene boundary (≈ 34my) as a result of a ruminant diversification associated with climatic and vegetation changes (Fernández and Vrba, 2005; Hassanin et al., 2012). At the end of the Oligocene and the beginning of the Miocene (≈ 24 my), all non-pecoran groups became extinct except the Tragulidae. In contrast, pecorans experienced a significant diversification (Cantalapiedra et al., 2015), marked by the acquisition of cranial appendages and hypsodonty (i.e. high-crowned dentition) (DeMiguel et al., 2014), giving rise to the most diverse group of extant large mammals (Fernández and Vrba, 2005; Hassanin et al., 2012; Sánchez et al., 2015) (Fig 1.4).

The first true cervids, with antler-like appendages, emerged in the early Miocene. The systematic analysis of Miocene deer has been a matter of discussion due to the controversial lagomericids (Heckeberg, 2020), recognised by Azanza & Ginsburg (1997) as an independent clade from Cervidae. As a result, the group of Miocene stem cervids is composed of the Procervulinae (*Procervulus* and *Heteroprox)* and the Dicrocerinae (*Dicrocerus*, *Acteocemas* and *Stehlinoceros*) (Azanza 2000). Both groups are characterised by proto-antlers, dichotomous antler-like appendages without a coronet or with a coronet-like structure that could be shed occasionally (Azanza et al., 2011). Based on the development of proto-antlers, the Dicrocerinae were thought to be an intermediate group between the subfamily Procervulinae (that includes the first recognised genus of the family) and modern cervids (deer with true antlers; Azanza et al., 2011). Stem cervids became extinct during the Miocene. However, recent phylogenetic analyses (Mennecart et al., 2017) have suggested that they may have reached the late Miocene.
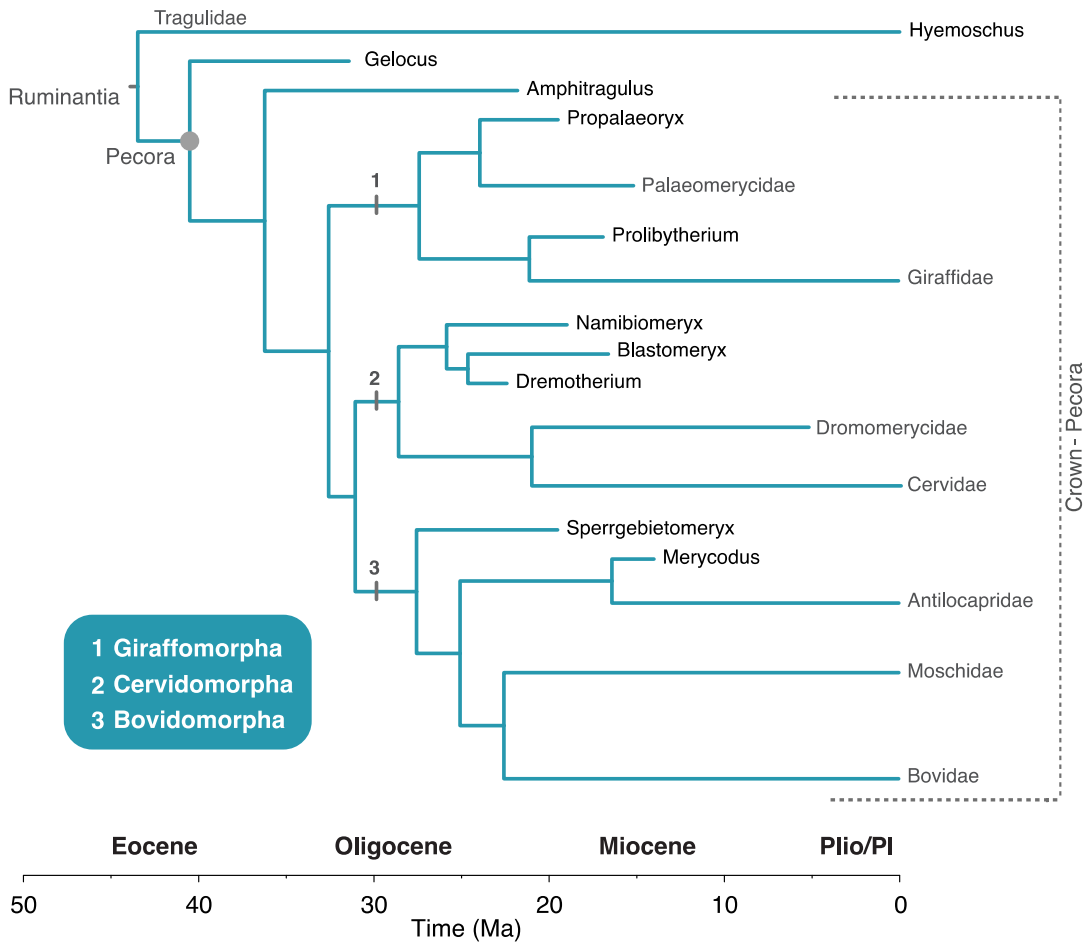
Figure 1.4. Phylogenetic hypothesis for pecoran ruminants. Modified from Sánchez et al. (2018, 2015).

Crown cervids emerged in the Middle Miocene, with the genus *Euprox* their earliest known representative (Azanza et al., 2013; Mennecart et al., 2017). True antlers are characterised by a monopodial morphology with true coronets and a regular cycle of shedding controlled by hormones (Bubenik, 1990). At the end of the Miocene, the two subfamilies of the crown cervid group (Cervinae and Capreolinae) underwent adaptive radiations, leading to the emergence of the earliest known members of Cervini and Capreolini including *Cervivatus*

and *Procapreolus* (Azanza et al., 2013) (Fig. 1.5). Deer reached the American continent between the late Miocene and the early Pliocene (Gentry, 2000). The subfamilies of deer evolved differently during Pliocene and Pleistocene: the clade Capreolinae was significantly depleted by the extinction of many subgroups during the climatic-geographic conditions of Northern Eurasia, while Cervinae remained mostly unchanged (Croitor, 2018, 2014; Geist, 1998). The first evidence of the genus *Cervus* comes from the early Pleistocene of Western Eurasia (*Cervus nestii*) (Croitor, 2018, 2014). During the Middle and Late Pleistocene, *Cervu*s underwent speciation driven by dispersal (towards Western Europe and the Eastern part of Asia and North America) and local evolutionary events associated with isolation in glacial refugia (Croitor, 2018; Ludt et al., 2004).
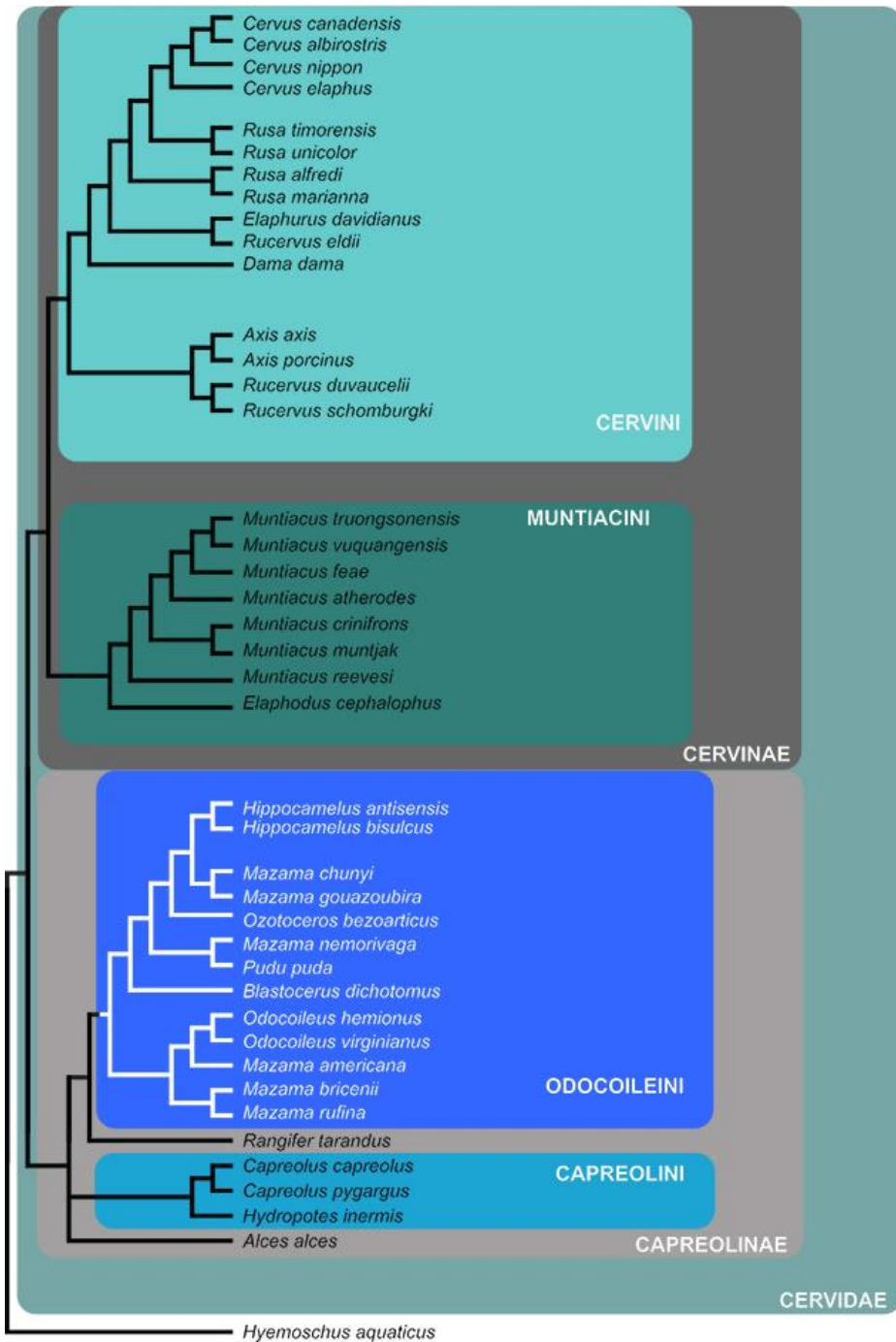
Figure 1.5. Phylogeny of crown-Cervidae. Figure modified from Heckeberg (2020).

1.3.2. Red deer distribution and subspecies

Most 20th century taxonomists considered red deer (*Cervus elaphus*) a single species of Holarctic distribution. In contrast, other authors (Clutton-Brock et al., 1982; Geist, 1998) maintained that *Cervus elaphus* (red deer) was confined between Western Europe and Central Asia, while a different species, *Cervus canadensis* (wapiti or elk), was dispersed from Central Asia to North America. This assumption was supported by molecular analyses demonstrating that red deer are differentiated into a western and an eastern clade (Ludt et al., 2004; Pitra et al., 2004; Randi et al., 2001; Stankovic et al., 2011). More recently, Lorenzini & Garofalo (2015) established two more *Cervus* species: *Cervus nippo*n (previously included in *Cervus canadensis*) and *Cervus hanglu* (previously included in *Cervus elaphus*).

Taking this into account, red deer is a species that inhabit several areas of the west Palearctic, although this species can also be found in some countries of South America, Australia and New Zealand due to introductions by humans (Lovari et al., 2016). Three different lineages of red deer from glacial refuges have been established based on mtDNA analyses (Skog et al., 2009a; Sommer et al., 2008; Zachos and Hartl, 2011): the Iberian, Balcanic, and African. These lineages split into a number of subspecies (e.g. *C. e. scotticus* [the United Kingdom], *C. e. hippelaphus* [central Europe], *C. e. atlanticus* [Scandinavian peninsula] and *C. e. hispanicus* [the Iberian peninsula]) based on phenotypic features, such as coat colour, and the morphological features of the cranium and antlers (Geist, 1998). The subdivisions of lineages into subspecies are not genetically supported by mtDNA analyses (Lorenzini and Garofalo, 2015; Ludt et al., 2004). However, Carranza et al. (2016) used nuclear markers to confirm that Iberian deer have a specific genetic identity (*Cervus elaphus hispanicus*).

1.3.3. Biology and ecology of red deer

Red deer is a polygynous species with marked sexual dimorphism: body masses of adult males (stags) range between 80–160kg, while those of adult females (hinds) vary between 50–100kg. Deer reside in woodland habitats either in mountainous or sea level planes, although some populations inhabit open moorlands, such as the Scottish population. They show a preference for ecotones (i.e. areas around woodland edges or the interface between woodland and grassland) due to their mixed feeding regime (Carranza, 2007; Clutton-Brock et al., 1982; Mitchell et al., 1977). Habitat selection and feeding habits are strongly seasonal and are influenced both by the production of different plant communities and by the deer requirements according to age, sex and breeding condition.

1.3.3.1. Life cycle of red deer

During most of the year, the basis of the red deer's social organisation consists of matriarchal groups of hinds, with stags dispersed throughout the territory (Mitchell et al., 1977). At the beginning of the reproductive season, known as the rut (October), stags start to associate with hinds, and harems are formed (Fig. 1.6a). During the rut, stags compete for their group of hinds and defend their territories by means of roaring (Fig. 1.6b) and, in some cases, fighting with other males (Fig. 1.6c). After conception (Fig. 1.6d), the gestation period begins and lasts approximately 230 days (Carranza, 2007). The life cycle is strongly determined by seasonality and synchronised so that that parturition and lactation (Fig. 1.6e) coincide with the period of maximum food availability (Lincoln, 1992). Hinds give birth to a single calf in May or June. To do so, pregnant hinds separate from the family group in order to avoid predators during birth. For the same reason, they keep their distance from calves, which remain hidden in the vegetation most of the time (Geist, 1998). Hinds and

calves only stay together during lactation bouts. It is possible to find a hind with more than one calf since allosuckling behaviour is common in deer (Landete-Castillejos et al., 2000). Shortly after birth, calves begin to incorporate vegetal material into their diet. As calves grow, they eat more vegetal material, and lactation bouts become shorter, with more time between bouts. Hinds gradually prevent calves from suckling until they are completely weaned (Clutton-Brock et al., 1982) (Fig. 1.6f).
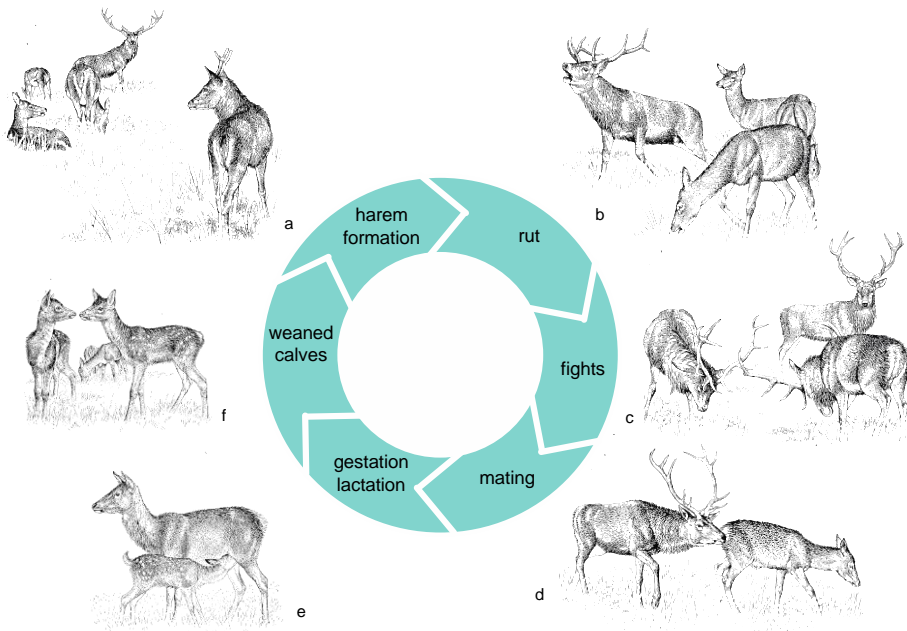
Figure 1.6. Life cycle of red deer. Figure modified from Clutton-Brock et al. (1982).

During this time, stags, which disperse again after the rut, cast their antlers at the end of winter. Shortly after, following endogenous annual rhythms, their antlers begin to regrow. Growing antlers are also called "antlers in velvet" due to their skin cover. Antlers size increases until mid-summer; then, stags remove the velvet skin by rubbing the antlers against trees, and they become ready for the coming rutting season (Lincoln, 1992). Antlers start to develop at the age of one in male deer (Carranza, 2017; Lincoln, 1971). Over the

years, antlers change their morphology by increasing their size and developing tines (Carranza, 2017). Antler morphology is indicative of a stag's body condition. Thus, antlers with asymmetrical morphology suggest that sub-optimal developmental conditions or stress has affected the annual cycle (Mateos et al., 2008). Although antler morphology reflects the fighting ability of the stag, it has been demonstrated that the morphology of these structures is also an indicator of the animal's reproductive quality (Malo et al., 2005).

1.3.3.2. *Life history of red deer*

Like other artiodactyls, the red deer species' life history strategy is characterised by a short juvenile period (from birth to first reproduction), a long gestation period, a long reproductive span, the birthing of a few well-developed offspring and a large body size (Gaillard et al., 1989). However, as a species with marked sexual dimorphism, some of these traits vary between males and females.

Calves typically weigh 6–10 kg at birth, and hinds grow rapidly until the age of three years, while stags reach their adult size at the age of six years. The males' longer growth period results in their larger body size. Their body size is also conditioned by the greater investment hinds make in male offspring before weaning (Clutton-Brock et al., 1982). However, the males' larger size comes with has costs common to polygynous and sexually dimorphic animals, such as shorter life spans and higher rates of heat loss (Clutton-Brock et al., 1982). Hinds and stags experience different reproductive costs for conception and calf rearing. The cost of fertilisation for stags is minimal compared with the high costs of gestation and lactation reproductive hinds experience (Clutton-Brock et al., 1989). As a consequence, hinds' reproductive success is determined by their ability to maintain an adequate nutritional status in order to minimise calf mortality, while stags' reproductive success depends largely

on their dominance and, if necessary, their fighting ability, which is determined by antler development and body size (Lincoln, 1992; Mitchell et al., 1977). The length of the reproductive span also differs between sexes. Hinds reproduce from the age of one or two years almost until death. In contrast, stags are sexually mature at the age of two or three years, but their reproductive span only lasts four or five years (Clutton-Brock et al., 1982; Carranza, 2007).

CHAPTER 2. AIMS AND OBJECTIVES

The histological analysis of bone microstructure has proven to be an excellent method for shedding light on the life histories of fossils and living vertebrates. The first histological studies focused on non-mammalian fossil groups, primarily providing age estimations for poikilotherms (e.g. amphibians and reptiles), as it was previously thought due that mammals, as homoeothermic animals, do not record growth marks (Chinsamy-Turan, 2005). However, the evidence that mammalian bones indeed record cyclical periods of growth that are synchronised with seasonal physiology (Köhler et al., 2012) initiated the use of histological analyses in mammals (Amson et al., 2015; Becker et al., 2020; Cambra-Moo et al., 2015; Jordana et al., 2016; Kolb et al., 2015b; Marín-Moratalla et al., 2013b, 2014; Martinez-Maza et al., 2014; Moncunill-Solé et al., 2016; Montoya-Sanhueza et al., 2020, 2021; Montoya-Sanhueza and Chinsamy, 2017; Nacarino-Meneses et al., 2016a, 2016b; Nacarino-Meneses and Orlandi-Oliveras, 2019; Orlandi-Oliveras et al., 2016, 2018). The information recorded in bone tissue and growth marks has allowed researchers to estimate mammalian growth dynamics and the timing of life history traits. However, most studies are dedicated to fossil groups, and additional research is needed to better understand the growth dynamics and ontogeny of extant animals (Padian, 2013). Furthermore, the biological triggers linked to certain histological features, such as the EFS record or non-cyclical marks, are not completely understood. The amount of time that growth marks (LAGs and annuli) represent has also not been thoroughly studied. Once these features are understood in wild animals, it will be possible to develop an inference model capable of making more accurate interpretations in fossil taxa (Padian et al., 2013).

Cervid evolutionary history is well known, and the bone microstructure of a few fossil species has been studied to reconstruct these animals' life history

traits (Amson et al., 2015; Kolb et al., 2015b, 2015a). However, despite the existence of abundant extant cervid species with available skeletal material and well-known life histories, no studies have focused on the bone growth dynamics of living members of this family. Therefore, to fill this gap, this dissertation provides histological analysis of the postcranial material of red deer (*Cervus elaphus* Linnaeus 1758), one of the most widespread species of living deer whose biology and ecology have been widely studied (Albon et al., 1987; Clutton-Brock et al., 1983, 1987, 1982; Nussey et al., 2008), to offer insight into the bone growth dynamics of extant deer.

Calibration of histological features with epiphyseal closure and dental eruption patterns together with known life history traits of individuals provide a firm basis for comparisons with other groups of mammals as well as for the study of fossil species. Moreover, in vivo labelling provides key information on the growth dynamics of deer during early ontogeny and sheds light on the deposition of non-cyclical marks. The diversity of the sample here used allows for the results between sexes, subspecies and feeding regimes to be compared.

This thesis addresses the following objectives:

i. To calibrate dental eruption pattern and epiphyseal closure with the histological features found in the bones of deer;

ii. To correlate the histological information contained in the limb bones of deer with key life history traits;

iii. To assess the reliability of skeletochronology for assessing mammalian bones and exploring the variations in the different bone elements as recording structures;

iv.   To analyse in detail the growth rates during the early ontogenetic stages
       of the deer;

v.   To shed light on the non-cyclical events that affect deer growth during
      early ontogenetic stages.

These objectives are addressed in the following chapters:

PhD chapter	Objectives addressed
Chapter 4. Calibration of life history traits with epiphyseal closure, dental eruption and bone histology in captive and wild red deer	I, II, III
Chapter 5. Labelling experiments in red deer provide a general model for early bone growth dynamics in ruminants	II, IV, V

Table 2.1. Summary of the chapters comprising the present dissertation and objectives addressed in each chapter.

CHAPTER 3. MATERIALS AND METHODS

3.1. Materials

3.1.1. Cranial and postcranial material

The sample studied in the present PhD dissertation consists of skeletal material from 51 red deer (*Cervus elaphus)* from two different red deer subspecies: one from the Iberian Peninsula (*C. e. hispanicus)* and one from Central Europe (*C .e. hippelaphus*).

The entire sample consisted of 99 long bones from the forelimbs (the humerus, radius and metacarpus) and hindlimbs (the femur, tibia and metacarpus) (Table 3.1). The material was prepared for histological analysis (see section 3.2.3.1.), resulting in a total of 191 thin sections. The material described is housed at the ICP (Institut Català de Paleontologia Miquel Crusafont) in Barcelona, Spain.

3.1.1.1. *Iberian red deer (Cervus elaphus hispanicus)*

Individuals from the Iberian subspecies belonged to three different wild populations in Spain: La Rioja and Lleida in the northern area and Badajoz in the southern area. Bones and mandibles were obtained from previous hunting seasons in these locations and were sent to the ICP installations accompanied by a report providing information about the sex of each individual.

3.1.1.2. *Alpine red deer (Cervus elaphus hippelaphus)*

Individuals of the Alpine subspecies belonged to a single captive population in Vienna, Austria. Animals were maintained in semi-wild conditions in facilities at the Research Institute of Wildlife Ecology, Department of Interdisciplinary Life Sciences, University of Veterinary Medicine Vienna. Four of these individuals were used for labelling experiments (see section 3.2.1.). After sacrifice, carcasses were sent to the ICP installations along with the following detailed life history data: sex, age, age at first birth (in the case of females), number of offspring (in the case of females), castration regime (in the case of males), weight at death, weight at birth, daily weight gain (in the case of the calves), feeding regime and age at weaning.

	subspecies	ID	males	females	limb bones	mandibles	thin sections
Ch. 4	*Cervus elaphus hispanicus*	19	11	8	25	13	54
	Cervus elaphus hippelaphus	13	8	5	20	13	27
Ch. 5	*Cervus elaphus hippelaphus*	6	5	1	54	-	110
Total	*Cervus elaphus*	38	24	14	99	26	191
	Cervus elaphus hispanicus	19	11	8	25	13	54
	Cervus elaphus hippelaphus	19	13	6	74	13	137

Table 3.1. Summary of the red deer sample studied in the present dissertation

3.2. Methods

3.2.1. Labelling experiment

As part of a long-running experiment carried out by the Institut Català de Paleontologia Miquel Crusafont (Barcelona) and the Research Institute of Wildlife Ecology (Vienna) under the planning and supervision of M. Köhler (ICP), four young individual deer were labelled with fluorochromes. A fluorochrome is a fluorescent substance that is incorporated in the mineralising parts of bone and teeth due to their calcium-binding properties (Erben, 2003). Once the fluorochrome is administered to the individual, the substance assimilates with the growing tissue, preserving its position (Klevezal, 1996) until the bone matrix is resorbed (Erben, 2003). In vivo labelling with fluorochromes provides important information on growing tissue, providing a calibration of the timing and the quantification of bone formation or remodelling (Erben, 2003; Klevezal, 1996).

Different fluorochromes can be used for the histological study of hard tissues. Alizarin is a plant dye that stains the tissue red. Alizarin red "S" was the first compound to be used in the hard tissue analysis (Schour et al., 1941) and fluoresces in red under blue or UV light (Erben, 2003; Klevezal, 1996). Alizarin complexone, on the other hand, fluoresces in red under green light. This type of alizarin is widely used because of its intense colour and low toxicity (Erben, 2003). In addition to alizarin, fluorescent labelling also relies on fluorochromes that produce other colours. Tetracyclines are antibiotics that bind to calcium ions and exhibit yellow fluorescence in response to excitation with UV light. Xylenol orange is a bone label that expresses orange fluorescence upon excitation with UV or blue light. Other common compounds include fluoresceins, such as green and blue calceins. Calcein green reacts with calcium, resulting in an intense green colour, while calcein blue, as its name indicates, is a blue dye, though it is rarely used due to its rapid fading.

29

Combining fluorochromes allows for multiple sequential labelling that is easily identifiable in hard tissues, as Suzuki & Mathews (1966) first demonstrated.

In previous studies supervised by M. Köhler on the European brown hare, the use of Xylenol orange caused harmful effects on some organs, while calcein blue, as noted above, faded rapidly (Meike Köhler personal comment). For these reasons, the present experiment did not use these fluorochromes. Instead, red deer calves were subcutaneously administered alizarin red and calcein green to obtain a red and green sequential labelling. Markers were prepared under sterile conditions at the pharmacy of the Vetmeduni Vienna and administered between birth and the 23rd week of age on an individual-specific schedule. In some cases, the procedures had to be carried out under anaesthesia (medetomidine; full details in Chapter 5). In those cases, the calves' vital signs were monitored. For euthanasia, animals were anaesthetised using ketamine and medetomidine and subsequently received an overdose of a combination of embutramide, mebezonium and tetracaine (full details in Chapter 5).

3.2.2. Determination of age classes

The degree of epiphyseal fusion and the dental eruption sequence provide information on age stages as well as the occurrence of key life history events (O'Connor, 2000). Epiphyseal fusion can be determined by examining the ossification centres of limb bones. In this way, it is possible to assign the status of "immature" (i.e. active growing stage) or "mature" (i.e. fully grown) to a mammal according to the degree of fusion of the diaphysis with the epiphyses (both proximal and distal) of its long bones. Mariezkurenna (1983) has estimated the age of epiphyseal fusion for several limb bones in red deer. The eruption of teeth (both deciduous and permanent) can also be used for age estimation (Anders et al., 2011; O'Connor, 2000). This approach examines the

degree of the emergence of a dental element from the alveolus of the maxilla or mandible. Azorit et al. (2002) and Brown and Chapman (1991) have described the sequence of dental eruption and replacement for red deer.

In this dissertation, the degree of epiphyseal closure and dental eruption of the red deer specimens were estimated by visual observation. First, the proximal (EP) and distal (ED) epiphyses of 45 long bones (femora and tibiae) were examined. According to their status, bones were assigned one of three different classifications: "unfused" indicated the epiphysis was completely separated; "fusing" indicated the epiphysis was fused with visible suture; and "fused" indicated the epiphysis was completely fused with no visible suture. The next step was to analyse and classify 26 mandibles according to their eruption stage. For that purpose, the degree of eruption of each molar was evaluated and classified as follows: "forming" for molars inside of the alveolus; "erupting" for molars that are not fully erupted; and "erupted" for fully erupted molars. Additionally, the term "complete" was used when all the three molars in the mandible had erupted.

Thereafter, the epiphyseal fusion and dental eruption categories were assigned age stages based on previous studies of this species (Anders et al., 2011; Azorit et al., 2002; Azorit, 2011; Brown and Chapman, 1991; Mariezkurenna, 1983) (Fig. 3.1). The resulting classification was later compared with the age of the semi-wild individuals (i.e. *Cervus elaphus hippelaphus* subspecies; see Chapter 4).
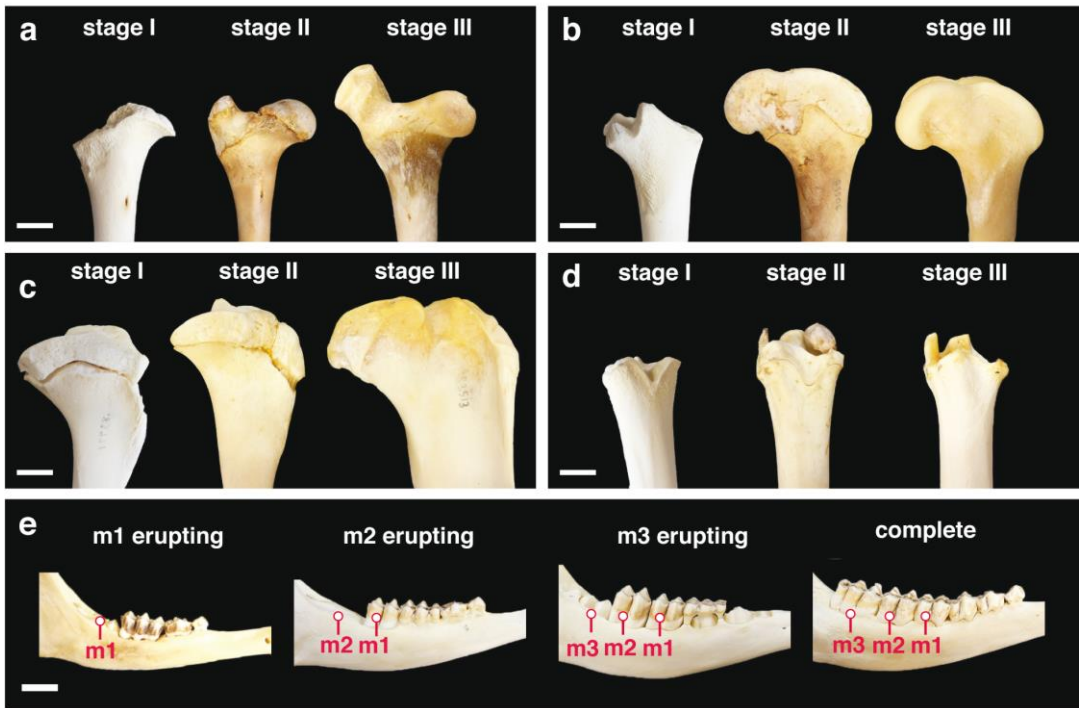
Figure 3.1. Different stages of bone development (a-d) and sequences of dental eruption pattern (e). Stage I: unfused epiphyses of the femur and tibia of the individual IPS-83491. Stage II: fusing epiphyses of the femur and tibia of the individual IPS-83506. Stage III: fused epiphyses of the femur of the individual IPS-60877 and tibia of the individual IPS-83513. (a) proximal region of the femur; (b) distal region of the femur; (c) proximal region of the tibia; (d) distal region of the tibia; (e) sequence of dental eruption pattern in buccal views. From left to right: mandible of the individual IPS-83492 with the first molar erupting; mandible of the individual IPS-60870 with the second molar erupting (still in alveolus); mandible of the individual IPS-60878 with the third molar erupting; mandible of the individual IPS-60877 with a complete dentition. Scale bar: 2cm

3.2.3. **Histological approach**

3.2.3.1. *Preparing the thin sections*

The preparation of thin sections involves a non-reversible alteration of the specimen (Lamm, 2013). With the aim to collect as much information as possible from the specimens prior to the histological preparation, all the material used in this thesis was photographed. Images were taken from the lateral, medial, anterior and posterior sides of each long bone. In addition, specimens were measured with a calliper and a metric tape in order to obtain the following dimensions:

- Maximum length;
- Functional length;
- Diaphyseal length (when epiphyses are not fused);
- Antero-posterior diameter of diaphysis at midshaft;
- Transversal diameter of the diaphysis at midshaft;
- Midshaft perimeter;
- Minimum perimeter;
- Antero-posterior diameter of epiphyses (proximal and distal);
- Transversal diameter of epiphyses (proximal and distal).

Measurements were added to a database file that contained information on the individual's degree of epiphyseal closure, molar eruption stage, sex and age. Subsequently, the preparation of thin sections was carried out following the well-defined laboratory protocol described below.

A chunk of approximately 3 cm from the middle of the diaphysis of each bone (from 1.5 cm above to 1.5 cm below the mid-shaft; Fig. 3.2a) was extracted with a small saw (Micromotor Navfram B120). Once the mid-diaphysis chunks

were obtained (Fig. 3.2b), they were degreased and dehydrated by a 24h immersion in successive alcohol solutions of 70%, 96% and 100%. Afterwards, the chunks were embedded in Araldite 2020 epoxy resin (Fig. 3.2c). Immediately thereafter, blocks were introduced in a vacuum chamber with the aim of eliminating any air bubbles.

After 24–48 hours, the block had solidified and was cut into two halves with a low-speed diamond saw (Fig. 3.2d; IsoMet, Buehler). The cut surfaces (Fig. 3.2e) were polished with a grinder-polishing machine (Fig. 3.2f; MetaServ 250) and fixed to a frosted glass using epoxy resin. Once the sample was fixed, it was cut with a diamond saw (Petrothin, Buehler) to a thickness of 100–120 microns (Fig. 3.2g). The next step consisted of polishing the slides with abrasive papers of decreasing particle size (CarbiMet and MicroCut abrasing paper, Buehler) and performing a final polish using a polishing cloth (MicroCloth, Buehler) in a diamond suspension (MetaDi, Buehler) in a grit-polishing machine (Fig. 3.2h; MetaServ 250). When necessary, samples were covered by a cover glass with DPX to improve the visibility of the section.
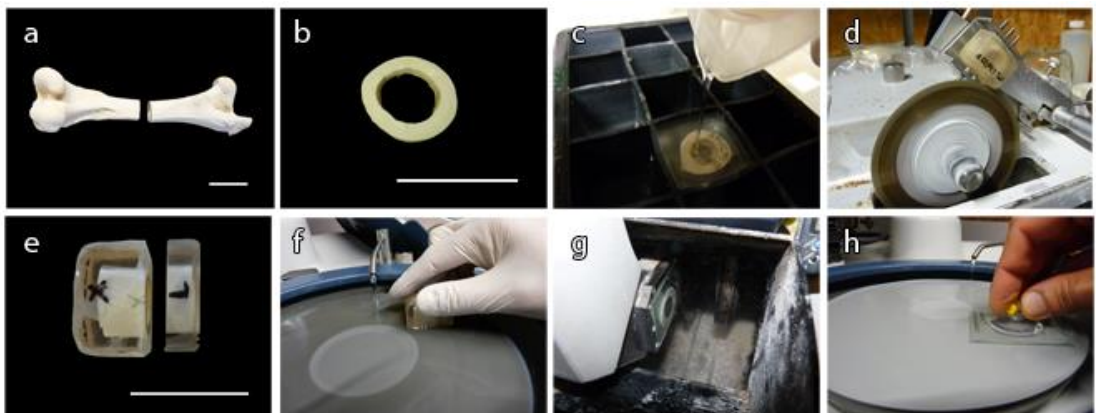
Figure 3.2. Methodology followed to obtain thin sections. (a-b) The midshaft region is extracted from a limb bone.; (c) chunks are embedded in the epoxy resin; (d) the resulting block is cut using a low speed diamond saw; (e) sectioned specimen; (f) the block is polished before fixing it to a frosted glass; (g) a block mounted in a frosted glass is cut; (h) the thin section is polished Scale bar: 5 cm

3.2.3.2. *Microscopic techniques*

The entire postcranial sample was studied under a Zeiss Axioscope A1 microscope located in the microscopic laboratory of the ICP at the Autonomous University of Barcelona.

Transmitted light and polarised microscopy

Transmitted light microscopy has been conventionally used in histological analyses for observing both cranial (Mitchell, 1967) and postcranial samples (de Buffrenil and Mazin, 1990). This kind of microscopy reveals the microscopic structure of the tissue (Fig. 3.3a). Polarizing microscopy, which enhances the contrast and the quality of the image, has also been used in histological analyses. Polarised light microscopes transform the unpolarised light into polarised light by means of two polarised filters that isolate the light vibration in one specific direction (Bromage et al., 2003; Bromage and Werning, 2013). The first filter or polariser is located between the light source and the sample. Thus, the sample receives light only in one direction of vibration. The second polarised filter or analyser is situated between the sample and the observer. Its vibration direction differs 90º from that of the polariser, blocking the light filtered by the polariser in case anisotropic materials are present in the sample. On the contrary, if the sample is composed of birefringent material (i.e. a sample with two refraction indexes), the vibration direction is modified by the sample; the light passes through the analyser and creates an image (Bromage and Werning, 2013). In this way, placing birefringent tissues, such as enamel or collagen fibres within bones, under polarised light creates a high-contrast image and reveals important information about the bone microstructure's arrangement (i.e. the orientation of various components) (Bromage and Werning, 2013).

Fluorescent microscopy

Fluorescence occurs when a substance absorbs light at a given wavelength and emits light at a different wavelength. For a fluorescence analysis, the sample must contain fluorescent compounds. The fluorescent emission of these compounds requires a very powerful light that is provided by a mercury arc lamp. This light is directed to an exciter filter that selects the excitation wavelength that is sent to the sample. At this moment, the sample emits light that is filtered by the barrier filter, indicating the emission wavelength. Finally, the light is converted into an image for visualisation or digitalisation (Fig. 3.3b).
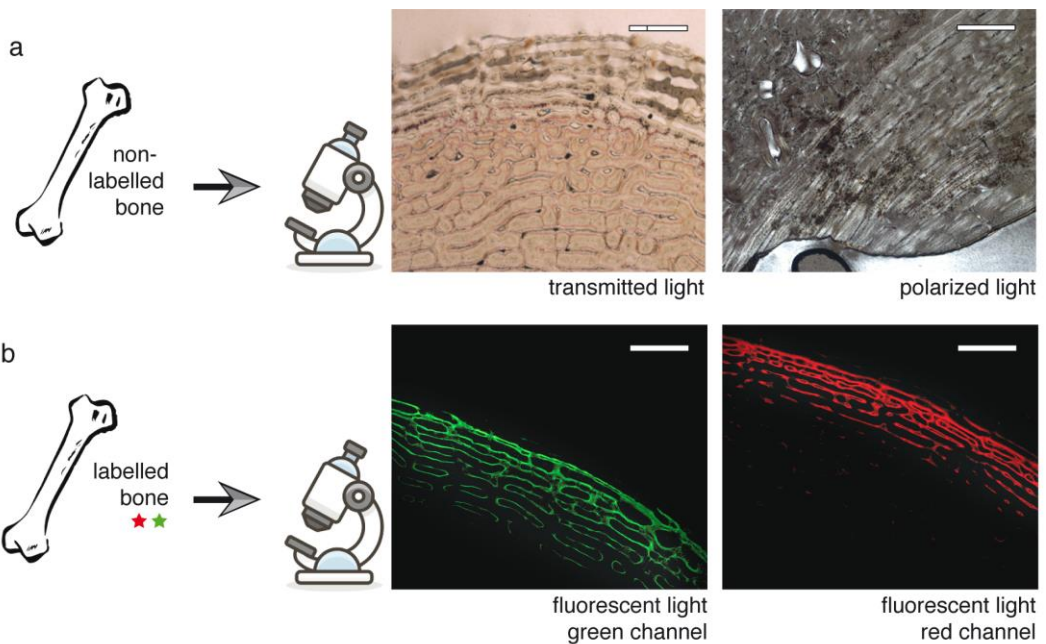
Figure 3.3. Imaging process with the different microscopic techniques employed in this dissertation. (a) Non-labelled bones were analysed under transmitted and polarized light. (b) Labelled bones were analysed under fluorescent light. Images are oriented with the medullary cavity towards the inferior part and outermost cortex towards the superior side. Scale bar: 500μm

In this dissertation, a double sequential labelling of alizarin complexone and calcein green was applied to six individuals of the *C. e. hippelaphus* subspecies following a specific schedule to shed light on the growth dynamics during the first stages of ontogeny. A detailed explanation of the experiment can be found in Chapter 5.

3.2.3.3. *Imaging*

The microscope used in this dissertation was equipped with an integrated camera (AxioCam ICc5), allowing for direct image capture. Images at different resolutions (1.25x, 5x, 10x and 20x) were taken under transmitted, polarised and fluorescent light (only in the case of the labelled samples). Combining the fluorescent and non-fluorescent images indicates the location of the fluorescent labels within the tissue. This combination is achieved by photographing the same area of the sample under the different lights.

The ZEN2011 software (Carl Zeiss) automatic performs this combination, resulting in a combined polarised or transmitted image with green, red or both fluorescent lines (Fig. 3.4.a). If a single image of the entire thin section was required, it was necessary to repeat the previous process along the entire area. Afterwards, images were aligned and composed using Adobe Photoshop CS3 (Fig 3.4.b-c).
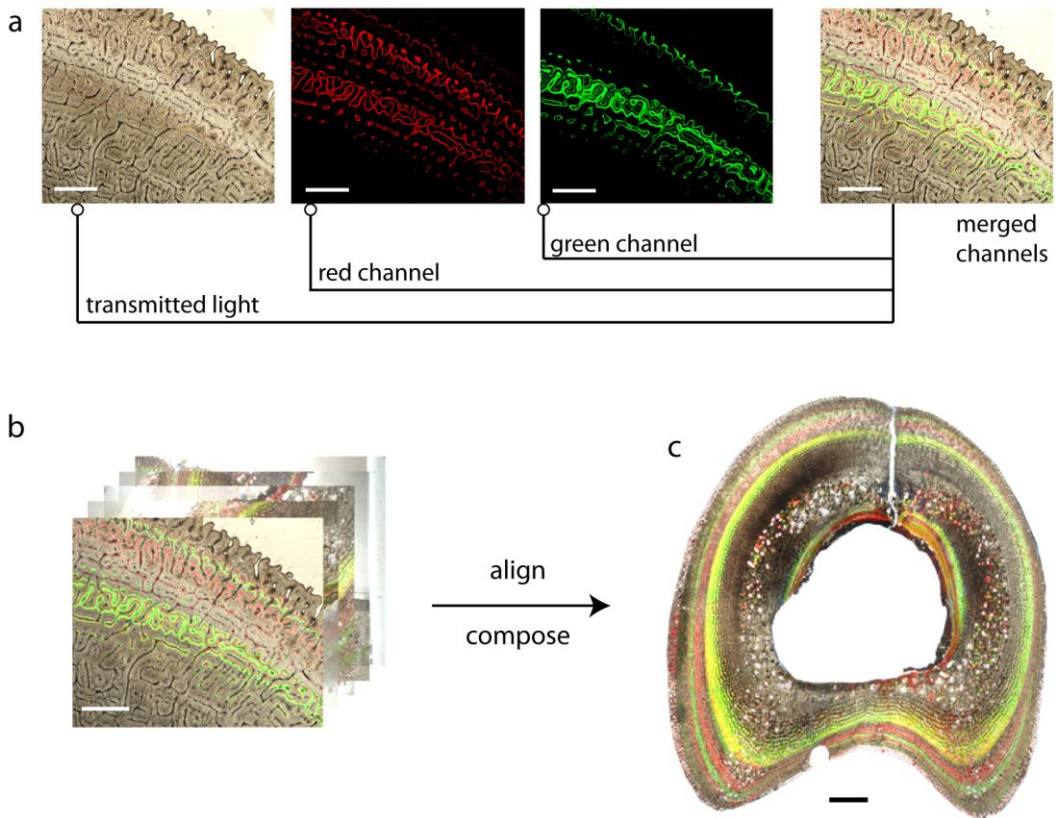
Figure 3.4. Combination and composition of images of the metacarpus (IPS-93664). (a) imaging of bone tissue under merged images of transmitted and fluorescent light. (b) successive imaging of bone cortex; (c) entire cortex composed from single images in (b). Images are oriented with the medullary cavity towards the inferior part and outermost cortex towards the superior side. White scale bar: 500μm. Black scale bar: 2mm.

3.2.3.4. *Bone histology*

Bone histology is a useful tool for reconstructing the life histories of both extant and extinct mammals (Amson et al., 2015; Cubo et al., 2012; García-Martínez et al., 2011; Köhler and Moyà-Solà, 2009; Kolb et al., 2015a; Marín-Moratalla et al., 2013a, 2014; Moncunill-Solé et al., 2016; Nacarino-Meneses et al., 2016b, 2016a; Nacarino-Meneses and Köhler, 2018; Nacarino-Meneses and Orlandi-Oliveras,

2019; Orlandi-Oliveras et al., 2016, 2018). Through bone tissue analyses, important life history traits, such the age at maturity, age at death and growth rate, can be estimated. In this dissertation, the histological analysis of red deer limb bones provided a description and quantitative analysis of two main structures: bone tissue and bone growth marks. Long bones were selected for this study because they preserve the most complete record of growth marks in tetrapods (Padian et al., 2013).

Bone tissue

Bone is a specialised tissue composed of a matrix of organic (mainly collagen) and inorganic (mainly hydroxiapatite) materials (Francillon-Vieillot et al., 1990; Klevezal, 1996). Bone formation or osteogenesis is the process through which osteoblasts deposit an organic matrix followed by the mineralisation of that matrix (Francillon-Vieillot et al., 1990). In addition to osteoblasts, the arrangement of the bone matrix is modulated by osteoclasts and osteocytes.

The first tissue formed early in ontogeny is called primary bone (i.e. bone deposited without bone matrix antecedents; Fig. 3.5a-f; Francillon-Vieillot et al., 1990). It contains primary osteons: vascular canals surrounded by centripetally deposited concentric bone lamellae. According to the arrangement of the collagen fibres within the bone matrix and the vascular canals, primary tissue can be classified into different categories. This dissertation refers to the nomenclature established by de Margerie et al. (2002) to describe the categories of the tissue.

Lamellar bone consists of successive thin layers (lamellae) of closely packed collagen fibres, resulting in a highly organised tissue. This structure appears as a dark and light pattern under cross-polarised light (Francillon-Vieillot et al., 1990; Huttenlocker et al., 2013). Tissue that contains a total

absence of vascular canals is called lamellar non-vascular bone (de Margerie et al., 2002). Tissue can also contain simple vascular canals or primary osteons, resulting in lamellar bone with simple vascular canals or primary osteons, respectively (de Margerie et al., 2002). Lamellar bone has the slowest apposition rates (de Margerie et al., 2002; Huttenlocker et al., 2013).

Parallel-fibered bone, often called pseudo-lamellar bone, consists of a large quantity of closely packed collagen fibrils with a parallel orientation (Francillon-Vieillot et al., 1990; Huttenlocker et al., 2013). Due to this arrangement the tissue is anisotropic under cross-polarised light (Huttenlocker et al., 2013), appearing bright or dark depending on the collagen orientation. As occurs with lamellar bone, parallel-fibered bone can be classified depending on the total absence of vascular canals, the existence of simple vascular canals or the presence of osteons within its matrix (de Margerie et al., 2002). Parallel-fibered bone exhibits a general slow deposition, although it is deposited at faster rates than lamellar bone.

Woven-fibered bone exhibits a highly disorganized pattern of loosely packed collagen fibres (Francillon-Vieillot et al., 1990; Huttenlocker et al., 2013) and contains randomly distributed osteocytes. It appears relatively dark under cross-polarised light due to its isotropic properties (Huttenlocker et al., 2013). The poor spatial organisation reflects the rapid osteogenesis of the tissue (Francillon-Vieillot et al., 1990; Huttenlocker et al., 2013). In fact, woven-fibered bone shows the fastest deposition rates. Additionally, a combined structure of woven-fibered bone and parallel-fibered bone, known as the fibrolamellar complex (FLC), exists (Francillon-Vieillot et al., 1990; Huttenlocker et al., 2013; Prondvai et al., 2014). This structure consists of a woven scaffold that contains primary osteons arranged in different orientations. Depending on the arrangement, the FLC can be classified as laminar (Fig. 3.5a), plexiform (Fig. 3.5b), reticular (Fig. 3.5c), longitudinal (Fig. 3.5d) and radial (Fig. 3.5e). This mixed type of bone can be found in fast-growing young individuals.

The arrangement of the bone matrix can be an indicator of the bone deposition rate due to the relationship between bone growth rate and bone vascularisation (Lee, A. H., Huttenlocker, A. K., Padian, K. & Woodward, 2013). A laminar orientation has the slowest rate of deposition, whereas a radial one has the fastest (de Margerie et al., 2004). In addition to the spatial arrangement of vascular canals, other factors, such as the quantity and size of the canals, also indicate the deposition rate: very porous tissues are formed at high rates, while a low percentage of canals within the bone matrix indicates a slow deposition rate (de Margerie et al., 2002)
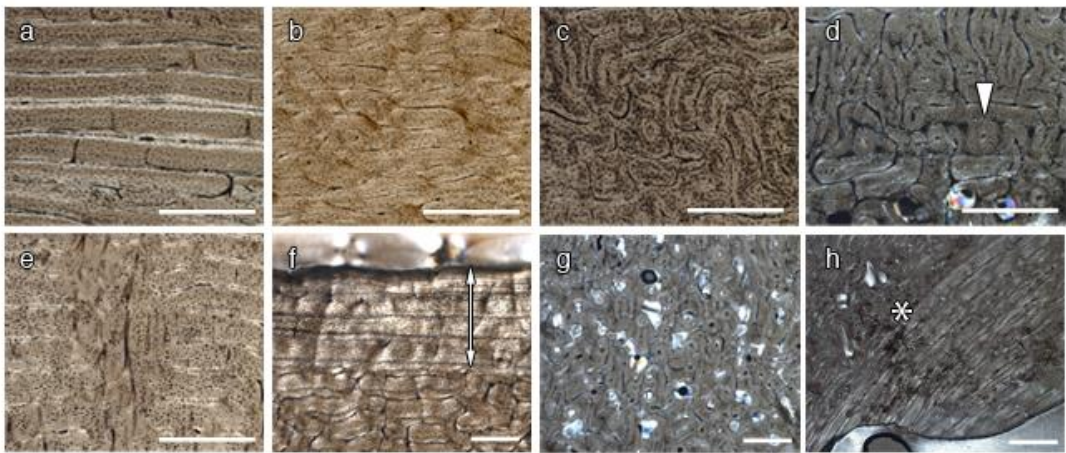
Fig 3.5. Histological detail of bone tissue. (a-f) primary bone; (g-h) secondary bone. (a) laminar; (b) plexiform; (c) reticular; (d) longitudinal (white arrowhead); (e) radial; (f) external fundamental system (EFS; white arrow); (g) Haversian bone. (h) endosteal bone (white asterisk: cementum line). Images are oriented with the medullary cavity towards the inferior part and outermost cortex towards the superior side. Scale bar: 500μm.

Due to the dynamic properties of the bone, primary tissue can undergo remodelling processes: primary bone is resorbed by the action of osteoclasts and subsequently, new tissue is deposited by the action of osteoblasts, forming the secondary bone (Fig. 3.5g-h). This type of bone is typically associated with cementing lines of resorption (Francillon-Vieillot et al., 1990; Klevezal, 1996)

and can be found within the cortex as secondary osteons. When secondary osteons are grouped together, the tissue is known as Haversian bone (Fig. 3.5g). Two of the main factors that can determine the deposition of Haversian tissue in the bone cortex are the restoration of bone tissue and the mechanical stress response (Currey, 2003; Enlow, 1962b). Moreover, secondary bone can also form the endosteal bone, a structure located in the innermost part of the bone, bordering the medullar cavity (Fig. 3.5f; Chinsamy-Turan, 2005; de Buffrénil and Quilhac, 2021; de Margerie et al., 2002; Enlow, 1962b; K. Padian et al., 2013).

In this dissertation, the bone tissue of six limb bones from two deer subspecies was analysed and described in detail. The main purpose was to identify variations in bone formation between limb bones, sex of individuals, subspecies and ontogenetic stages (Chapter 4 and 5). The presence or absence of the EFS in each bone was compared with data on epiphyseal closure and dental eruption as well as with the age of the individual to provide insight into the underlying causes of its formation (Chapter 4).

The labelled specimens were examined with the objective of analysing in-depth bone growth dynamics during the early stages of ontogeny, including the local changes associated with primary and secondary bone deposition, resorption processes and the expansion of the medullar cavity. In addition, the labelling schedule allows placing these growth processes into a specific timeframe. The density of the canals in the tissue was measured before and after two non-cyclical marks. First, an image of the tissue was taken of the area of interest under a 20x lens. Subsequently, the area containing vascular canals was selected by means of the image threshold and measured using ImageJ (Schneider et al., 2012).

Bone growth marks

Bone tissue is not deposited in a continuous manner but undergoes periods of slowdown or even a temporary interruption of bone growth. When this occurs, growth marks, annuli (Fig. 3.6a) and lines of arrested growth (LAGs; Fig. 3.6b) are laid down in the tissue. As a result, the bones of vertebrates show a succession of growth layers (i.e. a band of bone tissue; Klevezal, 1996) separated by these growth marks (Woodward et al., 2013).

Growth marks can be caused by periodical (cyclical) or single (non-cyclical) events (Castanet et al., 1993; Woodward et al., 2013). The presence of cyclical marks within the bone tissue indicates an annual rhythm of growth modulated by seasonal physiology (Köhler et al., 2012), while non-cyclical marks denote the occurrence of single events in an individual's lifetime such as hatching (Hugi and Sánchez-Villagra, 2012), birth (Nacarino-Meneses and Köhler, 2018), or metamorphosis (Sinsch, 2015). Some authors (Castanet et al., 2004; Morris, 1970) have also speculated that the weaning event, common to all mammals, could be recorded as a growth mark in some bones. Non-cyclical marks can also be caused by sudden changes in the direction and rate of deposition (cortical drift; Woodward et al., 2013). In this case, growth marks receive the name of cortical drift lines (CDLs; Woodward et al., 2013).

The cyclical arrangement of the growth marks allows them to function as skeletochronological indicators. It is therefore possible to calculate parameters such as age at maturity or age at death by counting these lines. However, this approach presents some caveats: the dynamic process of resorption and deposition of secondary bone may obscure some of these lines and could consequently lead to underestimates. Another problem is the expansion of the medullar cavity, which erodes the information contained in the inner part of the shaft. Furthermore, closely deposited cyclical lines can make counting difficult.
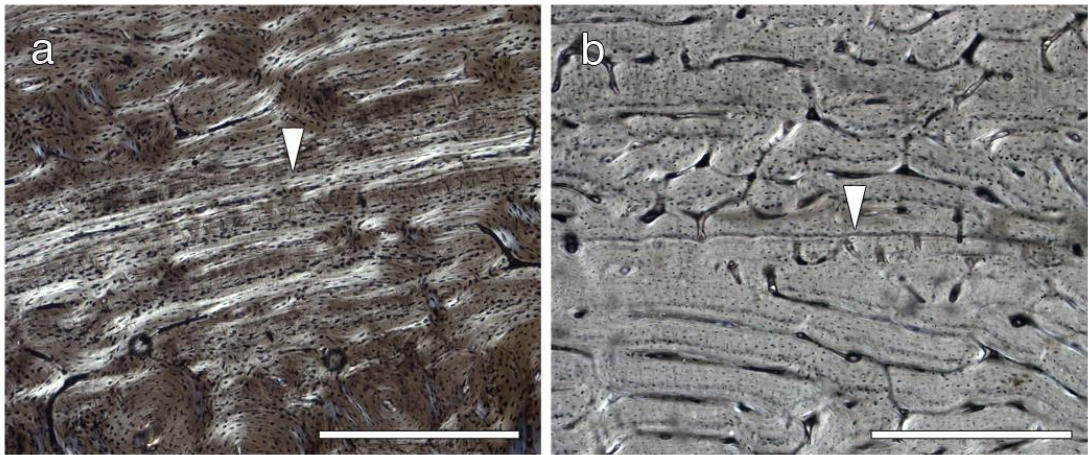
Figure 3.6. Detail of different growth marks within the cortex of limb bones (a) annulus in the anterior part of the humerus (IPS-88713); (b) line of arrested growth in the anterior part of femur (IPS-56308). Images are oriented with the medullary cavity towards the inferior part and outermost cortex towards the superior side. Scale bar: 500μm.

In this dissertation, both types of growth marks, cyclical and non-cyclical, were analysed to obtain age-related information on deer individuals and to shed light on the main events that affect their growth. To do this, a single image of the entire bone cortex was needed, which was obtained by aligning and merging several images using Adobe Photoshop CS3. The total number of cyclical marks within a bone was counted. Then, the number of growth marks was compared between bones from the same individual and assessed according to its known age (when possible). The number of growth marks within the FLC, excluding the lines contained in the EFS, was used for calculating the age at maturity (see Chapter 4). The ontogenetic series of each bone were superimposed to obtain the information lost by the remodelling or expansion of the medullar cavity (see Chapter 8). The presence of non-cyclical marks within the bone during the early stages of ontogeny was assessed with fluorescent labelling (Chapter 5).

Growth marks were also analysed to estimate the growth pattern and calculate tissue deposition rates in each bone. Previous studies on ungulates constructed bone growth curves using the perimeter of the cyclical growth marks (Jordana et al., 2016; Nacarino-Meneses et al., 2016a; Orlandi-Oliveras et al., 2018) or the distance between them (Nacarino-Meneses et al., 2016b) to calculate the amount of tissue deposition. In this dissertation, however, the area of the tissue contained in each of the growth marks was used since area is more related to body mass and consequently provides more reliable results.

The circumferences formed by the growth marks along the bone, were highlighted using Adobe Photoshop CS3 to improve their visibility. Afterwards, using a selection tool in ImageJ 2.0.0 (Schneider et al., 2012), the total area within a growth mark (included the medullary cavity) was calculated. Growth marks located in the inner part of the bone had smaller areas than external growth marks. To calculate the growth rates, the difference between the area of consecutive growth marks was divided by the interval between LAGs. It is important to remark that this interval is shorter than 365 days, as the LAGs themselves represent a period of arrest (Chapter 5). However, as the exact interval of a cyclical LAG is unknown, a three-month interval of growth arrest was assumed here. As a result, the area between growth marks was divided between 270 days (i.e. estimated time of formation of growth zones). Once obtained, areas and rates were plotted against time to calculate growth curves (Chapter 4), designating the first non-cyclical growth mark as time zero due to its correspondence with the birth event (Nacarino-Meneses and Köhler, 2018). As deer are born throughout May and June, the first cyclical growth mark is formed around the age of six months, corresponding to the first winter. Finally, the periosteum circumference correlated with the moment of death in individuals whose age was known.

For labelled individuals, it was possible to reconstruct a detailed growth curve for the first six months by using fluorescent labels as artificial growth

marks. Although other authors used the axial distance between labels to calculate daily bone apposition (Castanet et al., 2000; de Margerie et al., 2004, 2002), the preferred approach here was to use tissue area, as with cyclical growth marks. In this way, areas were obtained following the same procedure described above, while growth rates were calculated by dividing the area between two labels by the exact number of days between label injections. Additionally, the amount of tissue stained with fluorochromes was also quantified for each of the labels. For this purpose, each of the green and red labels was isolated from the shaft composition and converted into single images with Photoshop CS3. Thereafter, the coloured area was measured by using threshold tools in ImageJ 2.0.0 (Schneider et al., 2012) (Chapter 5).

CHAPTER 4. CALIBRATION OF LIFE HISTORY TRAITS WITH EPIPHYSEAL CLOSURE, DENTAL ERUPTION AND BONE HISTOLOGY IN CAPTIVE AND WILD RED DEER

4.1. Introduction

A significant research goal in biological disciplines is to gather information about age at death or estimate some life history patterns from mammalian remains. This approach could provide demographic data such as individual age, sexual and skeletal maturity, or the age structures of extant and fossil populations, and improve our knowledge about their way of life. This information is especially useful in policies of conservation and wildlife management and in the ecological studies of both extant and fossil organisms. However, correlated, age-calibrated anatomical data, which are the basis for correct life-history interpretations, are lacking in all mammalian groups.

The study of epiphyseal closure in limb bones is based on the degree of fusion of diaphyses and epiphyses. In juvenile specimens, epiphyses are unconnected, enabling the growth in length (O'Connor, 2000). As the specimen reaches the adult size, linear growth stops and the epiphyses start to fuse with the diaphysis (Popkin et al., 2012). When completely fused, the limb bone can only increase in width. The closure sequence differs between species. Data exist on some species of cervids such as white-tailed deer (Flinn et al., 2013; Purdue, 1983), fallow deer (Carden and Hayden, 2002) and roe deer (Ruddle, 1997). However, there is a lack of information about this sequence in red deer. It is also possible to estimate the specimen's age by its dental eruption pattern (O'Connor, 2000). Azorit et al. (2002) described the sequence of eruption and

replacement in Spanish red deer (*Cervus elaphus hispanicus*), and Brown and Chapman (1991) for English red deer (*Cervus elaphus elaphus*). Following this method, it is possible to determine the red deer age up to three and a half years. Other studies related with teeth were developed in cervids such the study of dental measurements (Cederlund et al., 1991; Cooper et al., 2013) or dental wear (Azorit, 2011; Veiberg et al., 2007).

The study of cyclical growth marks is also used in age estimations (skeletochronology). These marks are originated by growth alterations. Cementum marks or dental increments have been widely used as age-estimation method in cervids due to its annual periodicity (Azorit et al., 2004; Cederlund et al., 1991; Mitchell, 1967). Cyclical growth marks can also be found in mammalian limb bones (Köhler et al., 2012). This finding is supported by numerous histological studies in several mammalian groups such primates (Castanet et al., 2004; Castanet, 2006), rodents and lagomorphs (García-Martínez et al., 2011; Moncunill-Solé et al., 2016; Orlandi-Oliveras et al., 2016), and ungulates (Jordana et al., 2016; Köhler et al., 2012; Marín-Moratalla et al., 2013b, 2011; Nacarino-Meneses et al., 2016b, 2016a; Orlandi-Oliveras et al., 2018). Bone histology of extinct deer has been recently analysed to obtain data about growth rates and their relation with life history for these fossil forms (Amson et al., 2015; Kolb et al., 2015). However, a study of bone histology in extant deer in order to provide a firm basis for interpretation of fossil deer emerges as essential and has not been performed so far.

In view of this, the aim of this research is to correlate for the first time the data obtained from bone histology with the different techniques commonly used for ageing mammals (epiphyseal closure and dental eruption pattern), and to define a common pattern that describes the timing between these morphological traits and the life history characteristics of wild and captive populations of red deer (*Cervus elaphus*).

While the analysis of a wild population of known individual age could provide important information about the deer life history, monitoring a wild population is a difficult and expensive task, requiring large amounts of time. Results here obtained provide the basis for growth interpretation of deer and can be applied to other groups of hoofed animals.

4.2. Material and Methods

4.2.1. Sample of study

A total of 32 deer specimens of two subspecies (*Cervus elaphus hispanicus* and *Cervus elaphus hippelaphus*) were collected in four populations of different European geographic areas (Table S8.1). We studied individuals of three wild populations (*N* = 1, 8 and 10 specimens) of *C. e. hispanicus* from La Rioja (northern Spain), Badajoz (southwest Spain) and Lleida (northeast Spain), respectively, and of one captive population of *C. e. hippelaphus* (*N* = 13 specimens) from the Wildlife Institute of Vienna (Austria). This latter population was kept in semi-wild conditions in an area of 45 ha with additional fodder supply (pellets) during the winter season. Females gave birth in May-June (only exceptionally later) and they generally had one calf except for female 138-113, which had two calves at the age of seven. Most calves were hand-raised by bottle until their third month of life, coinciding with the time at which calves are able to feed independently in wild populations. For the Austrian red deer, we had very accurate information regarding age, weight, sex and some other important ecological and life history variables (i.e. diet, reproduction, castration in males, date of births for adult females, age at weaning, etc.) (Table 4.1). Specimens from Spanish populations were obtained from wild game. Sex was identified and age was estimated according dental parameters. In Spain, red deer together with wild boar (*Sus scrofa*) are the two wild ungulates most hunted due to its economic significance (Olea and Miguel-

ayanz, 2006). This activity has disrupted the wild condition of the deer, particularly in the Southwestern part of Spain, where the main habitat is the Mediterranean *dehesa*. *Dehesa* managers usually install fences in some hunting reserves, where artificial conditions are maintained and, consequently, deer density is raised (Olea and Miguel-ayanz, 2006). Some specimens of *C.e. hispanicus* here analysed belonged to this region (Badajoz) while two others lived in template forests. It is also important to bear in mind the loss of genetic variability caused by the trophy stalking or the introduction of European deer in some reserves in order to obtain larger trophies (Carranza, 2017), compromising the true wild status of the red deer in Spain.

After cleaning and selecting suitable specimens, we obtained a total number of 30 femora and 15 tibiae for study. We used femora and tibiae because long bones preserve the most complete record of growth marks in tetrapods (Padian et al., 2013). This material is housed at the ICP - Institut Català de Paleontologia Miquel Crusafont, Barcelona (Spain).

4.2.2. Epiphyseal closure and eruption pattern

The degree of fusion of long bone epiphyses and the eruption pattern (in specimens whose mandible was available) were used for estimating age at death. Proximal and distal epiphyses of femora and tibiae were examined and classified into three different categories according to their degree of closure (i.e. unfused [Un] when the epiphyses were completely separated, fusing [Fg] when it was possible to appreciate the suture between epiphyses and diaphysis and fused [Fd] when it was not possible to observe the suture previously mentioned). In the absence of literature specific for red deer, we considered the study of Flinn et al. (2013) on white tailed deer (*Odocoileus virginianus*) to age specimens according their epiphyseal closure. Thus, we established two age groups: <3,5 years when epiphyses are Un or Fg, and ≥3,5 when they are

completely fused (Table 4.1). According to Brown and Chapman (1991), who defined dental age classes from radiographies in red deer, we established 8 age categories that allow classification of erupted teeth disregarding stages (hidden in bone) of root development or resorption, or teeth that are still in their crypts. Thus, we used 7 stages from Brown and Chapman (1991) original classifications and added one additional category (Table 4.2):

0-5 months: First lower molar erupting; 5 months: First lower molar erupted but still unworn (Brown and Chapman, 1991; Fig.1a); 10 months: First lower molar erupted, wear has started; 13 months: Second lower molar erupted but still unworn; 15 months: All lower premolars are mineralizing; 18 months: Second lower molar erupted, wear has started; 27 months: Third lower molar erupted but still unworn; lower premolars are all erupting and will replace the lost deciduous precursors; 38-40 months: All teeth are completely formed and initial wear is observable on all teeth. Beyond this age, it was possible to age individuals from their teeth using the dental wear approach. Anders et al. (2011) established a formula of six IDAS (individual dental age stage) based on the dental wear of different groups of eutherians to distinguish the categories of prenatal, infantile, juvenile, adult, late adult and senile. More specifically, Azorit (2011) recognized four age groups from 4 to 13 years after the complete dental eruption for red deer: 3.0-4.0 years; 4.5-6.5 years; 5.5-8.5 years and 8.5-13.5 years.

With this information, we defined skeletal maturity as the moment at which all epiphyses are completely fused, and all teeth are completely erupted.

ID	Sex group	Year of birth	Year of death	Known age (years)	Weight (kg)	Number of offspring	Age at first birth (years)	Feeding regime
IPS-56303	Female	2006	2011	5	104	3	3	Natural feeding
IPS-56304	Female	2006	2011	5	94.5	2	4	Natural feeding
IPS-74171	Female	1998	2011	13	133	12	3	Hand-raised
IPS-56306	Female	2007	2011	4	95	0	-	Natural feeding
IPS-56307	Female	1998	2011	13	148.5	11	3	Hand-raised
IPS-56308	Male	2011	2011	0.91	56	-	-	Natural feeding
IPS-106838	Male[c]	2011	2016	5	225	-	-	Hand-raised
IPS-106839	Male	2015	2016	1.17	116	-	-	Natural feeding
IPS-106840	Male	2015	2016	1.08	117	-	-	Natural feeding
IPS-106841	Male[c]	2011	2016	5	210	-	-	Hand-raised
IPS-106842	Male	2015	2016	1.25	127	-	-	Natural feeding
IPS-106843	Male	-	2017	-	-	-	-	Natural feeding
IPS-109289	Male	2017	2017	0.58	79	-	-	Natural feeding

Table 4.1. Available data of *C. e. hippelaphus*. See Supporting Information for further information about the entire sample. ID, specimen; kg, kilograms; c, castrated specimens. Table obtained from Calderón et al. (2019).

4.2.3. Histological analysis

After taking the necessary metrics (i.e. maximum length, functional length, length of the diaphysis, antero-posterior diameter, total diameter, minimum perimeter of the diaphysis and antero-posterior and total diameter of both, distal and proximal, epiphyses) for each bone, thin sections of 30 femora and 15 tibiae were prepared following the protocol of the ICP laboratory. A chunk of approximately 3 cm from the middle of the diaphysis was extracted from

each femur (from 1.5 cm above to 1.5 cm below the mid-shaft) and embedded in Araldite 2020 epoxy resin. This block was cut into two halves with a low-speed diamond saw (IsoMet low speed saw, Buehler). The cut surfaces were polished with a MetaServ polishing machine and fixed to a frosted glass using ultraviolet curing epoxy resin. Once the sample was fixed, it was cut with a diamond saw (Petrothin, Buehler) up to a thickness of 100–120 microns and finely polished again to perfect the slide. Finally, sections were covered with DPX to improve the visualization under the microscope.

After preparation, thin sections were studied using a microscope ZEISS Scope A1, with integrated camera, under polarized light in order to analyse the different types of bone tissue and growth marks. Here, we employed the term "bone growth mark" in order to describe a growth line regardless of whether its nature is cyclic and "cyclical growth mark" to describe those that follow a cyclical pattern (Woodward et al., 2013). Afterwards section images were combined in order to reconstruct the mid-shaft surface using Photoshop CS4. We obtained the measurements of area and perimeter of each growth mark using specific software (ImageJ). These data allowed us to calculate the growth rate for each growth zone. Although the annual period of growth arrest is still unknown, here we supposed three months of growth arrest (i.e. ca. 270 days of formation of growth zones), in order to calculate an approximation of the daily bone growth rates for each growth zone. In the case of specimens that showed the NL, it was also possible to calculate the growth rate of the first growth zone. In this case, we calculated the rate considering 135 days of formation. Finally, we compared the obtained results of the different groups of data through statistical analysis (Kruskal-Wallis test).

4.3. Results

4.3.1. Epiphyseal closure, eruption pattern and dental wear

The stage of epiphyseal closure (unfused, fusing and fused) and dental eruption pattern and wear were examined in order to determine the specimen's age (Table 4.2). We detected that the time of epiphyseal closure differs in tibiae and femora, being the distal part of the tibia the first to fuse followed by the proximal part of the femur, the proximal part of the tibia and, finally, the distal part of the femur (i.e. Td>Fp>Tp>Fd) (Table 4.2). We observed different stages of dental eruption in the mandibles. Three females from Lleida showed the earliest eruption stage. The mandible still had the deciduous premolars and the M1 was erupting. On the other hand, 14 specimens possessed their complete dentition, showing the third cusp of the M3 completely erupted and, in some cases, worn. According to the dental wear, we observed the stages from infant to late adult, with no senile deer in our sample.

We also found an association between the stage of fused epiphyses and complete dentition. All fused specimens had a completely erupted dentition, and those with unfused or fusing stages of their epiphyses showed an incomplete dentition, excluding the male IPS-60871 from Lleida. In this male, all teeth had erupted but its epiphyses were still fusing.

| ID | EFS | | Epiphyseal fusion | | Dental eruption | | Dental wear | | Age group |
	Femora	Tibia	Femora (p/d)	Tibia (p/d)	Stage	Estimated age in months	Stage	Estimated age in years	
IPS-56303	Yes	-	Fd/Fd	-	complete	38-40	IDAS 3 (adult)	5.5-8.5	Ad
IPS-56304	Yes	-	Fd/Fd	-	complete	38-40	IDAS 3 (adult)	5.5-8.5	Ad
IPS-74171	Yes	-	Fd/Fd	-	complete	38-40	IDAS 4 (late ad.)	7.5-13.5	Ad
IPS-56306	Yes	-	Fd/Fd	-	complete	38-40	IDAS 3 (adult)	4.5-6.5	Ad
IPS-56307	Yes	-	Fd/Fd	-	complete	38-40	IDAS 4 (late ad.)	7.5-13.5	Ad
IPS-56308	No	-	Un/Un	-	M2 erupting	10	IDAS 2 (juvenile)	<3.5	Juv
IPS-106838	No	No	Fd/Fd	Fd/Fd	complete	38-40	IDAS 3 (adult)	4.5-6.5	Juv-Ad
IPS-106839	No	No	Un/Un	Un/Un	M3 forming	15	IDAS 2 (juvenile)	<3.5	Juv
IPS-106840	No	No	Un/Un	Un/Un	M3 forming	13	IDAS 2 (juvenile)	<3.5	Juv
IPS-106841	No	No	Fd/Fd	Fd/Fd	complete	38-40	IDAS 3 (adult)	4.5-6.5	Juv-Ad
IPS-106842	No	No	Un/Un	Un/Fg	M3 forming	15	IDAS 2 (juvenile)	<3.5	Juv
IPS-106843	Yes	No	Fd/Fd	Fd/Fd	complete	38-40	-	-	Ad
IPS-109289	No	No	Un/Un	Un/Un	M2 erupting	10	IDAS 2 (juvenile)	<3.5	Juv
IPS-60869	Yes	-	Fd/Fd	-	complete	38-40	IDAS 3 (adult)	4.5-6.5	Ad
IPS-60870	No	-	Fg/Fg	-	M3 erupting	18	IDAS 2 (juvenile)	<3.5	Juv
IPS-60871	No	-	Fg/Fg	-	complete	38-40	IDAS 3 (adult)	3.0-4.0	Juv-Ad
IPS-60872	Yes	-	Fd/Fd	-	complete	38-40	IDAS 3 (adult)	3.0-4.0	Ad
IPS-60873	No	-	Fg/Fg	-	M3 erupting	27	IDAS 2 (juvenile)	<3.5	Juv
IPS-60874	Yes	-	Fd/Fd	-	complete	38-40	IDAS 3 (adult)	3.0-4.0	Ad
IPS-60875	Yes	-	Fd/Fd	-	complete	38-40	IDAS 3 (adult)	5.5-8.5	Ad
IPS-60876	No	-	Un/Un	-	M2 erupting	10	IDAS 2 (juvenile)	<3.5	Juv
IPS-60877	Yes	-	Fd/Fd	-	complete	38-40	IDAS 3 (adult)	5.5-8.5	Ad
IPS-60878	No	-	Un/Un	-	M2 erupting	10	IDAS 2 (juvenile)	<3.5	Juv
IPS-83490	-	No	-	Un/Un	M1 erupting	<5	IDAS 1 (infant)	<3.5	Juv

IPS-83491	No	No	Un/Un	Un/Un	M1 erupting	5	IDAS 1 (infant)	<3.5	Juv
IPS-83492	No	No	Un/Un	Un/Fg	M1 erupting	<5	IDAS 1 (infant)	<3.5	Juv
IPS-83503	No	No	Fg/Fg	Fg/Fd	-	-	-	-	Juv-Ad
IPS-83505	No	No	Un/Un	Un/Fg	-	-	-	-	Juv
IPS-83506	No	No	Fg/Fg	Fg/Fg	-	-	-	-	Juv
IPS-83507	No	No	Fg/Un	Un/Fg	-	-	-	-	Juv
IPS-83513	-	No	-	Fd/Fd	-	-	-	-	-
IPS-62075	Yes	-	Fg/Fg	-	-	-	-	-	-

Table 4.2. Information about the stage of epiphyseal closure, stage and estimated age according dental eruption (Brown and Chapman, 1991), stage and estimated age according dental wear (Anders et al., 2011; Azorit, 2011), presence of EFS of subspecies of Cervus elaphus and estimated age group of each specimen. Juv: juvenile; Ad: Adult. Table obtained from Calderón et al. (2019).

4.3.2. Histological analysis

Fast growing tissue interrupted by bone growth marks or annuli was found in every sampled specimen, except for three females (IPS-83490, IPS-83491, IPS-83492), one male (IPS-83506) from Lleida and one male (IPS-109289) from Vienna, which did not show any growth interruption (Table S8.2). The tissue consisted of fibro lamellar complex (FLC) with different vascular orientations depending on the bone and the location within it. Bone growth marks were often surrounded by slow growing tissue, indicating the decline and increase in growth rate before and after the growth hiatus respectively. The specimen from Vienna previously mentioned shows this tissue change in the anterior part of its periosteum both in femur and tibia. In this part, the disorganized woven-fibered bone shifts to a more organized tissue (parallel-fibered bone), indicating the slowdown in growth. The full data set about this specimen (Table 4.1) allow us to identify that the decrease in growth rate occurred shortly

before its death. This coincides with the beginning of the winter season and, hence, it represents the first cyclical growth mark of the specimen.
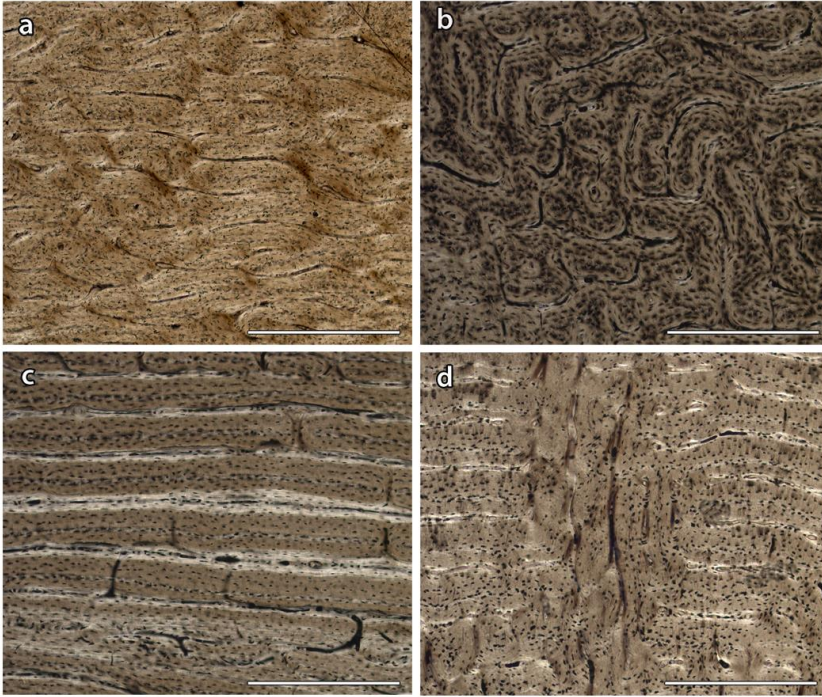
Figure 4.1. Long bones histology of *Cervus elaphus*. (a) Plexiform bone in the femur of an adult male (IPS-60877). (b) Reticular bone in the femur of a juvenile female (IPS-83490). (c) Laminar bone in the femur of an adult male (IPS-83513). (d) Radial canals present in the tibia of a juvenile male (IPS-83508). Scale bar: 500μm. Figure obtained from Calderón et al. (2019).

In the cortex of the 29 femora, we found plexiform orientation (Fig. 4.1a) with small areas of reticular vascularity mainly in the medial part near the medullar cavity and in disperse zones (Fig. 4.1b), which is indicative of the presence of biomechanical forces acting on the bone shaft (Francillon-Vieillot

et al., 1990). However, in the cortex of 9 of the 15 tibiae prevailed a laminar orientation (Fig. 4.1c). Some specimens also showed in their tibiae radial orientation of vascular canals in their very first bone growth mark (Fig. 4.1d), which indicates very fast deposition of bone (Francillon-Vieillot et al., 1990). Secondary bone (high density of secondary osteons) due to remodelling processes was present in the region of the linea aspera of each femur. As the age increases, secondary bone expands radially into the cortex from the inner region to the external cortex of femora and tibiae. Two 13 years old specimens (IPS-74171 and IPS-56307) also showed secondary osteons in the outermost cortex. Moreover, in 12 of them, there was a somewhat broad band in the periosteal zone of the femora forming the EFS, an edge of slow growing tissue without vascularisation formed by parallel fibered bone (i.e. lamellar non-vascular bone, LNV). In contrast, none of the tibiae showed EFS in its outermost cortex (Table 4.2). All specimens with EFS shared the feature of having complete dentition and fused epiphyses (Fig. 4.2). But, in the female IPS-62075 and the males IPS-60871, IPS-106838, IPS-106841, these features were not shown together (Table 4.2).

We considered a single bone growth mark as the circumferential structure formed by one or several well-defined lines which are situated very close together and which can be followed over the surface of the cortical slide (Huttenlocker et al., 2013). Our results demonstrate that bone growth marks are recorded in both periosteal bone types, the FLC and the EFS. In the bone cortex of specimens that showed EFS it was possible to count a constant of 4 bone growth marks within the FLC in the case of the females and 5 in the case of the males of both subspecies, with the last bone growth mark forming the border between the FLC and the EFS. Ontogenetic series of femora were reconstructed for each population by superimposition of histological slides to account for lost growth marks (Woodward et al., 2013). This allowed us to find bone growth marks that are partially erased by expansion of the medullary

cavity in three females of *C. e. hippelaphus* (IPS-74171, IPS-56306, IPS-56307) (Fig. S8.1; Table S8.2). In most of the analysed bones, the first bone growth mark was discontinuous and interrupted by growing tissue, or it changed into an annulus instead of a well-defined bone growth mark. Moreover, we found a sudden change of tissue in the inner region of most of the tibiae analysed and in the femora of IPS-56308, IPS-106840, IPS-83491, IPS-83505, IPS-83506 and IPS-83507.
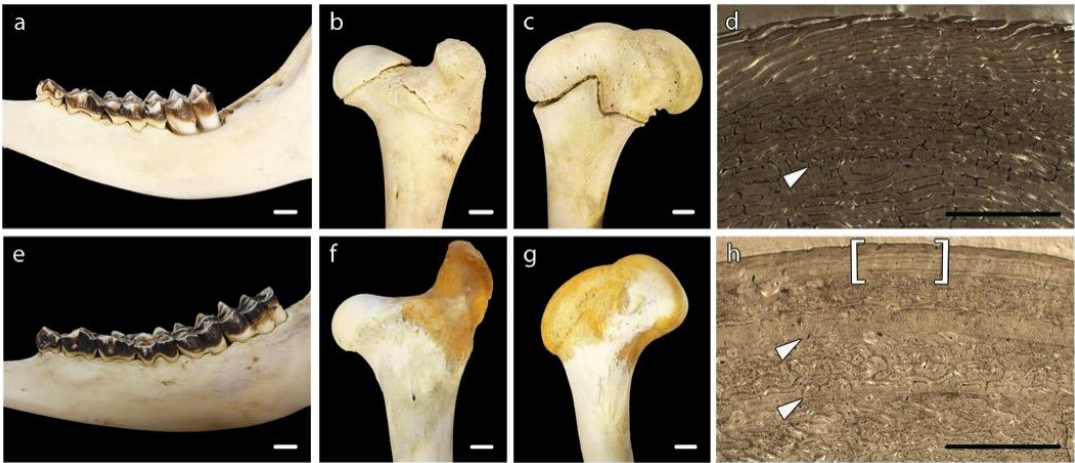
Figure 4.2. Dental eruption (a, e), stage of epiphyseal closure at the proximal (b, f) and distal region (c, g) and anterior cortex of femora (d, h) of a juvenile male (IPS-56308) (a, d) and an adult female (IPS-56304) (e, h). White arrow indicates the presence of EFS. White scale bar: 1cm. Black scale bar: 500μm. Figure obtained from Calderón et al. (2019).

4.3.3. Growth curves

We plotted the growth curves using accumulative growth zone areas of femur (Fig. 4.3a) and tibia (Fig. 4.3b) (i.e. active bone deposition between two bone growth marks). We used area instead of perimeter as a variable because it is more related with body mass and, hence, it better reflects the ontogenetic stages. Growth follows a sigmoidal curve, showing a section of linear fast growth and another of asymptotic or slow growth. In both subspecies, females reached the inflection point at an earlier age than males (third and fourth bone growth mark, respectively).

Mean growth areas of femora for *C. e. hispanicus* and *C. e. hippelaphus* were 270,71 mm^2 and 421 mm^2, respectively, during the first year of growth, and 58.38 mm^2 and 81.90 mm^2 in the last year before the formation of EFS (Fig. 4.3c). Regarding total growth zone areas of femora, significant differences (p = 0,013) were found between subspecies but no between sexes (p = 0,0924). In the case of the tibiae, significant differences were not found between subspecies neither in total growth areas (p = 0,617) nor in single areas. We calculated the growth rates for each growth zone both for tibia and femur using bone growth areas, instead of distance between bone growth marks (Jordana et al., 2016; Kolb et al., 2015b; Marín-Moratalla et al., 2014, 2013b). It is important to highlight that the specimens from Lleida exhibited a different growth pattern than the other two populations, both in femora (Fig. 4.3a) and tibiae (Fig. 4.3b). With increasing age, growth rates in the femora suffered an abrupt decrease, being very low the year before the formation of the EFS (Fig. 4.3c-1). By contrast, growth rates in the tibiae suffered a strong decline during the first year of growth (from 2.216 mm^2/day to 0.344 mm^2/day); after that, bone growth occurred slowly and continuously (Fig. 4.3c-2).

a

C. e. hispanicus
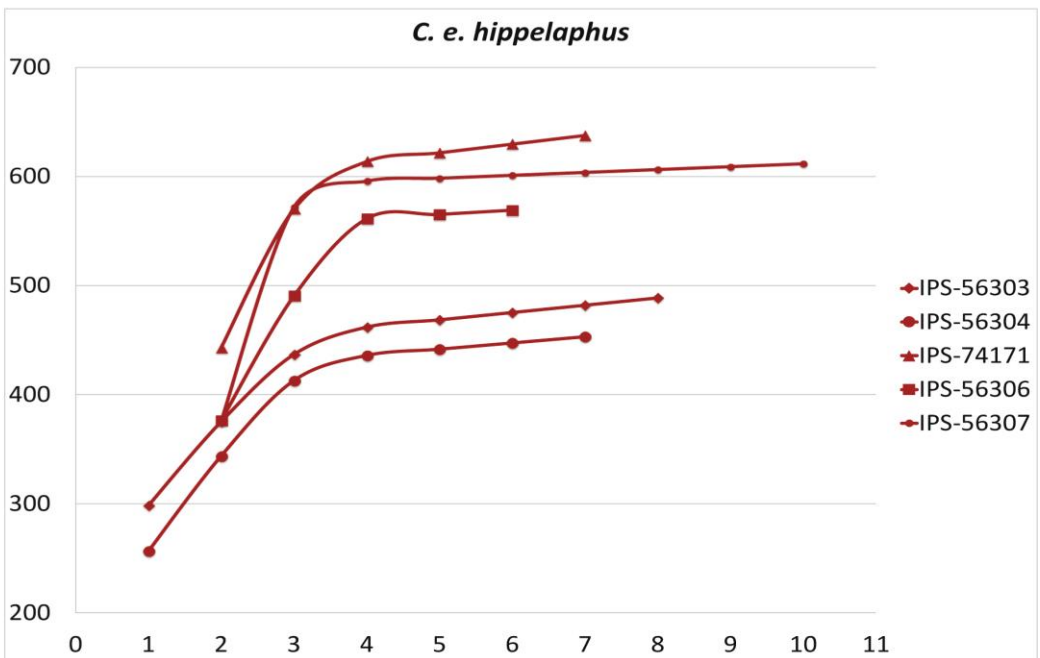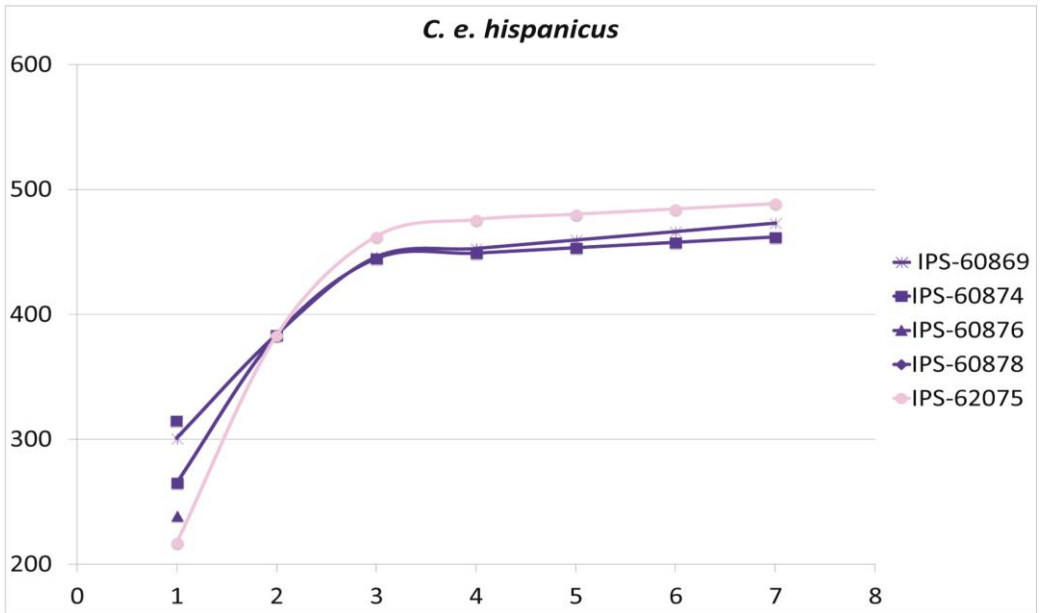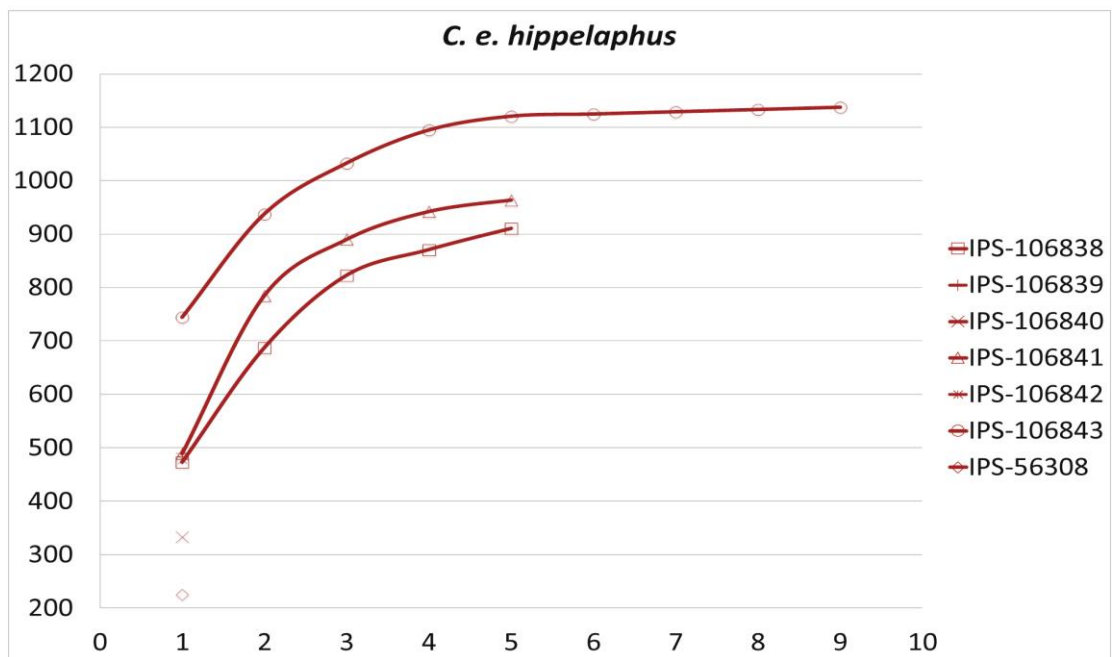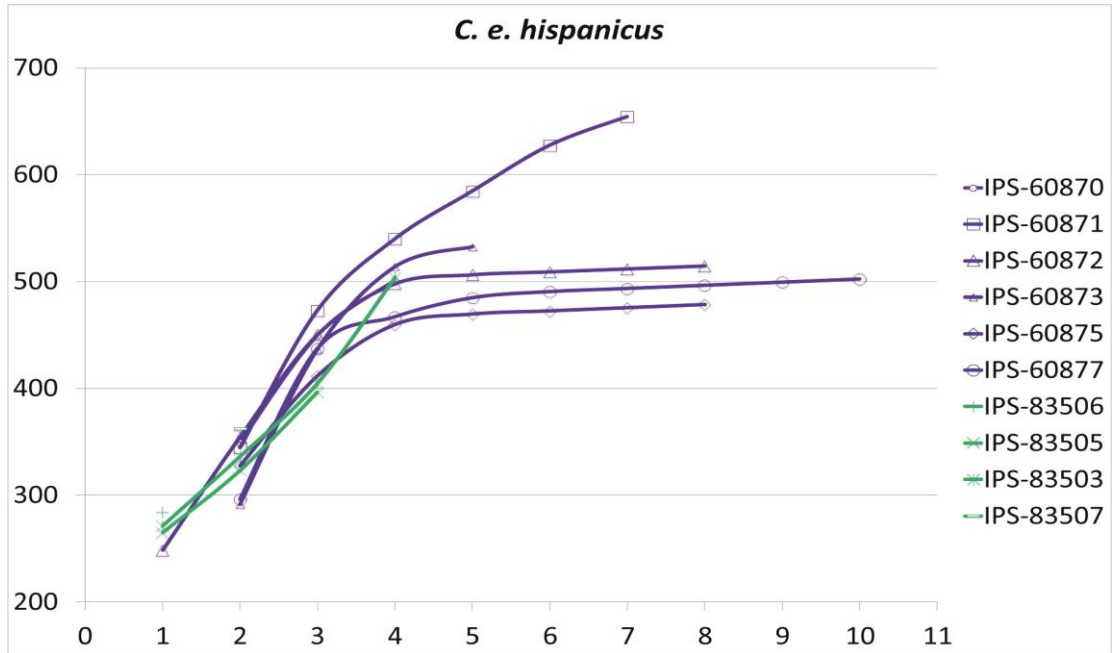
C. e. hippelaphus

b
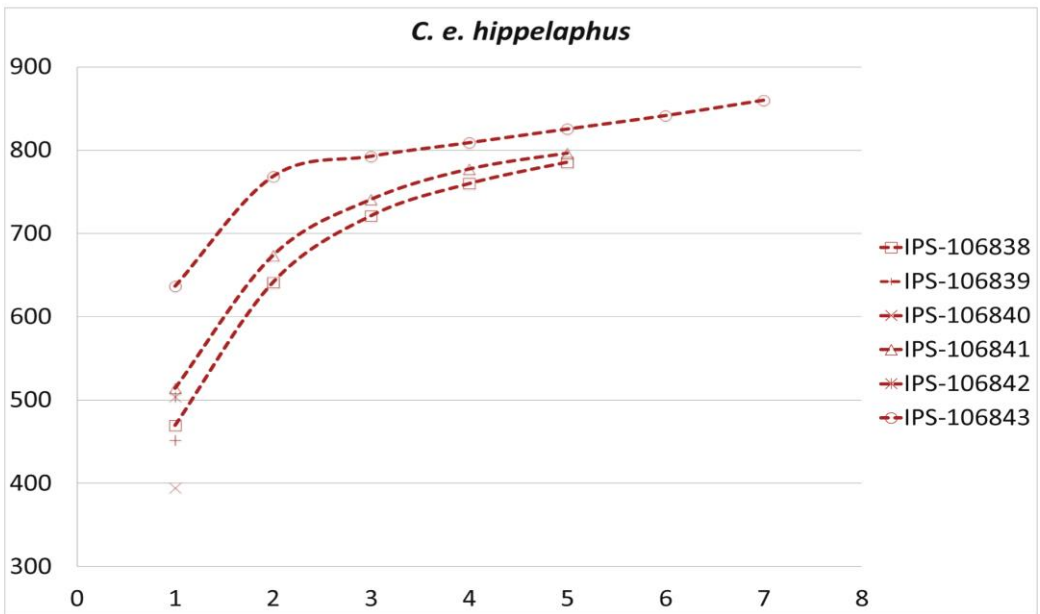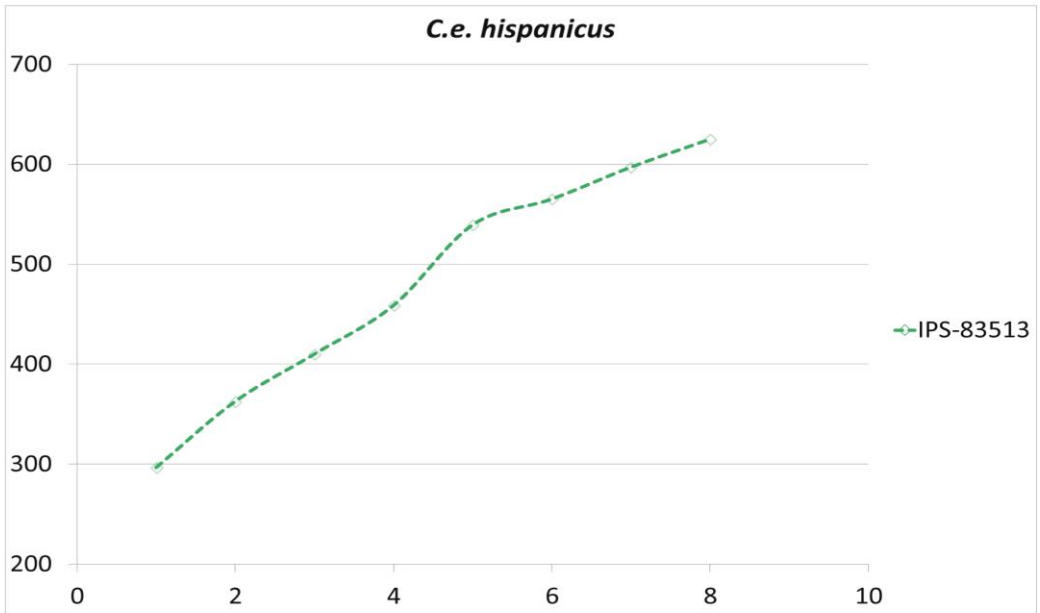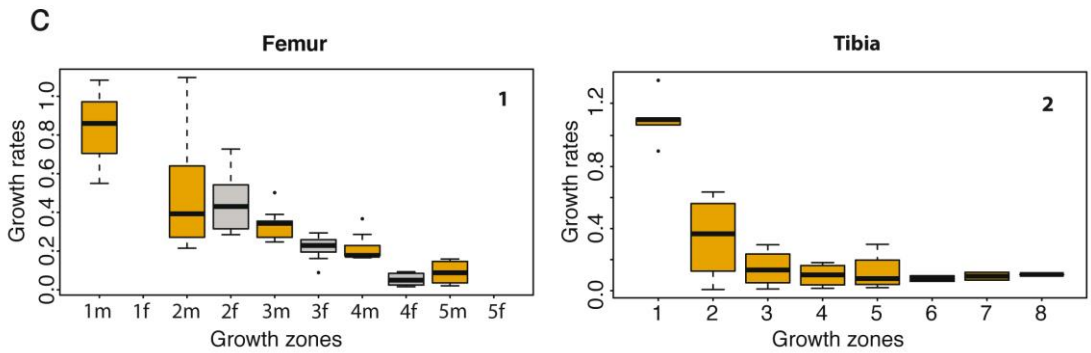
Figure 4.3. Representation of growth curves and growth rates of subspecies of *Cervus elaphus*. (a) Growth curves based on growth zone areas represented in mm² of femora for *C. e. hispanicus* and *C. e. hippelaphus*. (b) Growth curves based on growth zone areas of tibia for *Cervus elaphus*. Filled symbols represent female specimens, unfilled symbols represent males. Purple lines: Spanish deer population from Badajoz. Green lines: Spanish deer population from Lleida. Pink line: Spanish deer population from La Rioja. Maroon lines: Austrian deer population (c) Growth rates represented in mm2/day for each growth zone of sampled femora (1) and tibia (2). Orange boxes: males sample. Grey boxes: Females sample. m: growth zone of males. f: growth zone of females. Figure modified from Calderón et al. (2019).

4.4. Discussion

Data here obtained allow for the first time the calibration of eruption pattern and epiphyseal closure with bone histology and key life history traits (age at skeletal and reproductive maturity) in two subspecies of extant *Cervus elaphus*.

Summarizing the results, femora and tibiae of the individuals of our red deer populations showed the same number of annual marks in their FLC, with the exception of one adult male of *C. e. hippelaphus*, where the femora had less bone growth marks within the FLC than the tibia. Hence, both long bones

appear to be equally useful for skeletochronology. The analysis of dental eruption pattern and epiphyseal fusion allowed us to establish different age categories for both deer subspecies.

4.4.1. Ageing

Deposition of zonal bone is triggered by photoperiod (Castanet et al., 2004) and seasonal environmental cycles of resource availability (Köhler et al., 2012), recording seasonal physiological cycles of hypometabolism during the unfavourable season (i.e. winter) (Köhler et al. 2012). The total number of bone growth marks from the FLC and the EFS are expected to provide the age at death of the individual. This has been claimed to be true for ruminants in a study based on femora of wild individuals of unknown age (Jordana et al., 2016), but has been shown to be not fully reliable in equids with known age (Nacarino-Meneses et al., 2016b). Here, we discuss the results of our approach for the red deer.

4.4.1.1. Material of known age

Our aged material from the Vienna enclosure belongs to some but not all possible age categories, lacking animals of ages between 1-3 years and 7-13 years. The analysis of the *C. e. hippelaphus* population confirms that the total number of bone growth marks is not as reliable for deer as expected from previous publications (Jordana et al., 2016). The provided data about the age of these deer show that the number of bone growth marks present in tibiae corresponds to the known age. In the case of the femora, however, the number of bone growth marks only corresponds to the age before the deposition of EFS. When EFS is present, some individuals show more bone growth marks than

expected from their age, indicating that after attainment of skeletal maturity growth does not only slow down but it also ceases more frequently than before. On the other hand, there appears to be an age at which no further bone growth marks are deposited in the femur, leading to a lower final number of bone growth marks, as occur in the oldest individuals. This agrees with previous findings by Castanet et al. (2004) for the small primate *Microcebus*, and suggests that growth ceases definitely a few years after attainment of reproductive maturity.

Epiphyseal closure stages match the age, being females as reliable as males. Dental eruption stages also correspond precisely to the age up to 3.5 years. After this age, we only can age individuals by means of the analysis of their dental wear. Age classes and dental wear stages correspond to the age from the youngest (0-6 months) to the oldest specimen (13 years). Our findings determined that the specimens with all epiphyses unfused are younger than 1.5 years. Though a delayed epiphyseal fusion has been described in castrated specimens of sheep (Davis, 2000), we did not find variation in the maturation time of the skeletal elements of the castrated specimens.

4.4.1.2. *Material of unknown age*

We estimated the age for the specimens of *C. e. hispanicus* considering cyclical growth marks only within the FLC (Table 4.2). The Spanish sample is broader than that from Austria and contains a wide variety of age categories between 0.5-8 (estimated) years. As occurs with the *C. e. hippelaphus* sample, the dental eruption and epiphyseal closure stages agree, with a few exceptions, with the age estimated from histological analyses in both in males and females.

Although most of the data from our sample supports that femur and tibia are equally useful for skeletochronology, there are some important

remarks to mention here. The tibiae of two adult males of the *C. e. hispanicus* (IPS-83513) and *C. e. hippelaphus* (IPS-106843) populations, showed 8 and 7 cyclical growth marks within the FLC and were still lacking the EFS, while the maximum number of cyclical growth marks within the FLC of the femora was five. This variation between the number of cyclical growth marks found in long bones, as well as the absence of EFS in the tibia agrees with findings in equids (Nacarino-Meneses et al., 2016a). This can be explained by the low and fairly continuous growth rate of bone deposition in tibiae. This bone takes more years than the femur until radial growth rate decreases, leading to more cyclical growth marks than expected in the FLC.

Since births in red deer take place in summer (May-July in *C. e. hippelaphus* from the Wildlife Institute Vienna), fawns show their first cyclical growth mark at ca. 6 months coinciding with their first winter season. In our specimens, this first winter cyclical growth mark appears either faint or as an annulus as a consequence of the rapid growth of deer calves (Woodward et al., 2013). Considering this, the change of tissue detected in the innermost cortex of some specimens could represent the moment of birth (i.e. the neonatal line, NL), as Nacarino-Meneses & Köhler (2018) describe in their study of *Equus*. Specimens younger than 6 months showed this shift in the central part of the cortex, which supports its non-cyclical origin. The change of tissue, both in femora and tibiae, often accompanied by radial canals, could be produced by the beginning of locomotion and weight bearing in new-borns (Nacarino-Meneses and Köhler, 2018).

4.4.2. Attainment of skeletal and reproductive maturity

The effects of the attainment of skeletal or reproductive maturity on the bone cortex are still controversial. Some researchers assume that the formation of the EFS is correlated with the attainment of sexual maturity or with first

reproduction in ungulates (Jordana et al., 2016; Marín-Moratalla et al., 2014; Nacarino-Meneses et al., 2016a). On the other hand, some authors circumvent this problem relating the EFS with the attainment of skeletal maturity both in extant and extinct groups (Martinez-Maza et al. 2014; Amson et al., 2015; Kolb et al., 2015). Here, we demonstrate for the first time the strong correlation between the presence of EFS, complete dental eruption and epiphyseal fusion of long bones of known age specimens and corroborate the presence of an EFS in femora as indicator of skeletal maturity in red deer.

The moment of deposition of the EFS is reflected in the growth curves as an asymptotic slowdown of the growth (Fig. 4.3a). We calculated the age at which specimens reach the skeletal maturity by counting the cyclical growth marks within the FLC before the EFS formation (Chinsamy-Turan, 2005): Females attain skeletal maturity prior to males (shortly after 3.5 and 4.5 years, respectively), which is more than one year earlier than estimations by Jordana et al. (2016) who estimated ages of 5 and 6 years respectively. The difference between female and male reveals how important is the sex factor in this life history trait. The early cessation of growth in females has also been shown in other deer species such as White-tailed deer (Flinn et al., 2013) and Fallow deer (Carden and Hayden, 2002). The different investment in body size between sexes is attributable to the extended period males keep growing in order to attain dominance in intraspecific competition, while females invest in reproduction (Flinn et al., 2013).

The absence of EFS in the castrated specimens could be conditioned by the fact that their age (five years) is comprised within the threshold of EFS formation in males. Further studies are needed to establish the effects of castration on the formation of EFSs.

According to data gathered from the captive population, we strongly affirm that reproductive maturity in females of *C. e. hippelaphus* is reached at the age of 3 years because most of the females gave birth to their first calf at this age. There are no data about birth dates in Iberian deer but, according to the literature, *C. e. hispanicus* females can give birth as early as the age of two years (Carranza, 2017). First reproduction in males occurs later than in females, at the age of 5-7 years (Clutton-Brock et al., 1983; Ibler and Fischer, 2016). This phenomenon of bimaturism, the different onset of maturity between sexes, is typically found in polygynous species such as various species of hoofed mammals and some primates (Stearns, 1992). With these results, we conclude that, in deer, reproductive maturity precedes the attainment of skeletal maturity (Lee, A. H., Huttenlocker, A. K., Padian, K. & Woodward, 2013).

4.4.3. How fast do deer bones grow?

Dissimilarities found in the growth of subspecies might be due to *1*) genetics, as *C. e. hispanicus* is one of the smallest subspecies of *Cervus elaphus* (Garde et al., 2010); *2*) life conditions, because specimens of *C. e. hippelaphus* were bred in captivity while *C. e. hispanicus* were born in the wild; and *3*) environmental conditions, as the populations belong to different geographical regions with variable climatic conditions.

Biological differences between subspecies are based on the genetic differentiation of *C. e. hispanicus* due to the isolation of the territory by the Pyrenees (Garde et al., 2010). Genetic studies (Skog et al., 2009b; Zachos and Hartl, 2011) support the existence of different lineages (Iberian for *C. e. hispanicus* and Balkan/Carpathian for *C. e. hippelaphus*) belonging to different glacial refuges.

The captive population receives proper veterinary care and has better

food availability and quality than the wild populations of Spain, which could lead to differences in growth rates (Dmitriew, 2011). Notwithstanding, it is difficult to attribute these variations to the captive conditions due to the absence of samples of wild specimens of the same location with which these could be compared, and to the non-constant variability of other attributes like genetics or environmental conditions (Turner et al., 2016). Moreover, the possible semi-wild conditions of some *C. e. hispanicus* populations make difficult to establish clear differences. Both subspecies belong to different geographical regions with different climatic conditions and resource availability, which implies body size variations according to Bergmann's Rule (McNab, 2010; Rosvold et al., 2014). Accordingly, the environmental factor could be also an element that affects body size.

Growth variations between *C. e. hispanicus* populations of Badajoz and Lleida could be attributed to their belonging to different lineages (Carranza et al., 2016). But it is also possible that their different habitat and management cause variations in growth. Faster growth rates of specimens from Badajoz could be triggered by their development in *dehesas* or Mediterranean forests and its possible food support due to the hunting management in order to guarantee the deer population (Olea and Miguel-ayanz, 2006). On the other hand, specimens from Lleida lived in a temperate forest of a rather native environment, where low nutrition conditions, common in hard seasons, could cause slower growth rates (Popkin et al., 2012).

4.4.4. Growth caveats

The wide variety of growth patterns within the *C. e. hippelaphus* population could be attributed to the captivity regime maintained in the Wildlife Research Institute of Vienna for several generations. This is supported, for instance, by

studies of captive populations (Trut, 1999) in which morphological and body size variations are described to evolve within few generations of foxes.

4.5. Conclusions

An understanding of the life cycle of extant deer clarifies the relationship between their bone growth patterns and their life history events. The formation of the EFS in femora occurs at the same time as the epiphyseal fusion of proximal and distal femur and tibia and the complete eruption of the dentition, showing the attainment of the skeletal maturity. It is also possible to find some differences at histological level between sexes, with females attaining skeletal maturity earlier than males. Finally, we conclude that reproductive maturity, in deer, occurs slightly before skeletal maturity.

CHAPTER 5: LABELLING EXPERIMENTS IN RED DEER PROVIDE A GENERAL MODEL FOR EARLY BONE GROWTH DYNAMICS IN RUMINANTS

5.1. Introduction

Growth rate is a fundamental variable of an individual's life history (Dmitriew, 2011; Gotthard et al., 1994; Pontier et al., 1989) as it plays a major role in the timing of onset and offset as well as in the duration of life history events. In mammals, growth rate is particularly high early in life when the individual is under time constraints to attain a minimum weight and size for reproduction (Arendt, 1997), and it decreases after maturity when the animal ages (Gaillard et al., 1997). The rate at which an individual grows depends on both intrinsic (e.g. genetics, age, disease; Brown et al., 2004; Gillooly et al., 2002) and extrinsic factors (e.g. cyclical and non-cyclical changes in resource availability and thermal conditions; Roff, 1992; Stearns, 1992).

Life history events like birth and weaning fall within the category of non-cyclical episodes that potentially affect growth rate temporally via resource bottlenecks (transitions in the nutritional environment accompanied by modifications in energy metabolism). This is especially the case for early life history events which are characterised by profound changes in source and type of nutrients obtained during the period of maximum growth, i.e. a change from placental nutrient supply (glucose, amino acids and lactate) to maternal milk (high fat - low carbohydrate diet), and subsequently a change from milk to autonomous feeding (in herbivores typically low fat-high carbohydrate) (Ferré et al., 1986). Later life history events like sexual maturity, reproductive cycles, or onset of senescence involve changes in the allocation of acquired resources

to reproduction and maintenance (Gadgil and Bossert, 1970).

A widely used approach to identify and evaluate changes in growth rate is bone histology (Lee, A. H., Huttenlocker, A. K., Padian, K. & Woodward, 2013). One of the methods is the analysis of bone tissue types (Amprino, 1947). Times of decrease in resource availability or increase in energetic requirements are identified by bone growth marks leaving lines of arrested growth (LAGs) when growth stops, annuli (bands of slow growth) when growth is almost residual, or transitions from fast to slower growing tissue when growth rate is more or less reduced. Growth marks are either cyclical reflecting seasonal changes in growth rate, or non-cyclical supposed to be caused by life history events, unusual periods of resource constraints, or illness. Non-cyclical growth marks have been convincingly attributed to birth (neonatal line; Nacarino-Meneses and Köhler, 2018), or weaning in skeletochronological studies, where such "extra lines" have been found ("weaning line" by Morris (1970); "discordance" by Castanet et al. (2004); "adhesion line" by Klevezal & Kleinenberg (1967); "dark band" by Barker et al. (2003)). However, experimental confirmation that these non-cyclical growth marks are indeed due to the supposed early life history events is a still pending matter, particularly for weaning.

A further issue that needs to be addressed is how much time is compressed within a LAG or an annulus. A method frequently applied in skeletochronology to study this is, for instance, to divide the space between cyclical LAGs by the days of a year, and use this daily growth distance as a measure for estimating the number of days elapsed for forming a particular growth rate (Amson et al., 2015; Kolb et al., 2015a). However, this approach is false whenever growth marks produced by growth arrest imply periods of complete halt when no change in space is formed over time.

In vivo fluorochrome labelling is currently the most precise method to

gain insight into bone growth dynamics, to assess the timing (onset and offset) of growth mark formation (LAGs, annuli, resorption lines), and to reliably calibrate life history events with variations in growth rate and their corresponding growth marks. Nevertheless, labelling is a costly and time-consuming technique and therefore rarely applied. Fluorochrome labelling has previously been used to test the validity of skeletochronological methods in mandibles of small carnivores (Buffrénil and Pascal, 1984) and long bones of primates (Castanet et al., 2004), to understand the relationship between growth rate and bone tissue type in chicks of different bird species (Castanet et al., 2000; de Margerie et al., 2004, 2002; Starck and Chinsamy, 2002), to evaluate the pattern of bone remodelling in small mammals (Montoya-Sanhueza et al., 2021), to assess periodicities of regular incremental markings (Kierdorf et al., 2013; Smith, 2006; Witzel et al., 2018) and variation of apposition rates (Kahle et al., 2018) in dental tissue and for standardisation of procedures and other technical aspects of labelling (Shim, 2016; van Gaalen et al., 2010). Bone labelling, however, has never been used to calculate the time at which possible sequels of early life history events form in bone tissue or to estimate the time span enclosed in a growth mark (LAG or annulus).

Here we used in vivo labelling to analyse the impact of life history events on bone tissue formation and to reconstruct early growth rate in a long-lived mammal, the red deer. We sampled an ontogenetic series of six red deer calves to obtain a tissue sequence that enables the detection of early events, reflected initially in bone tissue, but eroding at later ages by expansion of the medullary cavity. In this way, we describe how birth and weaning events affect growth in general (i.e. daily weight gain; DWG) and bone growth in particular (tissue apposition, drift and resorption), give and account of the growth marks these events leave in all limb bones, and settle the time of onset and duration of the impact of these early life history events on bone tissue growth rate.

5.2. Material and methods

5.2.1. Individuals and feeding regime

Six red deer (*Cervus elaphus hippelaphus*) (five males and one female) were used for this study. All animals belonged to the herd of red deer kept at the Research Institute of Wildlife Ecology, University of Veterinary Medicine, Vienna. The deer enclosure contained about 39 ha deciduous oak-beech forest and a meadow of about 6 ha, i.e. provided close to natural living conditions. The animals could forage on natural vegetation in the enclosure and received supplementary pellets and hay. Calves analysed were born between late spring-early summer of 2014, 2015 and 2016. All of them were weighed at birth to the closest 50g.

New-born calves were assigned to two groups with different raising conditions and feeding regimes. One group of calves (C1) consisted of two males (ID-23, ID-24) that naturally suckled at their mothers. Both remained in the herd until euthanasia at ages 64 and 24 weeks, respectively. The second group of calves (C2) consisted of two males (ID-1, ID-2), sacrificed at ages 2 and 15 weeks, respectively, and one male (ID-3) and a female (ID-4), both sacrificed when 43 weeks old. Group C2 was initially also left with their mothers to allow for sufficient intake of colostrum, but separated from them within 12h after birth and hand-raised by experienced animal keepers. Until an age of ~4 months C2 animals were individually housed at night, but kept together under supervision for 8 hours during daylight. From an age of ~4 months onwards, C2 animals were kept together in a ~0.75 ha enclosure, separating from the rest of the herd by a fence.

Hand-raised animals were bottle-fed with milk substitute (Alpmil Lämmermilch 22.5% crude protein, 22% crude fat, Garant, Austria). From week 1-10 after birth, they received an increasing daily ration of milk substitute from

~1000 ml (week 1) to 1200-1500 ml (week 10), distributed over 4-5 (week 1), 3 (weeks 3-5), and 2 (weeks 6-10) feeding bouts per day (for individual intakes see Table S8.5). From week 10 onwards the daily amount of milk substitute fed was reduced to introduce the weaning period, and to encourage the animals to feed on pellets (up to an age of 5 months: Lämmerkorn, Garant, Austria; older than 5 months: Trophy Ergänzungsfuttermittel Reh/Rotwild, Garant, Austria) and hay, provided ad libitum. Bottle-feeding was terminated during week 13 after birth (weaning), except for ID-1 that was sacrificed earlier. C2 animals were weighed daily until weaning (13 weeks) and ID-4 until 20 weeks.

Age	Marker (ml)					
	Group C2				Group C1	
	ID-1 IPS-88714	ID-2 IPS-88715	ID-3 IPS-93664	ID-4 IPS-88713	ID-23 IPS-109291	ID-24 IPS-109290
birth	3.1					
3 days	13.3	3				
15 days	4.8					
30 days		19.8				
9 weeks				9.1		
11 weeks				38		
13 weeks		10.3	10.9	11.3	10.9	11.2
15 weeks		42	44	43		
17 weeks			13.9	12.3		
23 weeks			70	58.5		

Table 5.1. Schedule of alternated green (calcein green) and red labelling (alizarin complexone) and the amounts of fluorochrome marker administered (Alizarin complexone 30 mg/kg; calcein green 8 mg/kg). Table obtained from Calderón et al. (2021).

5.2.2. Fluorescent markers

Calves were labelled subcutaneously between birth and age 23 weeks with fluorescent markers (Alizarin complexone and Calcein green), known to get incorporated into growing bone tissue (Klevezal, 1996), individuals of group C2 repeatedly (Table 5.1). Marker solutions were prepared under sterile conditions at the pharmacy of the Vetmeduni Vienna and buffered to 7.4 pH with NaHCO3.

Until the age of about three months, all procedures were carried out without anaesthesia, as the hand-reared animals were hand-tame and still small enough to be restrained briefly for injection. Thereafter, all manipulations were performed under deep sedation using 0.1 mg/kg medetomidine (Medetomidine-HCL 2%, magistral formulation, Richter Pharma AG, Vienna, Austria). During sedations, vital parameters of animals were monitored. Sedation was reversed using atipamezole (Narco Stop 5 mg/ml, Richter Pharma AG, Wels, Austria). For euthanasia, animals were deeply anaesthetized with a combination of ketamine (Ketamidor 100 mg/ml, Richter Pharma AG, Vienna, Austria) and medetomidine (2 mg/kg and 0.8 mg/kg, respectively). Thereafter, they received an overdose of a combination of embutramide, mebezonium and tetracaine (T 61, lntervet, Vienna Austria).

Our research questions could only be investigated in a living wild ruminant kept under (semi-) natural conditions. Animals were managed by keepers with decades of red deer experience and were checked daily. Veterinary care was constantly available. All experiments and procedures were approved by the Ethics Committee of the University of Veterinary Medicine, Vienna and the Austrian Federal Ministry of Education, Science and Research in accordance with the Animal Experiments Act 2012 (TVG 2012) (permit numbers (GZ) BMWFW-68.205/0100-WF/II/3b/2014 and BMWF-68.205/0170-

WF/V/3b/2016). These experiments were carried out in compliance with ARRIVE guidelines.

5.2.3. Bone samples

After euthanasia, we prepared from each individual six postcranial bones from sections of the hind- and forelimb (femur, tibia, metatarsus, humerus, radius and metacarpus). The total of 36 bones was sent to the ICP-Institut Català de Paleontologia Miquel Crusafont, Barcelona (Spain) for histologic analysis.

All bones were photographed and measured following standard ICP procedure before sectioning (Calderón et al., 2019). Bones were sectioned at the central part of the diaphysis. A chunk of approximately 3 cm from the middle of the diaphysis was extracted from each bone (from 1.5 cm above to 1.5 cm below the mid-shaft), degreased and dehydrated by alcohol immersion. Afterwards the chunk was embedded in Araldite 2020 epoxy resin. The block was cut into two halves with a low-speed diamond saw (IsoMet low speed saw, Buehler). The cut surfaces were polished with a MetaServ polishing machine and fixed to a frosted glass using epoxy resin. Once the sample was fixed, it was cut with a diamond saw (Petrothin, Buehler) up to a thickness of 100–120 microns and finely polished again to perfect the slide.

5.2.4. Histological study and label examination

Thin sections were examined under Zeiss Scope A1 microscope with an integrated camera. Firstly, the sample was studied under transmitted and polarized light in order to obtain bone tissue information (e.g. tissue type, vascularity, growth marks). The description of bone tissue types was done following the nomenclature proposed by Prondvai et al. (2014). The FLC was

described as longitudinal, laminar, plexiform, reticular or radial regarding according Francillon-Viellot et al. (1990). Subsequently, the sample was exposed to fluorescent light, alizarin complexone (red) and calcein green with the purpose of obtaining information about the deposited bone at each date scheduled. Images of different sections were taken using Zeiss software and channels were merged in order to obtain a combination of red and green fluorescent image first, and polarized and fluorescent images together. Afterwards, combined section images were aligned and fused using Photoshop CS3 with the purpose of creating the entire surface of the cross-section (see Supplementary material). Although most individuals were labelled several times over a complete year, we focused on the period from birth to 23 weeks with the aim to avoid the overlap with seasonal disruptions (since births took place in June the beginning of winter occurred short time after the 23th week of life).

The complete cross-sectional areas between labels were measured on combined polarized and fluorescent images. For this purpose, the entire area contained in each one of the labels (i.e. fluorescent circumferences along the cortex), including the medullary cavity, was selected. We included the area of the medullary cavity in each measurement in order not to bias the data as the variation of its size over time cannot be estimated. Also, because our purpose is to study variations in deposited area between labels and not the precise amount of area. We measured areas instead of linear measurements (i.e. thickness between labels) as hitherto used (Castanet et al., 2000; de Margerie et al., 2004, 2002; Montes et al., 2007; Starck and Chinsamy, 2002), because area is related to body mass and, hence, better reflects the ontogenetic stages, which was the main purpose of our study. Besides, this method also allowed avoiding the bias caused by asymmetry of bone shafts.

For calculating daily growth rates, the area between labels was divided by the days between injections, which resulted in 7 stages: stage 1: Birth-3days; stage

2: 3-15days, stage 3: 3-30days; stage 4: 30days-13weeks; stage 5: 13-15weeks; stage 6: 15-17weeks and stage 7: 17-23weeks. Due to the short intervals between the first injections in the specimen ID-4 (Table 5.1), the fluorochrome lines overlapped in the bone tissue. Hence, it was no possible to calculate growth rates for ID-4 at ages from 9-15 weeks. As calves left with their mothers (C1) were labelled only at the age of 13 weeks, we could not measure the growth rates during discrete periods in their ontogeny. However, we could measure the growth rates of the six months old specimen ID-24 from birth until the age of 13 weeks and from there to the age of 24 weeks at euthanasia by using the birthmark and the outer circumference of the bone as natural labels.

We quantified the area of the fluorochrome deposited for each label. With that purpose, we created the entire composition of the shaft of red and green fluorescent images separately using Photoshop CS3. Basing on the disposition of the last fluorochrome label deposited (animals were sacrificed 2 days later), we estimated the time of complete pigment deposition and, hence, the time represented by a label as ≈48 hours in deer. We measured the area of each isolated label in single images using FIJI software. As the increasing diameter of the bone tends to bias these measurements, we standardized the data considering the ratio between the areas of each label (see Table S8.6). In addition to the labelled tissue that was deposited increasing the periosteal area of the shaft at the time of the injection, it was also possible to find concentric stained lamellae in the inner regions of the cortex (i.e. the area that was filling the woven matrix of FLC at that time).

The density of the canals was quantified in the anterior region of all bones for each labelling interval and also for the prenatal period where possible. We used ImageJ software (Schneider et al., 2012) to obtain the area occupied by vascular canals contained in a limited area of 0.370 mm^2 using a 20x lens. Finally, the area occupied by vascular canals was expressed as a percentage in order to facilitate comparisons with other measured areas.

5.2.5. Statistical analysis

Statistical analyses and charts were performed using RStudio (Team, 2019) software. Shapiro-Wilk test and Levene's test were performed to evaluate the normality and homoscedasticity, respectively, of our data. Once these conditions were confirmed (Saphiro Wilk W>0.95; Levene test p>0.05), ANOVA tests were performed to analyse the variation of growth rates over ontogenetic stages and over bones. The variation in growth rates and vascular density between the two groups of calves in different age periods was analysed by applying two-way ANOVA tests. Tukey multiple comparison test was used to establish statistically significant differences between groups. The increase of body mass, bone area and deposition area over time were analysed with segmented regression analysis (Muggeo, 2017). To account for different apposition rates in different bones, we analysed scaled values of cumulative bone apposition areas. A scaled value is a measure of how many standard deviations a raw score is below or above the mean of all measurements of a particular bone. Therefore, scaled values have a mean of zero and include equal amounts of negative and positive deviations in the case of a symmetric distribution. Raw data (i.e. without scaling) can be found in Fig. S8.12, Fig S8.13, Table S8.3 and Table S8.6. We considered repeated measurements in linear mixed effects models by a random factor bone nested within individuals.

5.3. Results

5.3.1. Body mass

Continuous measurements of body mass were available only from one individual (Fig. 5.1). Starting from a birth mass of 10 kg, this specimen grew linearly with a rate of 0.38 kg per day until weaning at day 91. After weaning, body mass remained constant for 22 days. Growth resumed thereafter, but at a

slightly lower rate (0.34 kg per day, difference between slopes of regression before the first and after the second breakpoint (Fig. 1, t=-2.63, p=0.01).
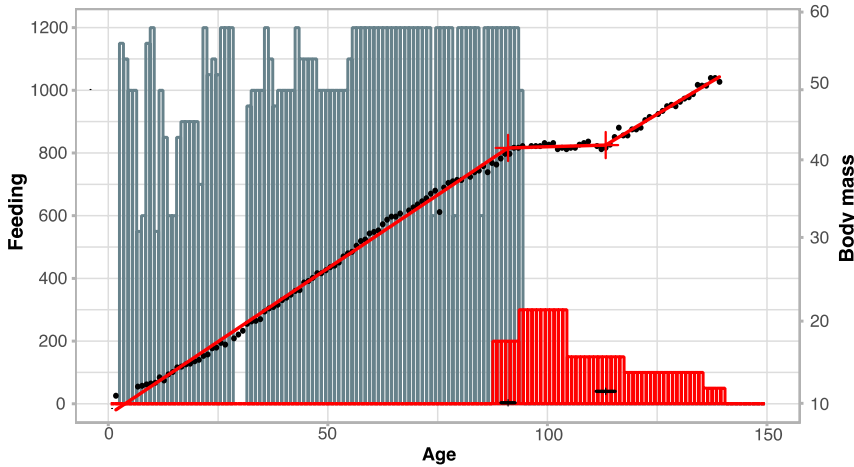
Figure 5.1. Daily body mass (in kilograms) (black dots) of the hand-raised female ID-4 and daily intake of food (blue and pink bars) plotted against age in days. Crosses indicate breakpoints estimated by segmented regression, horizontal bars above the x-axis 95% confidence intervals of breakpoint locations. Blue bars denote the amount of milk substitute ingested per day (millilitres); red bars the amount of fodder in (milligrams per litre). Slopes of regressions divided by breakpoints differed significantly (F(2,123)=148.69, p<0.0001; linear modelling without breakpoints yielded a significantly worse fit (model without breakpoints AIC=556.58; model with breakpoints AIC=42.36; ΔAICc=514, p<0.0001). Figure obtained from Calderón et al. (2021).

5.3.2. Bone growth rates

To calculate bone growth rates, we used the bone appositional area between labels instead of linear measurements (see methods). The complete record of measured areas can be found in Table S8.3, while the record of apposition rates and canal density can be found in Table S8.4.

We compared the growth rate of all six limb bones considering the entire interval from birth to 23 weeks and we did not find significant differences among them (ANOVA; $F_{(5,60)}$: 1.193; p=0.323). The quantitative analysis revealed the complete record of growth rate of the six limb bones analysed for hand raised (C2) red deer calves and those nursed by their mother (C1) over the first six months of life (Fig. 5.2a). Both groups showed high growth rate in the pre-weaning stage (birth-13 weeks), and substantially lower growth rate in the post-weaning stage (13-23 weeks; two-way ANOVA, effect of stage, $F_{(1,74)}$=36.06, p<0.001; difference between C1 and C2, $F_{(1,74)}$=1.54, p=0.218; difference between slopes, $F_{(1,74)}$=2.60, p=0.111). For the C2 calves, we had more detailed information and could analyse growth rates on a finer time scale over the first six months of life. We found significant differences among seven different age stages (stage 1: Birth-3days; stage 2: 3-15days, stage 3: 3-30days; stage 4: 30days-13weeks; stage 5: 13-15weeks; stage 6: 15-17weeks and stage 7: 17-23weeks) (Fig. 5.2b; ANOVA, $F_{(6,59)}$=19.11, p<0.001). Pairwise comparisons demonstrated the degree of differentiation between age stages. Growth rates were highest during stages immediately after birth (1: 1-3 days) and previous to weaning (4: 30 days -13 weeks), and lowest immediately after weaning (5: 13-15 weeks). This minimum growth rate corresponded to the almost null apposition of bone (see below) and was characterized by the presence of a growth mark. Growth rates recovered again thereafter (6: 15-17 weeks, 7: 17-23 weeks).
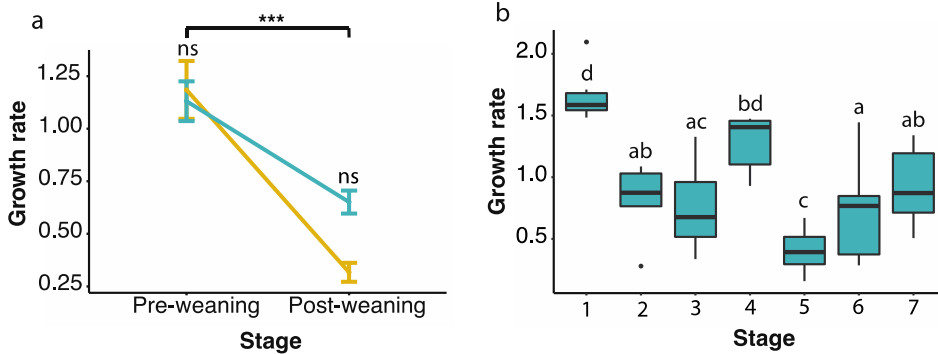
Figure 5.2. Average growth rates of the six bones analysed (in mm2/day) (a) for the pre- and post-weaning stages of calves nursed by their mothers (C1; orange colour, means ± standard errors of means) and hand raised calves (C2; blue colour) and (b) for the seven growth stages of hand-raised specimens (C2; blue colour). (b) Box plots of growth rates of C2 individuals with finer resolution of time (stage 1: Birth-3days; stage 2: 3-15days, stage 3: 3-30days; stage 4: 30days-13w; stage 5: 13-15w; stage 6: 15-17w and stage 7: 17-23w). In graph (b), different letters above each box indicate significant differences according to Tukey post-hoc comparisons (p<0.05). Figure obtained from Calderón et al. (2021).

5.3.3. Cumulative bone tissue apposition

Data from cumulative bone apposition areas measured between successive labels in six different bones revealed fast growth up to an age close to weaning (between 90 and 110 days according to the confidence interval) and a slightly slower growth thereafter (Fig. 5.3). Unlike the hand-raised calves (C2), labelled several times, calves nursed by their mother (C1) were labelled only at the age of 91 days. However, at this age bone apposition did not differ significantly between both groups (F(1,3)=2.68, p=0.200).
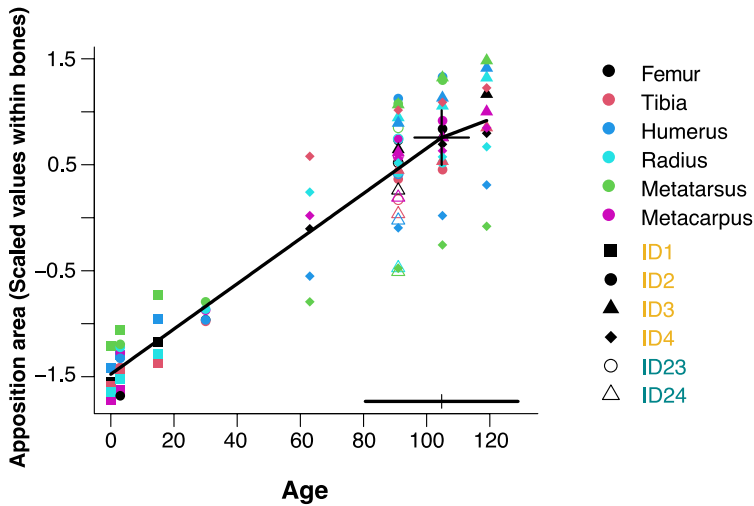
Figure 5.3. Cumulative apposition areas of bone tissue in six different limb bones during early life (scaled values of bone apposition area in mm2, plotted against age in days), of calves nursed by their mothers (C1: ID-23, ID-24), and hand-raised calves (C2: ID-1, ID-2, ID-3, ID-4). The cross indicates a breakpoint estimated by segmented regression, the horizontal bar above the x-axis the 95% confidence interval of breakpoint location in which the weaning event (occurred at the age of 90 days) is included. Slopes of regression below and above the breakpoint differed significantly (F(1,57)=6.25, p=0.015; linear mixed modelling without a breakpoint yielded a significantly worse fit, (model without breakpoints AIC=32.14; model with breakpoints AIC=11.22; ΔAICc=19.92, p<0.0001). Figure obtained from Calderón et al. (2021).

Further, we quantified the deposited area of each fluorochrome injection. This approach provided a quite narrow and, hence, temporally discrete bone appositional rate. It corroborated the result found with the cumulative bone apposition areas, but delivered a more detailed picture (Fig. 5.4). The area of pigment deposition decreased substantially after birth, resumed until weaning and was followed by a second, less pronounced decrease.
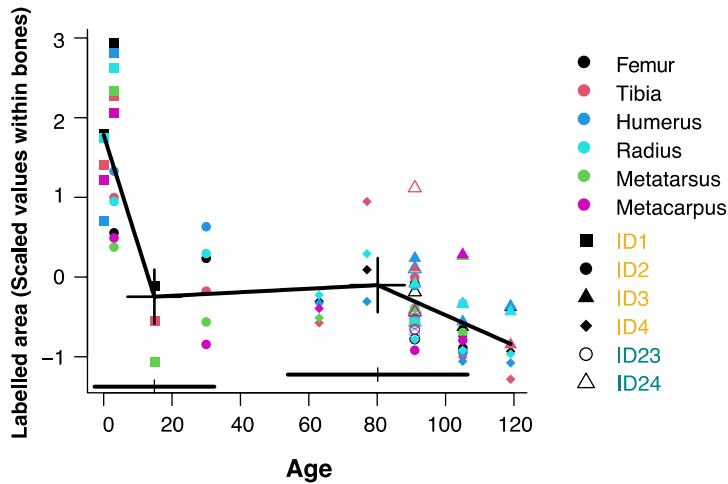
Figure 5.4. Amount of bone area stained with fluorochromes for each of the labels in six different limb bones. Plotted are scaled values of deposition areas in mm2 of calves nursed by their mothers (C1: ID-23, ID-24), and hand-raised calves (C2: ID-1, ID-2, ID-3, ID-4. Crosses indicate breakpoints estimated by segmented regression, horizontal bars above the x-axis 95% confidence intervals of breakpoint locations. Slopes of regressions divided by breakpoints differed significantly ($F_{(2,46)}=14.33$, $p<0.0001$; linear modelling without breakpoints yielded a significantly worse fit, (model without breakpoints AIC=179.66; model with breakpoints AIC=132.59; ΔAICc=47.07, $p<0.0001$). Figure obtained from Calderón et al. (2021).

Lastly, we calculated the canal density, another independent indicative of bone deposition rate (Lee, Huttenlocker, Padian & Woodward, 2013) for four ontogenetic periods: just before and after birth, and just before and after the weaning (Fig. 5.5). Results revealed differences between these ontogenetic periods in hand-raised specimens (Fig. 5.5a; ANOVA, $F_{(3,41)}=5.283$, $p=0.004$). When comparing data from the two groups of calves, we found differences also conditioned by feeding regimes (Fig. 5b; two-way ANOVA, $F_{(1,50)}=4.503$, $p=0.038$). Both groups (C1 and C2) experiment a decreasing trend between pre- and post-weaning period, but in a different way: The group of hand-raised calves (C2) show a higher density than calves nursed by their mothers (C1) in

the pre-weaning period while both groups show almost the same density after the weaning event (Fig.5.5b).
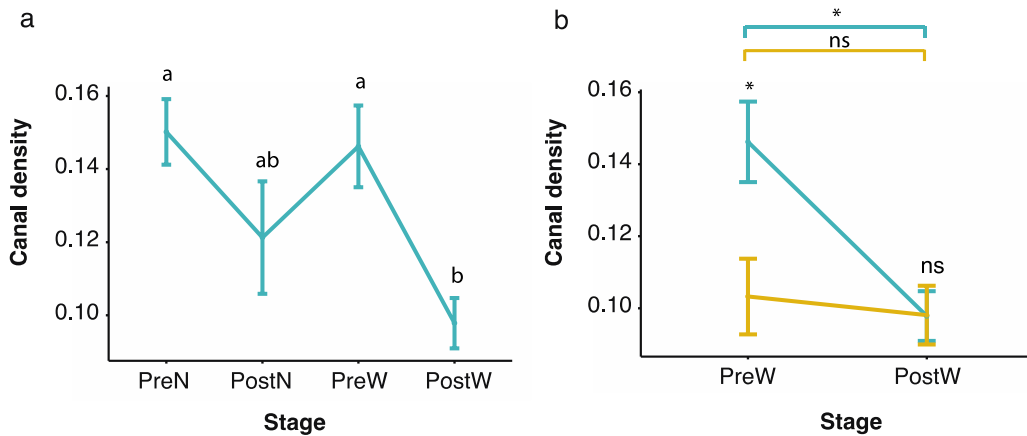
Figure 5.5. Representation of canal density (mean ± SE in % of the total area contained in a square of 0.370mm^2) (a) by ontogenetic periods of hand-raised calves (C2): prenatal (before birth), post-natal (from birth to 30 days), pre-weaning (from 30 days to 13 w) and post-weaning (from 13 to 23 w) and (b) for the pre-weaning (from 30 days to 13 w) and post-weaning (from 13 to 23 w) periods of both groups of calves (C1 and C2). Specimens staying with their mothers (C1) are represented in orange; hand-raised specimens (C2) are represented in blue. In graph (a) different letters above each point indicate significant differences (when groups show different letters) and non-significant differences (when groups share a letter) between groups according to Tukey post-hoc comparisons (p<0.05). In graph (b), ns: no significant differences. Figure obtained from Calderón et al. (2021).

5.3.4. Histological representation of growth rate variation

All the detailed histological descriptions of every bone section can be found in Chapter 8 (section 8.2.1.).

Every bone of the individuals here analysed was still actively growing at the time of death. The patterns of bone apposition displayed by the same label over different bone sections revealed different rates of cortical growth. Thus, a wide and spaced arrangement of successive labels indicated areas with elevated rates of bone apposition (fast-growing areas), while a compact arrangement of successive labels revealed areas of low rates of bone apposition (slow-growing areas) (Fig. 5.6a, b). Regardless of area, C2 individuals showed a general period of low apposition that starts at 13 weeks and lasts until 17 of age. (FIG 5.6a, b)

5.3.4.1. *Bone tissue formation*

Primary bone mainly consisted of woven-parallel complex (see methods for nomenclature), specifically of fibrolamellar tissue (FLC). Prenatal tissue showed a greater amount of primary parallel-fibered bone than postnatal tissue (Table 5.2; Fig S8.2a), which facilitated the visual recognition of this boundary under polarized light in all bones of the individuals here studied. As postnatal bone increased in proportion over ontogeny, the prenatal bone is being resorbed, though even the oldest individuals showed remnants of prenatal tissue (i.e. 43 weeks-old) (Table 5.2). We distinguished three main types FLC: laminar, plexiform and reticular. Radial orientation predominated in some areas of the tibiae and some longitudinal areas can be recognized in metapodials. These FLC types varied widely throughout the bone matrix (Table 5.2). Bones of C2 individuals experienced a shift in the type of FLC tissue towards a more organized pattern after weaning (i.e. 13 weeks of life) (Table 5.2; Fig. 5.6c) while bones of C1 individuals show a uniform deposition (Fig. 5.6d). Moreover, specimens of both groups showed local differences in transversal area (i.e. fast-growing areas frequently showed radial and

plexiform FLC, while laminar and plexiform FLC was common in areas of slow-growth).

Secondary bone such endosteal tissue and Haversian systems was present in the limb bones from an early age onwards (Table 5.2). Although growing centripetally, the endosteal tissue found in our sample was deposited following the same pattern as primary tissue (i.e. FLC). A woven-bone scaffold started to form and, subsequently, it was refilled with lamellar tissue following different FLC arrangements (Fig 5.6e; Fig. S8.3f; Fig. S8.4f). Deposition of Haversian bone started at the age of 15 weeks; their presence was restricted to particular areas depending on the bone (Fig. 5.6f).

5.3.4.2. *Indicators of growth arrest*

There was a correlation of growth marks with birth and weaning events. Describing incomplete circumferences, these growth marks did not follow the entire former bone circumference, but they only formed within the areas of low apposition.

A partial LAG or an annulus (depending on the bone and the location, but usually in the slow-growing areas) appeared in the moment of birth bordering the prenatal area (Fig. 5.6g). This growth disruption was associated with a local decrease in growth rate (Fig. 5.4) until approximately 3-days after birth. We found another growth disruption after the moment of weaning (13 weeks) in the slow-growing areas of all bones of hand-raised individuals (C2) older than 15 weeks (Fig. 5.3-5.4). This disruption was represented by a partial LAG located between the labels deposited at 15 and 17 weeks (Fig. 5.6h) or shortly after the 15-weeks label in all the bones of C2 individuals but only in the radius of a C1 individual (Fig. S8.4d). Taking this into account we estimated that limb bones of C2 group arrested growth for one to two weeks within the

slow-growing areas in response to weaning. There was no evidence of LAGs in the fast-growing areas of the shaft, though in most of the specimens there was no increase in bone area from 13 to 15 weeks.

These birth and weaning growth marks were accompanied by local cortical resorption in the slow-growing areas of radii, tibiae and metapodials of C2 individuals and of the radius of one C1 individual (Fig S8.4). A scalloped interruption of the tissue in combination with a growth mark was visible in these areas. In addition to these intervals, and apparently independent of any life history event, there were some marks on the lateral side of the radius both in C1 and C2 individuals.

Perinatal growth
Rounded shape and narrow bone cortex
The medullary cavity occupies a high percentage of the cross-section
Cortex formed mostly by prenatal tissue with reticular orientation (FLC with high percentage of PFB in the prenatal area)
Absence of annulus and LAGs
Endosteal bone present in radius and metapodials at the age of three days in the anterior part (metapodials) and in the antero-posterior areas (radius).
Haversian bone absent

Pre-weaning growth
Bone cortex slightly irregular but still rounded
Medullary cavity area increased
Prenatal bone still present. Variable types of FLC in group C2. Mostly plexiform in group C1
Growth marks bordering the prenatal area in radii of C1 and tibiae, radii and metatarsii of C2
Endosteal bone starts to form at 13weeks in proximal bones and tibia
Incipient Haversian bone in the linea aspera (femur), medial part (tibia and radius) and posterior area (metapodials)

Post-weaning growth
Shape similar to adults. Thick cortex
Large medullary cavity except for radius and metapodials
Low portion of prenatal tissue. Shift in FLC arrangement in group C2. Mostly plexiform tissue in group C1
Growth marks bordering the prenatal area in both groups (C1 and C2) and between the 13th and the 17th weeks label only in the C2 group. Growth marks with cortical resorption bordering the pre-weaning area in tibia and radius.
Well-developed endosteal bone but already reduced by resorption to few small areas
Well-developed Haversian bone in the linea aspera (femur) and some prenatal areas (rest of the bones), which continues spreading around the shaft

Table 5.2. Description of thin-sections. FLC = Fibrolamellar complex; PFB = Parallel-fibered bone; LAG = Line of arrested growth; C1 = calves left with their mothers; C2 = hand-raised calves. Table obtained from Calderón et al. (2021).
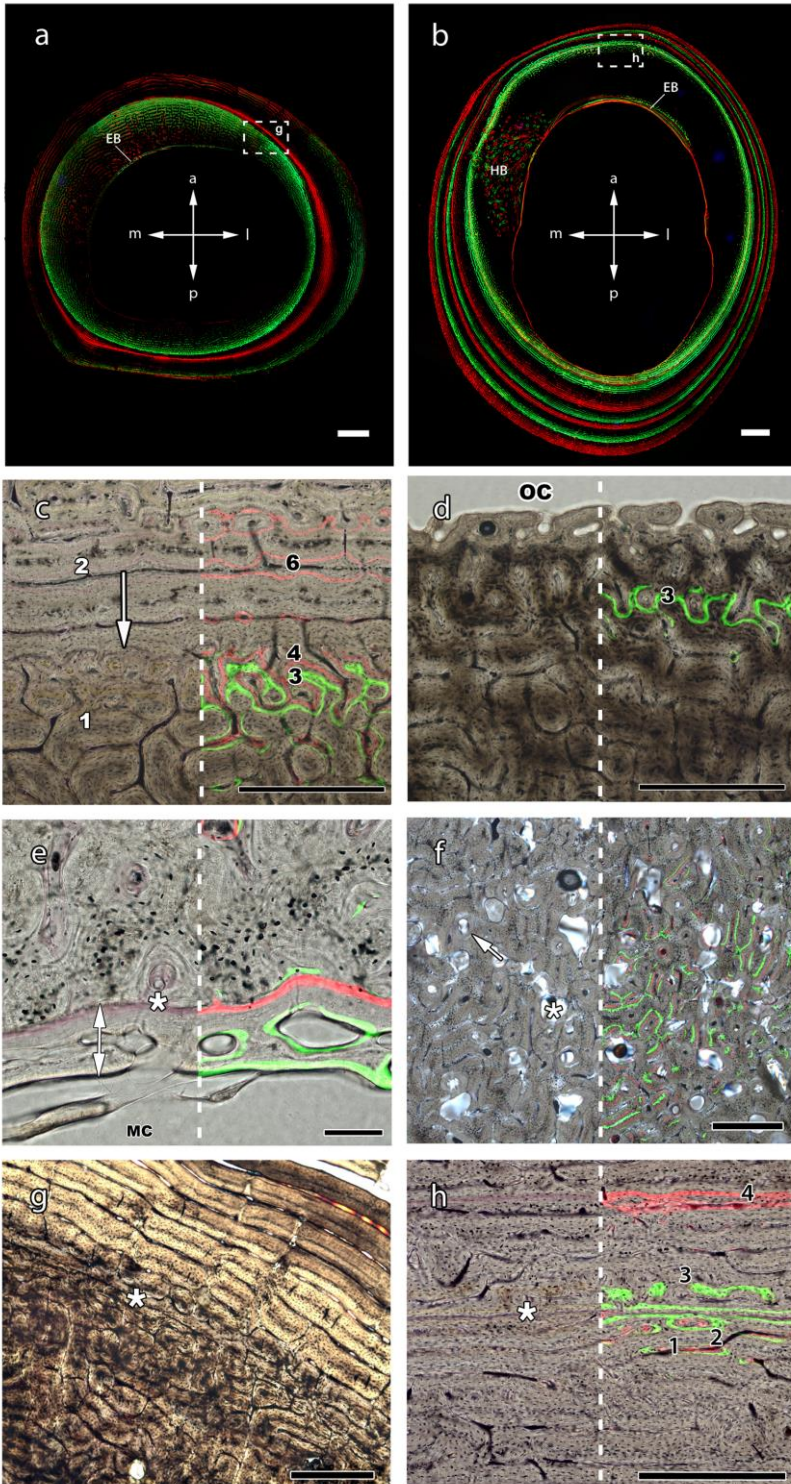
Figure 5.6. Limb bones under fluorescent light (a, b) and their histological details under transmitted (g) and combined transmitted and fluorescent light (c,d,e,f,h). (a) Bone expansion (bone drift) towards the postero-lateral side of the tibia of a 15-weeks old individual (ID-2). An initial cortical layer (endosteal bone: EB) formed around the antero-medial part of the medullary cavity as a consequence of bone drift. In this sector, later tissue (red label 30 day) has locally been arrested (upper part of first red label) to remodel the shape of the bone. Inner green label: 3rd day after birth; red label: 30 days after birth; outer green label: 13 weeks after birth; outer red label: 15 weeks after birth. Scale: 2 millimetres. (b) Bone expansion towards the posterior side of the humerus of a 43 weeks old individual (ID-3). The EB appears in the opposite site while a section of Haversian bone (HB) can be seen towards the medial sector. Inner green label: 13 weeks after birth; red label: 15 weeks after birth; second green label: 17 weeks; second red label: 23 weeks; subsequent labels were not considered in this study. Scale: 2 millimetres. (c) Abrupt shift of the FLC from reticular pre-weaning tissue (white 1) to a plexiform-laminar post-weaning tissue (white 2) in the anterior region of the metacarpus of a hand-raised individual (ID-3). A resorption process has eroded the deposition between labels 4 and 6. The white arrow indicates the transition between pre- and post-weaning periods. 3: label deposited at 13 weeks; 4: label deposited at 15 weeks; 6: label deposited at 23 weeks. Scale: 0.5 millimetres. (d) Uninterrupted deposition of tissue in the anterior part of the metatarsus of an individual nursed by its mother (ID-24). 3: label deposited at 13 weeks. Scale: 0.5 millimetres. (e) Endosteal bone (white arrow) in the anterior sector of the metatarsus of ID-1 delineated by a cement line (asterisk). Red label: alizarin red deposited at the age of 3 days; Green label: Calcein green deposited at the age of 15 days. Scale: 0.1 millimetres. (f) Detail of a forming Haversian bone in the posterior sector of the metatarsus of ID-3. Resorption cavities are marked with an asterisk and cement lines of secondary canals with an arrow. (g) Birth LAG (white asterisk) in the antero-lateral part of the tibia of ID-2. A more disorganized tissue before birth (down) and a more organized tissue after birth (up) indicate a slowdown in the deposition rate. Scale: 0.5 millimetres. (h) Weaning LAG (white asterisk) in the anterior part of the humerus of ID-3. Black numbers indicate the different labels: 1: green label deposited at 13 weeks; 2: red label deposited at 15 weeks; 3: green label deposited at 17 weeks; 4: red label deposited at 23 weeks. The absence of tissue deposited corresponds to the period between 13 and 17 weeks,

making barely visible the 15-week label (number 2). Scale: 0.5 millimetres. Figure obtained from Calderón et al. (2021).

5.4. Discussion

Previous in-vivo fluorochrome labelling experiments were aimed at testing the reliability of skeletochronology, generally in reptiles and mammals (Buffrénil and Pascal, 1984; Castanet et al., 2004; Klevezal, 1996; Klevezal and Mina, 1984). However, a few studies focused on quantifying bone tissue growth rates using juvenile (and, hence, rapidly growing) birds. Despite the generally fast growth rates observed, these studies found both quantitatively and qualitatively much variation in absolute growth rates in different bones and even within each tissue type (Castanet et al., 2000; de Margerie et al., 2004, 2002; Starck and Chinsamy, 2002); nevertheless, they have so far failed to provide a uniform and general picture of the dynamics of bone growth during early ontogeny in vertebrates. This is essentially due to the design of the studies. As they were not aimed at determining the timing and duration of the observed variations nor their correlation with early life history events (hatching in birds, birth and weaning in mammals), but rather at finding a correlation between visually classifiable bone tissue types and quantifiable tissue growth rates (testing Amprino's rule). Here, by fine-scheduled, high-resolution labelling, we describe a general pattern for juvenile bone growth rates in red deer as an almost continuous decrease with age. This trend shows two events of growth disruption that coincide with the life history events birth and weaning. In this way, results on bone tissue apposition and body mass gain, suggest that the bone development from birth to post-weaning in deer calves represents indeed a general 4-stages pattern for ruminants, described by birth (three days of growth decrease / arrest), the period between birth and weaning (vigorous growth), weaning (growth decrease / arrest for one-to-two

weeks), and post-weaning (modest growth resumption).

A birth line has been first identified and described by Nacarino-Meneses & Köhler (2018) as neonatal line, homologous to the birth line found in teeth (Smith et al., 2006), by superimposition of bone sections of aged individuals in several *Equus* species, evidencing the association between this non-cyclical growth mark and the event of birth in mammals. Our labelling results corroborate that the first growth mark (either a LAG indicating growth arrest or an annulus indicating a change in growth rate) deposited in the limb bones of red deer correspond to the birth event. The fact that we found both LAGs and annuli forming a neonatal line, as Nacarino-Meneses & Köhler (2018) did in *Equus*, indicates that not all long bones of a same individual uniformly arrest growth (LAGs); some do not stop but only decrease growth rate to a minimum (annuli). This corroborates previous findings that tissue growth rates vary both within and among long bones, which is especially obvious between legs and wings of birds (Castanet et al., 2000; de Margerie et al., 2004, 2002; Starck and Chinsamy, 2002).

The boundary between pre- and postnatal tissue in red deer calves is further emphasised by an abrupt transition in tissue type from predominantly parallel-fibered prenatal bone to postnatal fibrolamellar cortex with lower proportions of parallel-fibered bone, indicating acceleration in growth rate after the event of birth. This pattern is comparable to that found in equid foals (Nacarino-Meneses and Köhler, 2018) and elephantidae (Curtin et al., 2012) and opposed to the pattern found in dinosaurs and reptiles (Chinsamy and Hurum, 2006; Hugi and Sánchez-Villagra, 2012).

A weaning line was found in the jawbones of hedgehogs (Morris, 1970). The dark band found by the authors was attributed to the reduced growth caused by the food disruption of weaning. Posteriorly, Castanet et al. (2004) describe a discontinuity in the inner part of the long bones that may indicate

the weaning event due to the date of deposition and which they did not consider for age estimation. In a similar way, the "dark line" discounted in skeletochronology of yellow-pine chipmunks by Barker et al. (2003) could correspond to a weaning line; alternatively, their "extra adhesion line" might instead represent a neonatal line. However, Barker et al. (2003) provided no description so that an exact determination is impossible.

Results provided by our labelling schedule evidences that this early growth mark, mainly present in the hand-raised individuals (C2 group), corresponds to the weaning process. In addition to the growth mark, the transition from pre- to post-weaning period is marked by a shift in the type of FLC that reflects the change from high to low bone growth rates (de Margerie et al., 2004) in hand-raised specimens (C2). The weaning process is also the responsible of the temporal stagnation of the daily body mass gain during approximately 4 weeks (Fig. 5.1).

Unlike the hand-raised specimens (C2), we could not weigh the C1 group daily because these individuals were untamed. Thus, we had to restrict the weight measurements to the labelling at approximately weaning and at death. Notwithstanding, the fact that we found a weaning LAG in most of the specimens of the C2 group and only in a single element of C1, could be due to either the different pre-weaning feeding regimes or to the less gradual and more abrupt artificial weaning experienced by the hand-raised group. As in all ruminant artiodactyls, the digestive system of red deer calves changes during early life, specifically during the pre-weaning period. The rumen development is highly conditioned by the addition of vegetal material during the pre-weaning period. When the rumen is fully developed and functional (i.e. around 12 weeks), calves are able to feed entirely on vegetal materials (Teagasc, 2017). Despite the gradual modification of diet before weaning in the hand-raised deer (i.e. a decreasing amount of milk and an increasing amount of vegetal material), it is possible that this shift could have been not smooth

enough as in naturally weaned calves. As a consequence, the rumen could have undergone an incomplete development, making difficult the absorbance of the only-vegetal feeding and hence, causing a marked growth disruption.

The negative effects of weaning on growth rate of juveniles is widely studied in domestic breeds (Warren et al., 1998). This is because domestic species experience an abrupt weaning that often starts too early compared to the gradual weaning of wild animals (e.g. foals; Holland et al., 1996, beef calves; Enríquez et al., 2011). Therefore, the improvement of the weaning process with the aim of maximizing production efficiency (Pollard et al., 2002) is in the foreground of many studies on farm animals. In this way, farm managers use to employ artificial feeding (i.e. milk-based diet), as we have employed in the hand-raised calves (C2), as a method for improving the production efficiency. Various studies (Pluske et al., 2003; Wolter and Ellis, 2001) have demonstrated that milk replacer allows for an accelerated growth rate in piglets. This supports the different pre-weaning vascular density found between our hand-raised calves (C2) and those fed by their mothers (C1). In our case, this is conditioned by the composition of powdered milk, richer in nutrients than natural deer milk (Landete-Castillejos et al., 2000; Wang et al., 2017). This high energy diet fed to hand-raised animals most likely led to a fast periosteal bone apposition generating a highly vascularized matrix (Fig. 5.5b) (Lee, , Huttenlocker, Padian, & Woodward, 2013; Stein and Prondvai, 2014).

However, the accelerated growth triggered by the high nutrient diet of powdered milk could have caused long-term effects. Fast calf growth during lactation positively determines adult body size and mating success (Clutton-Brock et al., 1982; Festa-bianchet et al., 2000). Moreover, larger calves are more able to tolerate nutritional deficiencies and harsh winter conditions (Cook et al., 2004), even in farmed environments (Moore et al., 1988). In contrast, accelerated growth could also cause negative effects. Some authors (Ozanne and Hales, 2005; Van Eetvelde and Opsomer, 2017) have explored the

mismatch between a low prenatal and high postnatal growth conditioned by milk substitutes in different groups of mammals (mice and cattle, respectively). Based on life history theory, they concluded that fast growth could potentially lead to reduction in longevity, and a decrease in fertility and metabolic activity. For these reasons, it is important to have a good understanding of this pre-natal stage as the accelerated growth of C2 individuals feeding on milk replacer could cause similar detrimental long-term responses.

Our labelling study provides, for the first time an estimate of the duration of non-cyclical LAG formation during weaning: decrease or even cessation of bone growth during this event lasts one or two weeks depending on the nutritional conditions (environmental food availability and conversion of acquired nutrients into energy), which can lead either to a rather smooth decrease in bone growth rate in naturally nursed, healthy calves or to an abrupt deposition of a non-cyclical partial LAG under conditions of artificial weaning. The weaning LAG is especially visible where the direction of radial bone growth is constrained by shape (biomechanics) through growth arrest, and is almost imperceptible where bone growth is only reduced but not arrested (Calderón et al., 2019). Accordingly, the expression (imperceptible, incomplete or complete) of LAGs and annuli within long bones is conditioned by bone growth rates: the slower the rate the easier the formation of rest lines. The absence of cyclical marks in juvenile dinosaurs led to similar conclusions (Horner et al., 2000a; Padian et al., 2001).

Additionally to the growth marks caused by birth and weaning events, we relate structures formed by cortical resorption, generally termed "dark lines" and attributed to temporary changes of bone deposition (Woodward et al., 2013), to growth arrest because of the frequent incidence of these resorption lines with non-cyclical rest lines. Accordingly, we consider these darks lines as LAGs. The fact that resorption in bones is restricted to marked cortical drifts indicates that this phenomenon is related to changes in shape. LAGs deposited

at the age of birth and weaning and associated to resorption result from reduced bone apposition triggered by these events combined with a concomitant biomechanical re-adjustment of shape. In some bones, especially in the radius, such biomechanical adjustments are not restricted to these events but happen throughout ontogeny, leading to deposition of several non-cyclical partial LAGs where the bone faces an adjacent bone (here ulna), which limits expansion in this area.

In addition to the histological changes associated with specific life history events, other variations in bone microstructure were observed. Though a bone tissue type can have different absolute growth rates, the factor "tissue type" has been found to have the strongest correlation with bone growth rate (de Margerie et al., 2004). Not surprisingly, hence, postnatal deposited fibrolamellar bone in our red deer calves varies importantly among skeletal elements. The slowest-growing tissue (longitudinal microarchitecture) is typically found in metapodials, while the fastest-growing tissue is found in tibiae where it frequently shows the unusual and rarely observed radial orientation, which has significantly higher growth rates than other fibrolamellar bone types (de Margerie et al., 2004; Pratt and Cooper, 2018). This agrees with the dissimilar growth pattern of limb bone length in which the distal segments grow slower after birth than the proximal segments (Starck and Chinsamy, 2002). Moreover, all bones showed internal variation, revealing different local apposition rates and indicating cortical drift toward a specific area depending on the bone, as corroborated the arrangement of the fluorescent labels. Bone drift activity can be also appreciated by the resorption processes occurred in the inner region of the bone (i.e. expansion of the medullary cavity) and the subsequent endosteal deposits of bone found from an early age in our sample. Despite the endosteal bone has been commonly described as a lamellar or parallel-fibered bone tissue (Chinsamy-Turan, 2005; de Buffrénil et al., 2021; de Margerie et al., 2002; Enlow, 1962a; Padian et al.,

2013), this work documents an endosteal bone mainly composed by FLC, suggesting fast rates of osteogenesis. Recently, Montoya-Sanhueza et al. (2021) have described in detail the patterns of bone remodelling in long bones of naked mole rat by using in vivo fluorescent labelling. However, the results obtained form that work and for another study including juvenile specimens (Montoya-Sanhueza et al., 2020) showed that the endosteal bone of this species was composed by lamellar tissue. This may due to the fact that these studies are focused in small-size mammals. Further research on the bone microstructure of large mammals is needed to shed light on this issue. Moreover, according to our findings, this structure formed early in ontogeny is partially resorbed after, highlighting the importance of research focused on the early stages of ontogeny in order to obtain the most complete record of information.

In summary, our labelling study provides, for the first time, a general pattern of juvenile bone growth rates in red deer calves, shows how weaning and different feeding regimes affect bone tissue formation and yields an estimate of the timing of non-cyclical LAG deposition. In this way, the results gathered here allow reconstructing ontogenetic bone growth patterns, provides a firm ground for inferences of growth rates for histological bone structures of hitherto unknown time intervals, and bridges the gap between bone histology and interpretations of life history strategies.

CHAPTER 6. **DISCUSSION**

The principal objective of this PhD thesis is to illustrate how bone in red deer develops during ontogeny and how different life history events and feeding regimes affect early growth. By analysing these factors, this thesis provides new insights into bone growth that contribute to the knowledge of ruminant bone histology. This goal has been addressed through two histological analyses: the first on different limb bones from individuals of different ages belonging to two subspecies of red deer, and the second on fluorochrome-labelled limb bones of calves from different feeding regimes. Calibrating the histological information with epiphyseal closure, dental eruption patterns and the known life history traits of the individuals of one of the subspecies here studied (e.g. birth date, weight, age at death, number of offspring) provide a firm foundation for comparisons with other groups of mammals as well as for the study of fossil species. Moreover, results from the labelling experiment provide important findings on the dynamics of early growth and the impacts of single life history events. This chapter discusses this dissertation's main findings. First, the chapter examines the primary outcomes of the ontogenetic analysis of the bone microstructure of red deer, emphasising its calibration with the known life histories of individuals from a captive population. Second, the chapter considers how life history traits vary according to factors such as age, sex, feeding regime, population and the occurrence of life history events, thus resulting in different growth patterns.

6.1. The study of red deer skeletal elements

6.1.1. Skeletal elements as indicators of age stages

Age stages have been established for red deer based on epiphyseal fusion (Mariezkurenna, 1983), dental eruption pattern (Brown and Chapman, 1991) and dental wear (Anders et al., 2011; Azorit, 2011), and these matched the known age of individuals in the *C. e. hippelaphus* population. Furthermore, as some morphological features such as the fused epiphyses of long bones and the eruption of the third molar are indicatives of skeletal maturity of the individual (Engström et al., 1983; Popkin et al., 2012), it was possible to estimate whether a particular individual had reached its adult size or was still in an immature developmental stage. It is noteworthy that the castrated males in our sample did not show a delayed pattern of epiphyseal fusion as have been reported in sheep (Davis, 2000).

It should also be noted that dental eruption patterns and the degree of epiphyseal fusion can only provide age estimations for a limited time until the adult size is reached. Moreover, these approaches, on their own, do not provide information about an individual's exact age but only allow for a rough attribution to a general age stage (Chinsamy-Turan, 2005; Hillson, 2005). The microstructural analysis of hard tissues, however, provides accurate information that is not available from the basic morphological examination (Padian, 2013).

6.1.2. Bone histology

The microstructure of ontogenetic series of bones has been widely studied in fossil groups (e.g. dinosaurs; Horner et al. 2000) with the purpose of understanding the process of bone development during an individual's

lifetime and to obtain key information about its life history. However, due to this bias towards fossil groups, some authors have expressed the need for ontogenetic studies of extant (and, if possible, wild) populations (Padian et al., 2013). Recently, there has been an increase in the number of ontogenetic studies of extant mammals such as ungulates (Jordana et al., 2016; Nacarino-Meneses et al., 2016b, 2016a; Nacarino-Meneses and Köhler, 2018; Smith, 2020), rodents (Montoya-Sanhueza et al., 2021, 2020; Montoya-Sanhueza and Chinsamy, 2017), marsupials (Chinsamy and Warburton, 2021) and xenarthrans (Heck et al., 2019). Life history information obtained from these studies is expected to contribute to improved conservation strategies for threatened species (e.g. Asiatic wild ass, Nacarino-Meneses et al. 2016a, b; addax, Marín-Moratalla et al., 2013b; and nine-banded armadillo, Heck et al. 2019) and also provide a foundation for life history inferences in fossil taxa (e.g. *Equus* genera; Nacarino-Meneses 2018). The present PhD dissertation aims to contribute to the understanding of bone development, with special emphasis on early life stages, through an exhaustive analysis of the limb bone microstructure of one of the most iconic species of extant deer, *Cervus elaphus*. However, in contrast to other histological studies of extant species, some of the histological traits here described were calibrated with an individual's life history events using fluorescence labelling. This method provides a firm and reliable basis for *Cervus elaphus* life history interpretation and its extrapolation to other ruminant species, both extant and fossil.

6.1.2.1. *Ontogenetic changes in bone microstructure*

The known ontogenetic ages of red deer individuals who provided this sample of femora and tibiae ranged from 15 days to >14 years. In addition, the fluorochrome labelling approach allows for bone growth monitoring during the first six months of life, providing detailed information on bone tissue

deposition during that time, including growth disruptions caused by life history events. Although fluorescent labelling has been widely used to obtain important insights in bone histology (e.g. to test the relationship between tissue type and bone growth rate; Castanet et al., 2000; de Margerie et al., 2004, 2002; Starck and Chinsamy, 2002, determine the reliability of skeletochronology; Buffrénil and Pascal, 1984; Castanet et al., 2004; Klevezal, 1996; Klevezal and Mina, 1984 and describe in detail bone remodelling processes; Montoya-Sanhueza et al., 2021), until now, this approach has not been used for in-depth studies on the bone growth dynamics of mammals during early ontogeny.

Perinatal apposition

Early in life, the cross sections of all of the limb bones analysed present a rounded shape and narrow bone cortex with a large medullar cavity. The bone tissue deposited before birth (assessed by fluorescent labels; see section 6.1.2.2.) shows a matrix mainly composed FLC with a high percentage of parallel-fibered bone, while after birth, the bone consists of an FLC matrix with a low percentage of parallel-fibered bone, a tissue often found in immature animals (Huttenlocker et al., 2013). This abrupt transition of tissue indicates a slow deposition rate during the prenatal interval followed by fast deposition rates after birth. This trend has also been observed in equids (Nacarino-Meneses and Köhler, 2018) and Elephantidae (Curtin et al., 2012), whereas the inverse pattern has been documented in reptiles before and after the hatching event (Chinsamy & Hurum, 2006; Hugi & Sánchez-Villagra, 2012).

As the bone grows, cortical bone thickness increases while the medullar cavity expands, destroying previously deposited tissues. In this way, the amount of prenatal tissue is reduced through ontogeny. However, unlike equids, in which the prenatal tissue is completely eroded during the subsequent postnatal stages (Nacarino-Meneses and Köhler, 2018), cervids

show remnants of prenatal tissue even in advanced growth stages. The expansion of the medullary cavity is especially noticeable in cervid metapodials because of the erosion of the antero-posterior column that separates third and fourth metapodials. In the perinatal stage, both metacarpal and metatarsal still exhibit the separation between the metapodials in the form of an antero-posterior central column consisting of reticular FLC, which is a remnant structure resulting from the fusion of the third and fourth metapodials (i.e. an artiodactyl feature). At 15 weeks of age, this column has been almost completely eroded by the expansion of the medullary cavity. This phenomenon has also been documented in giraffids (Smith, 2020).

The postnatal deposition of fibrolamellar bone exhibits different arrangement among skeletal elements, which, according to the strong correlation between tissue type and bone growth rate (de Margerie et al., 2004), reveals different absolute growth rates between limb elements. Thus, the slowest-growing matrix (i.e. the longitudinal orientation) is found in metapodials while the matrix arrangement of proximal elements is deposited at faster rates (e.g. the plexiform). Radial orientation, an unusual type of FLC that has the highest growth rates (de Margerie et al., 2004; Pratt and Cooper, 2018) is only found in tibiae, a particular feature also reported for giraffids (Smith, 2020). This arrangement has also been described in the tibiae of other extant and extinct deer genera (*Dama* and *Megaloceros*; Kolb et al. 2015). The arrangement of the FLC also varies within the bone, indicating that apposition of new bone does not occur in a symmetrical way along the cross-section, but that tissues within a bone grow at different rates depending on the area (e.g. the medial part of tibia grows slower than the anterior section). This irregular growth, together with the erosion and removal of the tissue in other areas of the bone, contributes to changes in the shape and size of the bone as the individual develops, a phenomenon termed "bone drift" (Chinsamy-Turan, 2005). The arrangement of the fluorescent labels within the tissue provides a

picture of asymmetrical bone apposition. In areas where tissue is deposited at slow rates (slow-growing areas), fluorescent labels appear tightly packed. In contrast, spaced labels denote regions where bone is rapidly deposited (fast-growing tissue). Fluorescent labels also permit the observation of the asymmetrical expansion of the medullary cavity, which follows a determinate pattern in each bone. In addition to these variations within the bone sections (i.e. anterior, posterior, medial and lateral), the FLC arrangement differs before and after key biological events. For instance, individuals weaned at the age of 13 weeks present an abrupt change from fast- to slow-growing bone just before and after the 13-week label. Vascular density, another indicator of growth rate (Lee, A. H., Huttenlocker, A. K., Padian, K. & Woodward, 2013), also reports significant changes from higher to lower densities before and after the weaning event, revealing a shift from faster to slower periosteal apposition.

According to the ontogenetic analysis of deer bone, secondary bone (i.e. bone deposited where the previous bone matrix has been resorbed; Francillon-Vieillot et al., 1990), is present in the limb bones of deer from an early age. Endosteal bone, a type of secondary bone deposited in the innermost cortex, is found in the radius and metapodials of red deer specimens as young as 3 days old. The histological analyses performed in this thesis demonstrated that, although this tissue grows centripetally, it is deposited early in ontogeny following the same pattern as primary bone (i.e. the FLC): a woven-bone scaffold starts to form and is subsequently refilled with lamellar tissue with different arrangements. This singular endosteal FLC pattern, which suggests fast rates of deposition, contrasts with the poorly vascularised lamellated endosteal bone that has been commonly described for vertebrates (de Buffrénil and Quilhac, 2021). Becker et al. (2020) have described endosteal deposits composed of FLC, such as the one described in this thesis, in the humerus of juvenile sheep from 13 to 33 months old. Alternatively, in a study discussing the histological changes during ontogeny in another ruminant species (*Giraffa;*

Smith, 2020), the author did not document FLC endosteal deposits in the two juvenile specimens analysed but observed resorption processes in the endosteal area and lamellar endosteal deposits in subadult and adult specimens. Given these results, it is possible to assume that this kind of fast deposited endosteal bone (i.e. the FLC) is associated with the early stages of ontogeny and is subsequently resorbed. This idea is supported by the labelling experiment performed here, which reveals how this structure, formed early in ontogeny, is partially resorbed shortly after deposition. This finding demonstrates how ontogenetic studies on early growth are important for obtaining complete ontogenetic information.

In the red deer sample studied in this dissertation, the deposition of Haversian bone (i.e. another type of secondary bone formed by the association of secondary osteons) started at 15 weeks of age; it first appears in the prenatal area, and as the individual's age increases, it expands towards the external surface of the cortex. The Haversian bone eventually occupies almost the whole cortex, as shown in the oldest deer in the sample, which hampers the identification of primary tissue and the presence of growth marks. The fact that this feature is restricted to particular areas depending on the bone could be attributed to the mechanical load. Some studies focused on the Haversian microstructure (Mayya et al., 2016; Zedda et al., 2015), have reported that this type of bone appears in areas of compressive stress in bovine and equine femora. Moreover, the distribution of Haversian systems could also be associated with shifts in muscle attachments during bone growth (Enlow, 1962b).

Sub-adult and adult apposition

Until the age of 23 weeks, bone deposition is only affected by non-cyclical events (Chapter 5). After this age (ca. 6 months), bone apposition shows the

first evidence of seasonal physiological cycles (chapter 4). As a result, in this sub-adult stage, deer bones are composed of bands of fibrolamellar tissue alternating with growth marks; (Klevezal, 1996). At the maximum age of 3.5 and 4.5 years in females and males, respectively (see section 6.2.), the EFS is deposited. None of the individuals in this sample shows an EFS in the tibia, a finding that agrees with a study on equids (Nacarino-Meneses et al. 2016). The appearance of this slow-growing structure in deer femora is associated with the eruption of the third lower molar as well as the epiphyseal fusion of all long bones analysed (Chapter 4). For these reasons, the EFS is here considered an indicator of red deer skeletal maturity (i.e. the individual has reached its adult size; Chapter 4) as has also been suggested for fossil cervids (Amson et al., 2015; Kolb et al., 2015a). However, other mammalian groups do not show this synchrony. For instance, in Asiatic wild ass, the deposition of the EFS occurs prior to the fusion of each epiphysis (Nacarino-Meneses et al., 2016a), while in nine-banded armadillo specimens patterns differ between individuals (Heck et al., 2019).

6.1.2.2. *Growth marks: Skeletochronology and timing of life history events*

Bone growth marks can be classified as cyclical or non-cyclical depending on whether the event is periodic o non-cyclic, respectively (Castanet et al., 1993; Woodward et al., 2013). Both photoperiod (Castanet et al., 2004) and seasonal environmental cycles of resource availability (Köhler et al., 2012) play an important role in the deposition of bone, which record seasonal physiological cycles of hypometabolism during the unfavourable season (winter in the case of red deer). These cyclical growth marks allow histologists to develop skeletochronological analyses and infer the timing of life history traits, including age at maturity or age at death. Bone deposition can also be affected

by single events, such as birth or hatching, and also by resorption processes. It is important to differentiate between these types of growth marks to avoid errors in skeletochronological studies.

Cyclical growth marks

Due to their annual periodicity, the total number of cyclical growth marks in a bone is expected to provide the individual's age at death. Jordana et al. (2016) stated this was true for ruminants in a study based on thes femora of wild individuals of unknown age. However, a crosscheck of the number of cyclical marks recorded in individuals of known ages does not fully support this assertion for red deer (Chapter 4).

The aged material (i.e. specimens from the *C. e. hippelaphus* subspecies) reveals that the number of cyclical growth marks within the FLC of both the tibia and femur of sub-adult individuals matches the individual's age, while the EFS (which, as indicated above, is only present in femora) is not a reliable structure for skeletochronological analyses. Some of the individuals of known age that presented EFSs have a larger number of cyclical marks than expected for their age, indicating that after skeletal maturity is reached, growth slows down and ceases more frequently than at earlier stages. In other cases, the total number of cyclical growth marks underestimates the age of the individual, which indicates that from a certain age onwards, bone tissue is no longer deposited. Although the growth marks recorded in the FLC suggest that femur and tibia are equally useful for skeletochronological studies, there are some noteworthy differences to consider. In the femur, a maximum of five growth marks was found in the FLC before the formation of the EFS. In contrast, the tibiae of some adult individuals (i.e. those with fused epiphyses and third molar erupted) showed up to eight cyclical growth marks in the FLC but did not yet develop an EFS. The absence of EFSs in the tibiae, together with the

variation of cyclical growth marks between bones, aligns with findings on equids (Nacarino-Meneses et al. 2016). It is still unknown whether the EFS is never deposited in the tibiae of deer or whether it takes longer to be deposited, as Heck et al. (2019) has found for armadillos. To clarify this issue, it would be useful to analyse the tibiae of older specimens to determine if the EFS appears at some point. With the data available thus far, one can conclude that, in deer, the tibia is very useful for estimating the age at death, while the femur is a strong indicator of the age at maturity.

Non-cyclical growth marks

As red deer births take place throughout May and June, the first cyclical growth mark is expected to appear at the age of six months, coinciding with the calves' first winter. However, the detailed analysis of the firsts ontogenetical stages reveals two growth marks before this age, which must therefore be related to non-cyclical events.

The labelling results corroborate previous findings that show that the first growth mark deposited in red deer limb bones corresponds to the birth event. This birth or neonatal line, homologous to the neonatal line found in teeth (Smith et al., 2006), was first identified and described in limb bones through the superimposition of bone sections of aged *Equus* individuals, evincing the association between this non-cyclical growth mark and the birth event in mammals (Nacarino-Meneses and Köhler, 2018). In red deer, the neonatal line was found in all six limb bones analysed. However, depending on the bone and the area of the bone cortex (e.g. the anterior), the mark was distinguishable as either a LAG or an annulus. These two features are indicative of different types of growth disruptions (an arrest of growth [LAG] or a slow-down in the growth rate [annulus]), suggesting that not all long bones within an individual, nor all of the areas within the same bone cortex,

respond to the birth event uniformly. This result supports previous findings that tissue growth rates vary both within and among bones (Chapter 5). In addition to the formation of the annulus or LAG, the transition from pre- to postnatal tissue is marked by the abrupt change of tissue, as previously mentioned.

Some authors have speculated on the origin of another early non-cyclical mark found in mammalian bones. A dark band found in the jawbones of hedgehogs was interpreted as a reduction in growth caused by food disruption associated with weaning (Morris, 1970). Castanet et al. (2004) later described a discontinuity in the inner part of the long bones of a small primate. These authors decided to not use this growth mark for age estimation since, based on the date of deposition, they supposed that it might indicate the weaning event. In another skeletochronological study, Barker et al. (2003) discounted a dark line found in the bones of yellow-pine chipmunks. However, the authors did not provide any explanation of the possible origin of that line, which, as researchers now speculate, could be caused by weaning. The results from labelling the red deer corroborate that this second early growth mark, mainly present in hand-raised individuals (C2), corresponds to the weaning process. Recently, the weaning event (among other physiological events) has also been documented in macaque dental microstructures (cementum; Cerrito et al., 2021). In addition to corroborating the presence of a weaning line in the limb bones of deer, the arrangement of labels reveals key information concerning the amount of time represented by the weaning LAG in this species. These structures depict a growth arrest of up to two weeks, although the amount of time may vary according to the area of the cortex. Moreover, the transition from the pre- to post-weaning period is marked by the shift in the osteon orientation and the decrease in the density of vascular canals, as previously described.

Additional non-cyclical growth marks, not triggered by life history events but formed by cortical resorption, are described in this thesis. These marks, generally termed "dark lines", are attributed to temporary changes in bone deposition (Woodward et al., 2013) and are often associated with changes in the shape of the bone (i.e. bone drift). In deer, the radius offers an excellent example of bone drift, as it shows the deposition of several non-cyclical partial LAGs in the area where another bone (the ulna) limits expansion. In some cases, these lines seem to be associated with birth and weaning marks, which indicate resorption processes linked to growth arrest events.

The microstructural analyses of bone tissue reveal that the expression of growth marks within long bones varies according to growth rate: the slower the rate, the easier the formation of growth marks. Non-cyclical growth marks corresponding to birth and weaning were not recorded along the entire bone cortex but were restricted to slow-growing areas. Moreover, the first cyclical mark (corresponding to the age of six months) appeared as either a slightly recorded LAG or as an annulus and is conditioned by the particular rapid growth rate of this early stage (Woodward et al., 2013). It has been suggested (Horner et al., 2000b; Padian et al., 2001) that the absence of cyclical marks in juvenile dinosaurs were triggered by similar causes.

6.2. Growth dynamics

The incremental records of growth within the bone tissue allow for the reconstruction of growth curves. For the deer analysed here, growth reconstruction was obtained by plotting the areas contained in each of the growth marks (mm^2) against the age at deposition (e.g. neonatal line = time zero, first cyclical mark = 6months and so on; Chapter 4) or, for labelled individuals, by plotting the areas of each label against the day of labelling

(Chapter 5). This quantitative analysis of bone microstructure provides data on one of the most important life history traits: growth rate. In general terms, the results from deer match the typical mammalian growth trend in which the juvenile stage is characterised by high rates of bone deposition that gradually decrease with ontogeny until the adult stage is reached. As explained in previous sections, histologically, these periods of high and low growth rates correspond to the deposition of fibrolamellar bone (i.e. the FLC) and the deposition of an EFS, respectively. This shift produces an asymptotic growth curve, in which the linear part corresponds to high juvenile deposition rates. At a particular age, which varies according to the sex of the individual (see below), the growth rate decreases and linear growth reaches a plateau (Lee et al., 2013). A correct interpretation of growth requires two main factors: an ontogenetic record that is as complete as possible and a strong knowledge of the life history of the species. Otherwise, misinterpretations could arise, as evinced by Lee et al. (2013) documentation of the false "indeterminate growth" attributed to crocodilians, which was caused by incomplete sampling.

Most mammals and birds follow a common growth trajectory in which, according to von Bertallanffy (1957) "growth rates are decreasing and growth eventually attains a steady state". However, growth is also conditioned by particular physiological and life history features (see below) and, therefore, a specific growth pattern cannot be directly applied to other taxa without previous studies (Lee et al., 2013). For instance, in red deer, different long bones exhibit different growth patterns. When the femur reaches the growth asymptote (i.e. when it experiences a considerable reduction in growth rate), the tibia is still growing, which explains why there are more cyclical growth marks than expected in the FLC of tibiae. These patterns are conditioned by the way growth rates decline with age in both bones. While femora display a gradual decline with age, tibiae show an abrupt decline followed by a continual low rate of deposition (Fig. 4C, Chapter 4).

It is important to distinguish between skeletal, sexual and reproductive maturity. While skeletal maturity is reached when an individual has completed its growth, sexual maturity indicates the maturation of reproductive organs and the production of gametes. Finally, reproductive maturity indicates the age at which an individual is capable of producing offspring. These events are not necessarily synchronous and may occur separately. In contrast to skeletal maturity, which is associated with the deposition of an EFS in the femur, sexual and reproductive maturity do not seem to be linked to any histological feature and cannot be inferred from microstructural analysis, at least for red deer. According to the literature, red deer females can give birth as early as 2 years of age (Carranza, 2017). This finding is supported by the fact that most of the hinds in the semi-wild population of *C. e. hippelaphus* here analysed gave birth to their first calf at the age of 3 years. On the other hand, studies focused on red deer biology reported that males reach sexual maturity at the age of 3 years, (in Spain; Carranza, 2007) while their first reproduction occurs between 5 and 7 years of age (in Scotland; Clutton-Brock et al., 1983; Ibler and Fischer, 2016). These ages, correspond to the inflection point of the growth curve projected from the red deer sample studied here, which graphically represents the shift from the rapid growth typical of the juvenile stages to a stage characterised by low growth rates. In other words, the available resources that are invested in growth during the juvenile stage are channelled towards reproduction when maturation is reached, leading to a marked slow-down in growth (i.e. a trade-off between growth and reproduction; Stearns 1992). Taking these findings into account, it is possible to conclude that, in deer, skeletal maturity (determined by the completion of the dental eruption pattern, the epiphyseal closure both in the tibia and femur and the deposition of the EFS in the femur) occurs slightly after reproductive maturity, as previously suggested for most vertebrates (Lee et al., 2013).

The results obtained in this dissertation show that males and females reach maturity at different times. This phenomenon, called bimaturism, is common in polygynous species, including various species of ungulates and primates (Stearns, 1992). The phenomenon of bimaturism can be inferred from growth curves as hinds and stags reach the asymptote of their growth curve (i.e. the attainment of skeletal maturity) at 3.5 and 4.5 years, respectively. For males, this study found that skeletal maturity occurs more than one year earlier than Jordana et al. (2016) estimated. Males' extended growth period and delayed maturity confer dominance in intraspecific competition, whereas females have shorter growth periods, as they invest in reproduction (Stearns, 1992).

In addition to the different growth patterns explained thus far, this dissertation illustrates growth differences between the two analysed subspecies from Central Europe (*C. e. hippelaphus*) and the Iberian Peninsula (*C. e. hispanicus*). These differences may be influenced by multiple factors. First, these subspecies constitute two distinct lineages that originated in different glacial refugia (the Iberian and the Balkan/Carpathian; Skog et al., 2009b; Zachos and Hartl, 2011). Second, the *C. e. hispanicus* population lives in wild conditions, while the *C. e. hippelaphus* subspecies receives feeding support and proper veterinary care, which could lead to differences in growth patterns between them (Dmitriew, 2011). Finally, these subspecies belong to separate geographical regions with different climates and resources, which may cause body size variations according to Bergmann's rule (McNab, 2010; Rosvold et al., 2014). Moreover, each of the subspecies shows intra-group variations. The variability of growth curves within the *C. e. hippelaphus* population could result from the captivity regime that has been maintained for several generations. This idea is supported by a study that showed morphological variations developed in foxes living in captivity within a few generations (Trut 1999). On the other hand, growth variations among the *C. e. hispanicus* populations of

Lleida and Badajoz might be attributed to their different habitats and management. The slightly lower bone growth rates shown by members of the Lleida population compared to those of the Badajoz population could be explained by the fact that specimens from Lleida lived in a temperate forest consisteing of a native environment with poor nutritional conditions (Popkin et al., 2012), while individuals from Badajoz inhabit Mediterranean forests or *dehesas* (a human-modified Mediterranean forest) with a possible food support from hunting managers to ensure the persistence of the deer population (Olea and Miguel-Ayanz, 2006).

Cyclical growth marks on bones allow growth rates to be calculated in large (generally annual) intervals and provide information on general bone growth trajectories. However, the fluorescent study, which offered a detailed analysis of growth rate, reveals that the decrease in growth rate with age is not gradual but undergoes some variations. During early growth, bone growth rate is affected by disruptions caused by the birth and weaning events. These disruptions produce abrupt changes in growth rates, giving rise to a 4-stage pattern in the six bones analysed: birth (three days of growth decrease/arrest), the period between birth and weaning (vigorous growth), weaning (growth decrease/arrest for 1 to 2 weeks) and post-weaning (modest growth resumption). As described above, these disruptions can be recognised histologically, despite a large inter- and intra-bone variability, and by the recording of non-cyclical growth marks.

The results here presented further show how the weaning event for hand-raised individuals (C2) affects the body mass of the individual, reducing or even inhibiting body weight gain for an interval of 4 weeks. The effects of birth on bone tissue can be observed in the skeletal elements of all calves analysed in this study. However, the fact that the weaning line (and the associated tissue changes) is more noticeable in hand-raised (C2) individuals suggests that growth differences are caused by nutritional conditions. It is

likely that such differences are due to the artificial weaning experienced by the hand-raised group. As in all ruminant artiodactyls, the digestive system of red deer calves changes during early life. Rumen development is highly conditioned by the gradual addition of vegetal material during the pre-weaning period. Once the rumen is fully developed and functional (i.e. around 12 weeks), calves are able to feed entirely on vegetal material (Teagasc, 2017). Although this experiment aimed to recreate natural weaning conditions in hand-raised deer, it is possible that this shift did not occur as smoothly as in naturally weaned calves. Therefore, the rumen might not have developed completely, negatively affecting the absorbance of vegetal food at the time of artificial weaning and possibly resulting in a marked growth disruption. The different pre-weaning feeding regimes (i.e. the mother's milk for the C1 calves and milk replacer for the hand-raised calves) might also affect growth. The powdered milk used to feed the hand-raised calves was richer in nutrients than natural deer milk (Landete-Castillejos et al., 2000; Wang et al., 2017). This high energy diet most likely led to a fast periosteal bone apposition, generating a highly vascularised matrix in hand-raised animals. This notion is supported by various studies in piglets which have demonstrated that milk replacer accelerates growth rate. It is also worth noting that accelerated growth triggered by a high nutrient diet of powdered milk during the pre-weaning stage also has future consequences for the individual's life cycle (e.g. positive affecting mating success [Clutton-Brock et al., 1982; Festa-bianchet et al., 2000] and negatively affecting longevity [Ozanne and Hales, 2005; Van Eetvelde and Opsomer, 2017]).

The impact of early life history events on bone growth presented here provide key information, hitherto unknown, of the dynamics of growth at early ontogenetic stages. However, many questions remain to be answered. For instance, it was not possible to perform periodic labelling or weight measurements in naturally weaned calves (C1) because of their untamed

behaviour. A comprehensive study providing such data would offer a better understanding of the disruptions caused by weaning in deer living under natural conditions. It would also be useful to perform similar analyses in other wild ruminant subspecies, as well as in other groups of mammals with different feeding strategies, to improve the scientific knowledge of weaning effects on bone under different circumstances.

In summary, the histological analysis of extant deer bones bridges the gap between bone microstructure studies and strategies for interpreting life histories. Calibrating the results with known life history traits from a semi-wild population and using fluorochrome labelling during early life has allowed reliable ontogenetic bone growth patterns to be reconstructed. These findings contribute to a deeper understanding of how growth is modulated not only by ontogeny but also by sexual and environmental factors, providing a solid foundation for more accurate interpretations of other taxa.

CHAPTER 7. **CONCLUSIONS**

i. The histological analysis of the ontogenetic series revealed that in the initial stages of growth, bone tissue begins to be deposited at high rates, forming an FLC. It is possible to differentiate the tissue formed during the pre- and postnatal stages based on the percentage of lamellar fibres, which is higher before birth. During the juvenile stage, bone is composed of an FLC with different osteon orientations, which vary depending on the bone and the location within the bone. Secondary bone appears early in life as Haversian systems, which first form in the prenatal area and expand towards the outer cortex as the individual grows older, and an endosteal bone that shows FLC-like scaffolding. At a certain age, the FLC is no longer deposited, and a slow-growing tissue called the EFS appears in the femora. The appearance of the EFS in the femora occurs at the same time as the fusion of the epiphyses (both in the femora and tibiae) and the complete dental eruption, which is indicative that skeletal maturity has been reached.

ii. The limb bones of red deer contain both cyclical and non-cyclical growth marks. Prior to the age of 6 months, deer bones record non-cyclical lines associated with birth and weaning. After this age, coinciding with the first winter of the calf, cyclical growth marks begin to be recorded. Bones with marked bone drift (i.e. changes in bone shape) also reveal non-cyclical marks not associated with events that are formed by cortical resorption.

iii. In red deer, the sum of the cyclical growth marks does not always provide information about the age of the individual. Prior to the deposition of the EFS, the number of cyclical marks contained within the

FLC matches the individual's age. Once the EFS is deposited, the number of cyclical growth marks within the FLC indicates the age at skeletal maturity. Growth marks enclosed in the EFS, however, can lead to misinterpretations of the individual's age and should not be used in skeletochronological studies.

iv.   The reconstruction of growth curves based on the areas of cyclical growth marks reveals fast linear growth that corresponds to the sub-adult stage, which decreases abruptly and ends in an asymptote when skeletal maturity is reached. Furthermore, in deer, the age of reproductive maturity corresponds to the inflection point of the growth curve, indicating that the available resources that were invested in growth during the juvenile stage are allocated for reproduction when maturation is reached, leading to a marked slow-down in growth (i.e. a trade-off between growth and reproduction).

v.   Hinds and stags exhibit different growth patterns, as they reach the asymptote of the growth curve (i.e. attain skeletal maturity) at different times, a phenomenon called bimaturism. This phenomenon is common in polygynous species, in which males display an extended growth period and delayed maturity to attain dominance in intraspecific competition, whereas females invest in reproduction.

vi.   The labelling approach here employed provides detailed information on the growth dynamics of early in life and on the duration of growth disruptions for the first time. During the first six months, bone growth rate is disrupted by both birth and weaning, leading to a 4-stage growth pattern: birth, the period between birth and weaning, weaning and post-weaning.

vii.   At a microstructural level, birth and weaning events are represented by non-cyclical growth marks (either a LAG or an annulus) as well as by

shifts in the type of FLC. Qualitative and quantitative differences in the recording of growth marks and canal density during the pre-weaning period in hand-raised and mother-reared individuals reveal that the effects of the weaning event on bone are modulated by the individual's nutritional regime.

CHAPTER 8. APPENDIX

8.1. Chapter 4 appendix
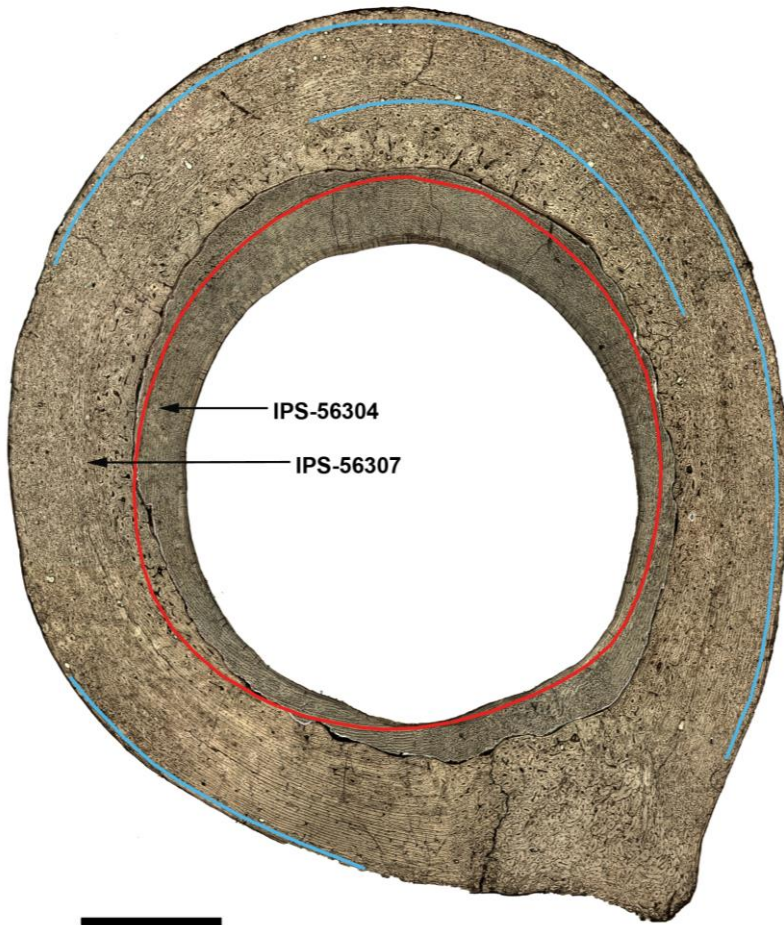
Figure S8.1. Superimposition of femora of 13 years old (IPS-56307) and 5 years old females (IPS-56304). Red line indicates the first CGM lost by the expansion of the medullar cavity. Blue lines are two CGM partially eroded within FLC. Scale bar: 2mm. Figure obtained from Calderón et al. (2019).

ID	Subspecies	Location	Sex group	Year of birth	Year of death
IPS-56303	C. e. hippelaphus	Vienna,A	Female	2006	2011
IPS-56304	C. e. hippelaphus	Vienna,A	Female	2006	2011
IPS-74171	C. e. hippelaphus	Vienna,A	Female	1998	2011
IPS-56306	C. e. hippelaphus	Vienna,A	Female	2007	2011
IPS-56307	C. e. hippelaphus	Vienna,A	Female	1998	2011
IPS-56308	C. e. hippelaphus	Vienna,A	Male	2011	2011
IPS-106838	C. e. hippelaphus	Vienna,A	Malec	2011	2016
IPS-106839	C. e. hippelaphus	Vienna,A	Male	2015	2016
IPS-106840	C. e. hippelaphus	Vienna,A	Male	2015	2016
IPS-106841	C. e. hippelaphus	Vienna,A	Malec	2011	2016
IPS-106842	C. e. hippelaphus	Vienna,A	Male	2015	2016
IPS-106843	C. e. hippelaphus	Vienna,A	Male	-	2017
IPS-109289	C. e. hippelaphus	Vienna,A	Male	2017	2017
IPS-60869	C. e. hispanicus	Badajoz,SP	Female	-	2013
IPS-60870	C. e. hispanicus	Badajoz,SP	Male	-	2013
IPS-60871	C. e. hispanicus	Badajoz,SP	Male	-	2013
IPS-60872	C. e. hispanicus	Badajoz,SP	Male	-	2013
IPS-60873	C. e. hispanicus	Badajoz,SP	Male	-	2013
IPS-60874	C. e. hispanicus	Badajoz,SP	Female	-	2013
IPS-60875	C. e. hispanicus	Badajoz,SP	Male	-	2013
IPS-60876	C. e. hispanicus	Badajoz,SP	Female	-	2013
IPS-60877	C. e. hispanicus	Badajoz,SP	Male	-	2013
IPS-60878	C. e. hispanicus	Badajoz,SP	Female	-	2013
IPS-83490	C. e. hispanicus	Lleida,SP	Female	-	2013
IPS-83491	C. e. hispanicus	Lleida,SP	Female	-	2013
IPS-83492	C. e. hispanicus	Lleida,SP	Female	-	2013
IPS-83503	C. e. hispanicus	Lleida,SP	Male	-	2013
IPS-83505	C. e. hispanicus	Lleida,SP	Male	-	2013
IPS-83506	C. e. hispanicus	Lleida,SP	Male	-	2013
IPS-83507	C. e. hispanicus	Lleida,SP	Male	-	2013
IPS-83513	C. e. hispanicus	Lleida,SP	Male	-	2013
IPS-62075	C. e. hispanicus	La Rioja,SP	Female	-	2013

Table S8.1. General information about the entire sample of *Cervus elaphus.*

126

ID	Subspecies	Location	Sex group	Weight (kg)	Known age (Years)	Femora		Tibiae	
						FLC	EFS	FLC	EFS
IPS-56303	HIP	Vienna,A	Female	104	5	3	4	-	-
IPS-56304	HIP	Vienna,A	Female	94.5	5	3	3	-	-
IPS-74171	HIP	Vienna,A	Female	133	13	3*	6	-	-
IPS-56306	HIP	Vienna,A	Female	95	4	3*	2	-	-
IPS-56307	HIP	Vienna,A	Female	148.5	13	3*	6	-	-
IPS-56308	HIP	Vienna,A	Male	56	0.91	1	0	-	-
IPS-106838	HIP	Vienna,A	Malec	225	5	5	0	5	0
IPS-106839	HIP	Vienna,A	Male	116	1.17	1	0	1	0
IPS-106840	HIP	Vienna,A	Male	117	1.08	1	0	1	0
IPS-106841	HIP	Vienna,A	Malec	210	5	5	0	5	0
IPS-106842	HIP	Vienna,A	Male	127	1.25	1	0	1	0
IPS-106843	HIP	Vienna,A	Male	-	-	5	5	7	0
IPS-109289	HIP	Vienna,A	Male	79	0.58	0	0	0	0
IPS-60869	HIS	Badajoz, SP	Female	-	-	3	3	-	-
IPS-60870	HIS	Badajoz, SP	Male	-	-	2	0	-	-
IPS-60871	HIS	Badajoz, SP	Male	-	-	5	0	-	-
IPS-60872	HIS	Badajoz, SP	Male	-	-	4	3	-	-
IPS-60873	HIS	Badajoz, SP	Male	-	-	4	0	-	-
IPS-60874	HIS	Badajoz, SP	Female	-	-	3	2	-	-

IPS-60875	HIS	Badajoz, SP	Male	-	-	4	3	-	-
IPS-60876	HIS	Badajoz, SP	Female	-	-	1	0	-	-
IPS-60877	HIS	Badajoz, SP	Male	-	-	4	4	-	-
IPS-60878	HIS	Badajoz, SP	Female	-	-	1	0	-	-
IPS-83490	HIS	Lleida,SP	Female	-	-	-	-	1	0
IPS-83491	HIS	Lleida,SP	Female	-	-	0	0	0	0
IPS-83492	HIS	Lleida,SP	Female	-	-	0	0	0	0
IPS-83503	HIS	Lleida,SP	Male	-	-	4	0	4	0
IPS-83505	HIS	Lleida,SP	Male	-	-	3	0	3	0
IPS-83506	HIS	Lleida,SP	Male	-	-	0	0	0	0
IPS-83507	HIS	Lleida,SP	Male	-	-	1	0	1	0
IPS-83513	HIS	Lleida,SP	Male	-	-	-	-	8	0
IPS-62075	HIS	La Rioja,SP	Female	-	-	3	3	-	-

Table S8.2. Available data of subspecies of Cervus elaphus and number of LAGs in both the fibrolamellar complex and the external fundamental system. HIP: *Cervus elaphus hippelaphus;* HIS: *Cervus elaphus hispanicus.* Table obtained from Calderón et al. (2019).

8.2. Chapter 5 appendix

8.2.1. Detailed histological description

8.2.1.1. Perinatal growth

Femur

Few days after birth, the cross-section is rounded with a narrow compact bone bordering a large medullary cavity. Most of the bone cortex, composed of primary bone, has been formed before birth, resulting in a disorganized matrix of prenatal fibrolamellar complex (FLC) with a high amount of parallel-fibered bone (PFB). The tissue within the prenatal tissue is mainly reticular except for the postero-medial and, inversely, for the antero-lateral regions. In these areas the bone tissue shows plexiform and longitudinal arrangments, respectively. After birth, the femur area increases towards the antero-medial part. Postnatal tissue is barely deposited in the postero-medial sector of the bone. In the subsequent days FLC is deposited following a pattern of plexiform orientation.

Humerus

A narrow bone cortex of mainly disorganized prenatal tissue with high proportion of primary PFB (Fig. S8.2a), encloses a large medullary cavity. The tissue shifts from reticular to a plexiform/reticular in the medial and lateral sectors during prenatal growth and barely increases in area after birth. The small area of postnatal tissue is deposited towards the posterior part.

Tibia

At this early age, the bone shaft is quite rounded and is almost entirely composed of prenatal tissue with FLC matrix. In the prenatal area, the FLC alternates between reticular and plexiform, showing a more organized pattern towards the outer part of the antero-medial sector of the bone. Some dispersed

radial canals are discernible in the lateral part (Fig. S8.2b). The cortical apposition of postnatal bone is arranged asymmetrically. Abundant bone is deposited towards the lateral portion. At the opposite site, the postnatal tissue forms an extremely thin band. The FLC in this area is plexiform/reticular.

Radius

The cross-section of this bone shows an elongated shape with considerable cortical thickness along the antero-posterior axis. Most of the cortex is composed of prenatal tissue. In the inner part of the medial portion the bone tissue is reticular. Afterwards, as FLC increases in area, the FLC becomes plexiform. The rest of the bone shows FLC with plexiform/reticular arrangement except for the postero-lateral sector, which presents plexiform/laminar arrangement. Postnatal bone is deposited only anterior and posteriorly with a plexiform/reticular pattern. The endosteal bone starts to deposit at the third day of life both in the anterior and posterior areas of the shaft. This tissue is separated from the primary bone by a cement line. A scaffold of woven bone forms this new tissue centripetally.

Metapodial bones

Metapodials are characterized by a rounded shape of two lobes separated from each other by a column in the centre of the medullary cavity. Most of the cortex is formed by prenatal reticular FLC that locally shifts to a plexiform as new bone is deposited. There is only little postnatal apposition towards the lateral side. In both metapodials, the endosteal bone starts to deposit on the 3rd day in the anterior half of the bone. From here on, a scaffold of woven bone is deposited centripetally thus reducing the area of the two semi-medullar cavities. In the metatarsus, a thin layer of lamellar bone precedes the woven scaffold.
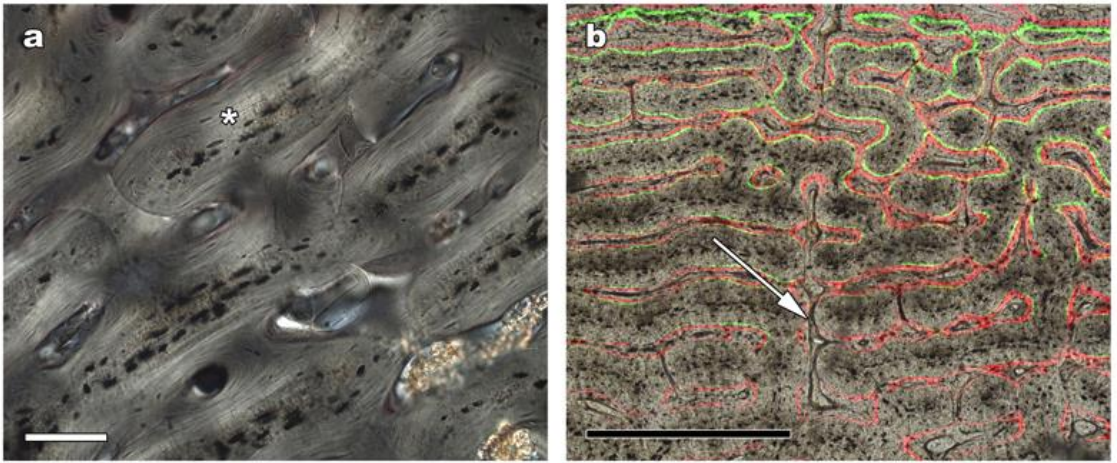
Figure S8.2. Histological details of the 15 days old individual ID-1 / IPS-88714 under polarized light (a) and fluorescent light (b). Images are oriented with the medullary cavity (MC) towards the inferior part and outermost cortex (OC) towards the superior side unless specified. (a) High proportion of PFB (asterisk) in the prenatal part of the humerus. (b) Detail of the radial canals (white arrow) in the prenatal tissue of the tibia. Black scale: 500 micrometres. White scale: 100 micrometres. Figure obtained from Calderón et al. (2021).

8.2.1.2. *Growth before weaning*

Femur

At the age of 15 weeks, the shape of the cross section still is quite rounded, but the linea aspera is identifiable in the postero-medial sector. At this stage, the area of postnatal tissue increases while the prenatal area has been eroded by the expansion of the medullary cavity (Fig. S8.3a). This expansion is more pronounced in the postero-medial sector, where the tissue formed before the third day of life has been partially deleted. As the area of postnatal tissue increases, the FLC becomes somewhat more organized: from an early plexiform/reticular orientation (from 3 to 30 days of life) to a plexiform or even plexiform/laminar organisation in the outer cortex (from 30 days to 15 weeks). In addition to this shift, tissue shows a compressed arrangement between days 3 and 30. The short distance between labels in the medial area reveals the slow growth of the tissue in this sector. There is scarce deposition of tissue from weeks 13 to 15 in all sectors. At the age of 15 weeks there is no formation of new scaffold, but tissue is deposited within the scaffold previously formed. In general, the pattern is more organized towards the medial and posterior sectors, except for the linea aspera, which shows a reticular orientation. In this area, a few cavities formed at 13 weeks are refilled with secondary bone in the two subsequent weeks.

Humerus

The prenatal tissue is practically non-existent in the posterior and postero-lateral areas due to the considerable directional expansion of the medullary cavity. There is a greater amount of cortical apposition towards the posterior and medial sectors than in the rest of the bone, resulting in a wider separation of the labels. By contrast, labels are closer spaced within the antero-medial

region. Bone tissue shows a great variability of FLC types: longitudinal in the antero-lateral part, plexiform in the posterior one and a band of laminar oriented canals is deposited in the outer part of the lateral and medial sectors. As occurs in the femur, bone is deposited in a more compact manner during the interval between 3 and 30 days of life than in the other intervals. There is no increase of bone area in the lateral portions between weeks 13 to 15. However tissue is deposited within the inner cavities of the previously formed scaffold. At this age, an incipient endosteal bone composed of lamellar tissue is deposited in the antero-medial region.

Tibia

The expansion of the medullary cavity towards the lateral part has partially eroded the perinatal bone. The labels evidence increased bone apposition on the lateral side. As a result, the proportion of pre- and postnatal tissue varies over the shaft. In the antero-medial portion, the prenatal tissue formed by reticular FLC still predominates in most of the area, while the lateral part is almost entirely formed by postnatal tissue. The organisation of the postnatal FLC varies depending on the bone area. Within the lateral portion of the shaft a significant amount of plexiform tissue has been deposited between the labels. The interval from 3-30 days shows higher compactness than the rest of the deposition. There is a marked bone drift in the anterior and medial parts of the tibia between pre- and postnatal tissue. In a small portion of these anterior and medial areas, bone deposited between 3 and 30 days has been resorbed, leaving a scalloped surface delimited by a line (these lines are associated to particular areas that show cortical drift and sometimes bone resorption; Fig. S8.3b). Newly deposited tissue shows a laminar orientation with a lower degree of compactness than in the rest of the bone (Fig. S8.3c). Bone apposition between weeks 13 to 15 is only observable in the lateral area of the tibia (i.e. new scaffold is formed at this age). At this stage secondary bone starts to form. A scaffold of woven bone builds the endosteal bone and incipient Haversian systems appear

in the antero-medial sector. According to the labels, both structures started to form some time before the age of 13 weeks and began to refill until the death of the individual after the 15th week.

Radius

The expansion of the medullary cavity through the anterior and posterior areas has deleted a small portion of prenatal tissue and the endosteal bone deposited at previous stages. Cortical apposition of bone also follows this asymmetrical trend. At the age of 3 days, there is no periosteal growth in antero-posterior direction. Bone is deposited within the cavities of the prenatal scaffold and also within the annulus that delimitates the prenatal tissue (Fig. S8.3d). The subsequent deposition of FLC follows a plexiform/reticular arrangment, but between days 3 to 30, bone is deposited with a higher degree of compactness than in previous and posterior intervals. Moreover, an area of reticular bone appears in the posterior sector. In a small section of the medial part the tissue deposited between 3 and 30 days has been resorbed and a line limits the area. Afterwards, FLC is deposited following laminar orientation. There is no increase of bone area in the lateral portions between weeks 13 to 15. At the age of 30 days, the endosteal bone starts to form at the medial side of the radius. This structure is formed by longitudinal and reticular FLC with some areas of highly organized and non-vascular tissue. Incipient Haversian systems appear in the medial part of the prenatal tissue. Cavities formed at 13 weeks are refilled with new tissue in the subsequent weeks.

Metapodial bones

At this stage, the expansion of the medullary cavity has removed completely the central column of the metatarsus, although this structure is still visible in the metacarpus. The postnatal tissue is deposited mainly towards the posterior sector both in metacarpus and metatarsus. The principal tissue fund is reticular FLC, with some small plexiform/laminar areas in the anterior and posterior

sectors. The label arrangement emphasises the scarce lateral and medial tissue apposition between days 3 and 30. In the postero-lateral sector of the metatarsus, the tissue formed during this interval has been resorbed and a line can be distinguished (Fig. S8.3e). A broad band rich in lamellar tissue appears along the outer part of the line. There is hardly bone apposition between 13-15 weeks. At this age, bone is only deposited within the cavities left by the previous scaffold. The endosteal bone, still present since its early formation, continued refilling the woven bone matrix following a longitudinal pattern throughout the cortex but the posterior sector (Fig. S8.3f). In the postero-lateral and the posterior-medial sectors of both metapodials, Haversian systems started to form at 13 weeks by actively refilling the cavities at the age of 15 weeks.
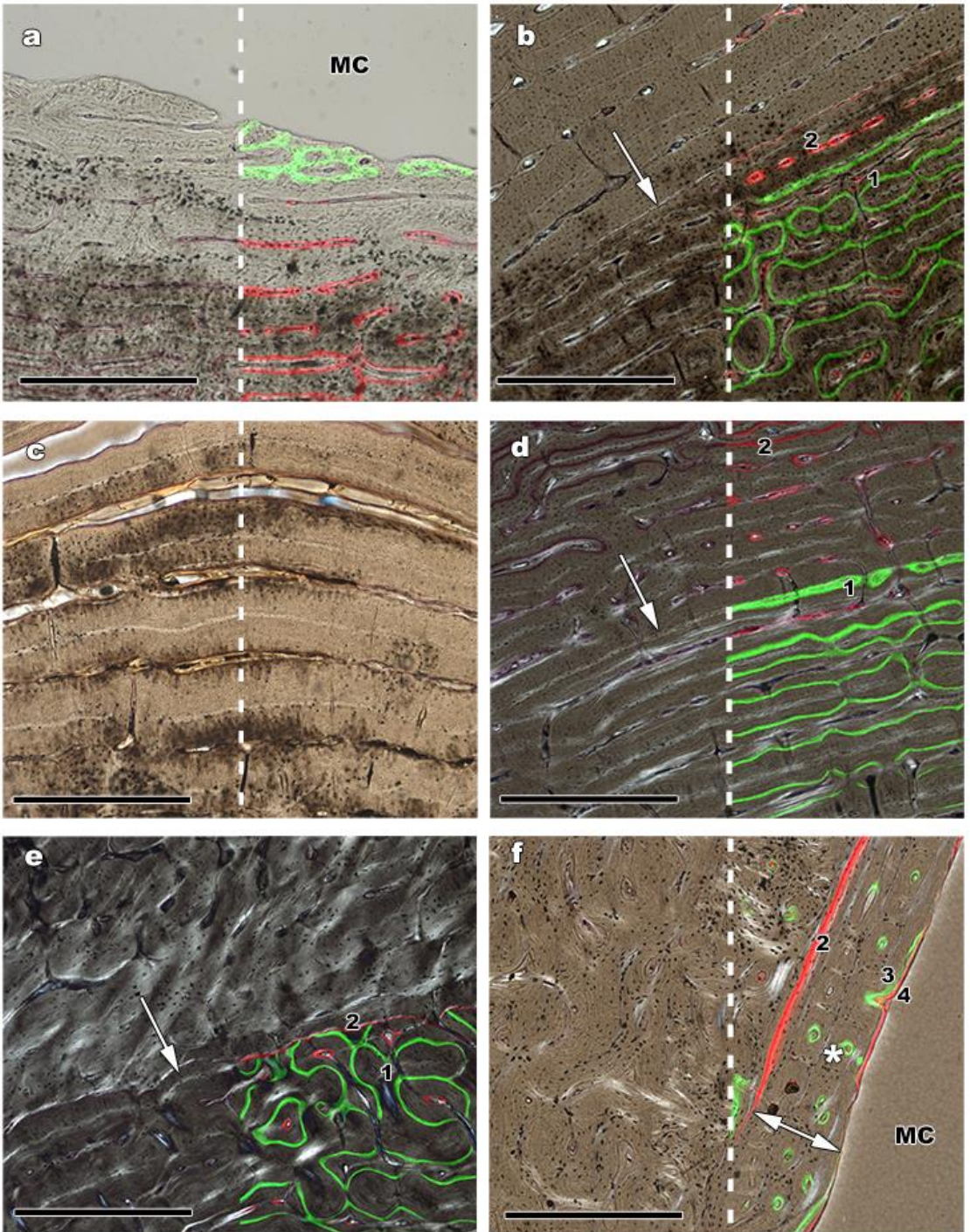
Figure S8.3. Histological detail of the 15 weeks old individual ID-2 / IPS-88715 under combined transmitted and fluorescent light (a), polarized light (c) and combined polarized and fluorescent light (d, e, f). Images are oriented with the medullary cavity (MC) towards the inferior part and outermost cortex (OC) towards the superior side unless specified. (a) Partial erosion of prenatal bone my medullary expansion. (b) LAG indicated by white arrow delimiting the resorbed cortex in the anterior sector of the tibia. (c) Laminar FLC in the antero-medial part of the tibia. (d) Annulus bordering the prenatal growth (white arrow) in the posterior part of the radius (e) Scalloped surface left by a resorption process in the postero-lateral sector of the metatarsus. (f) Endosteal bone in the lateral sector of the metatarsus (white arrow) composed of longitudinal canals (asterisk). 1: label deposited at 3 days; 2: label deposited at 30 days; 3: label deposited at 13 weeks; 4: label deposited at 15 weeks. Black scale: 500 micrometres. Figure obtained from Calderón et al. (2021).

8.2.1.3. *Growth after weaning*

Femur (hand-raised individuals)

At this stage, the prenatal tissue consists of a narrow band around the medullary cavity, which is slightly broader in the medial area. Despite, individuals ID-3 and ID-4 were not labelled during the perinatal growth, the shift from pre- to postnatal tissue is identifiable due to the different proportion of primary PFB within the FLC and the presence of an annulus surrounding part of the prenatal area in the case of the male ID-3. Postnatal tissue, composed of FLC, predominates within the bone section. As mentioned for the previous stage, we also observe a more organized pattern towards the posterior part or the bone. The labels of 13, 15 and 17 weeks are closely deposited throughout the entire shaft, indicating a limited bone apposition during this period. Indeed, there is almost no periosteal growth in some sections of the bone.

Instead, there are partial LAGs observable between the weeks 13 to 17 in the anterior parts of male ID-3 and female ID-4. In these areas, there is no increase in bone area between weeks 13 to 15, but tissue is refilling the previously formed scaffold. The green-labelled surface deposited at 17 weeks appears as a narrow line bordering the outer part of the LAG, indicating that bone apposition stopped for almost one month after weaning in these areas and restarted at week 17. Before and after this LAG, there are different types of FLC (Fig. S8.4a). Thus, a plexiform/reticular FLC shifts to plexiform/laminar in the anterior portion of the femur and from plexiform to laminar towards the posterior part. Endosteal bone is located in a small area of the lateral and anterior part of ID-3 and ID-4, respectively. This structure is separated from the primary bone by a cement line. In this tissue, a plexiform arrangement of the FLC prevails. The Haversian system can be found in area of the linea aspera and incipiently in the prenatal area, eroding the primary tissue. Some cavities are still forming in this area.

Femur (individuals nursed by mother)

In the two individuals analysed, the proportion of pre- and postnatal bone are the same as in hand-raised individuals, as well as the organisation of the endosteal bone and Haversian systems. Femora of these individuals, however, show a more organized pattern in the tissue of the posterior sector. These bones are composed of disorganized and reticular areas at the beginning of the postnatal deposition; thereafter, they show a constant deposition of plexiform FLC without any shift or disruption. In both individuals, ID-23 and ID-24, the endosteal bone is an only a thin layer.

Humerus (hand-raised individuals)

The section of the humerus shows a pronounced and directional expansion of the medullary cavity and bone apposition towards the postero-medial sector. The significant increase of the medullary cavity in these areas deletes almost

all tissue deposited before 13 weeks. In the opposite section, the prenatal tissue is still preserved and it is even possible to distinguish a partial annulus at the moment of birth. The tissue of the medial sector is reticular, while it is plexiform in the posterior sector (slightly more organized in the female individual ID-4). Plexiform FLC is deposited at the lateral side of the bone until week 13. Labels deposited between weeks 13 to 17 are narrowly spaced throughout the entire section with exception of the posterior portion, where they are wider spaced, which denotes the scarce tissue deposition along most of the periosteum during this interval. Actually, in the antero-lateral sector of both individuals (ID-4 and ID-3) there is no periosteal apposition for two weeks (13 to 15); however, bone continues to be deposited within the previously formed scaffold. A partial LAG can be identified between this scaffold and the subsequently formed new laminar bone shortly before week 17. There is a thick layer of endosteal bone enclosed within a small area of the anterior sector formed some time before week 13. At its beginning, the endosteal bone consists of lamellar tissue, but later in ontogeny the patterns shifts to plexiform. The Haversian systems appear enclosed within a small area in the medial sector of the humerus.

Humerus (individuals nursed by mother)

As well as in the hand-raised group, the humerus of individuals nursed by mother shows an area of reticular FLC in the medial sector, while plexiform tissue predominates in the rest of the section. None of the individuals shows a shift in bone tissue after 13 weeks. As well as in the femora, the endosteal bone forms a thin layer bordering the medullary cavity.

Tibia (hand-raised individuals)

The tibia is mainly composed of postnatal tissue at this stage, though there still remains a well distinguishable residual prenatal area surrounded by an annulus or a partial LAG in the posterior area of both individuals ID-3 and ID-

4 (Fig. S8.4b). The postnatal bone tissue is plexiform/laminar during the first 13 weeks. We observe a marked bone drift in the anterior part of the tibia. In this area, cortical resorption has eroded parts of the tissue deposited between weeks 13 to 17, leaving a scalloped edge limited by a line. Between 17 and 23 weeks, tissue deposition resumes but it follows a different tissue arrangement. Radial canals are distributed within the entire cross-section, being the highest densities of these canals in the postero-lateral region. The Haversian systems spread almost throughout the entire prenatal area and new cavities are still forming. The expansion of the medullary cavity erodes the endosteal bone formed at previous stages and a small area of new endosteal tissue starts to form around the 13th week following reticular and longitudinal orientation.

Tibia (individuals nursed by mother)

This bone is composed of a plexiform FLC, with the medial part slightly more organized than the lateral one. The prenatal tissue is bordered by a partial LAG in the anterior sector of the ID-23 tibia. The medial sector shows a small area of reticular bone in ID-24 after the 13th week. The endosteal bone has a longitudinal orientation while in ID-23 a plexiform FLC alternates with lamellar bone.

Radius (hand-raised individuals)

At this stage, this bone shows a thick cortex and a small medullary cavity. As a result, the prenatal tissue still occupies a considerable area within the cross-section, delimited by an annulus in the medial sector. As a particularity, the early postnatal tissue of ID-3 shows some longitudinal canals in the anterior sector. From now onwards until week 13, cortical apposition follows the plexiform FLC described previously, with dispersed reticular areas in the anterior and posterior sectors. Towards the medial and lateral sides of both individuals, a resorption process has eroded part of the tissue deposited between weeks 13 and 17 (Fig. S8.4c). As a result these areas show well-marked

lines and an abrupt shift in orientation. Some lines form in the lateral part in subsequent post-weaning weeks; endosteal bone is reticular, plexiform and laminar. Well-developed Haversian systems can be found within the almost entire prenatal tissue. They also spread within the lateral part of the bone.

Radius (individuals nursed by mother)

At the beginning of the postnatal deposition, bone shows a plexiform FLC that shifts rapidly to a reticular, which prevails after weaning. Tissue deposited at 13 weeks is resorbed in subsequent stages as testify the eroded label and a line in the medial and lateral sectors of ID-24 (Fig. S8.4d). These structures are also visible in the medial and lateral part of ID-23 shortly before and after week 13. The endosteal tissue in this bone is formed by FLC with plexiform and laminar orientation in ID-23 and longitudinal orientation in ID-24.

Metapodial bones (hand-raised individuals)

The medullary cavity shows a reduced size at this stage, but their expansion has completely removed the central column in both bones. The prenatal bone is visible within most of the bone shaft but in the posterior sector, being delimited by a partial LAG in the ID-3 metatarsus. As in the radius, metatarsus and metacarpus of ID-3 show a band of longitudinal canals just at the beginning of the postnatal deposition in the antero-lateral part of the bone (Fig. S8.4e). In general, during the first 13 weeks bone matrix is deposited following a continuous reticular FLC. Labels from 13 to 17 weeks are closely spaced except for the posterior area, which indicates a slower tissue apposition during this period. Indeed, in the anterior sector a partial LAG represents an arrest of growth between weeks 15 and 17. At the inner side of this LAG there is a thin layer of bone deposited at week 15, while bone deposited at week 17 surrounds the LAG externally. The tissue deposited at week 17 shows plexiform/laminar FLC. In the medial sector of ID-4 metapodials, a band of laminar bone appears even after the 13th week. A broad band of endosteal bone is present in the

anterior sector of the bones (Fig. S8.4f), occupying a comparatively larger area in the metacarpus. The Haversian systems are limited to the postero-lateral and postero-medial regions, though large erosion cavities penetrate throughout the whole prenatal tissue zone.

Metapodial bones (individuals nursed by mother)

At the age of six months, there still remains a part of the central column in the medullary cavity of ID-24 metacarpus but not in that of ID-23. The main FLC pattern in these bones is uniformly reticular, although there is a more organized arrangement, even plexiform, towards the medial and lateral sides. In the medial part of the ID-24 metacarpus, a partial LAG delimitates the prenatal tissue. The endosteal bone in the metatarsus is composed by reticular and plexiform FLC, while the metacarpus shows a longitudinal pattern.
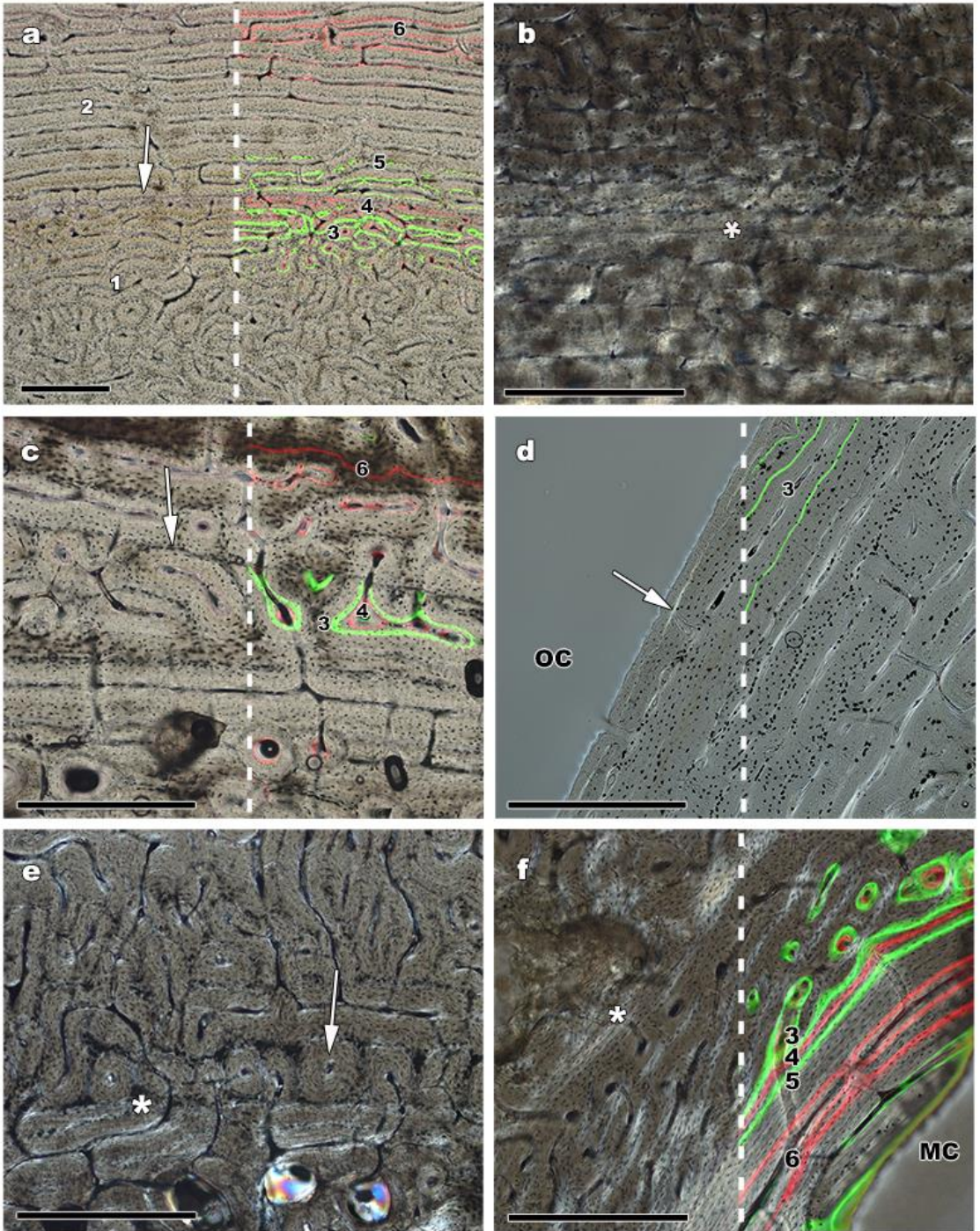
Figure S8.4. Histological detail of individuals older than 15 weeks under combined polarized and fluorescent light (a, c, d, f) and polarized light (b,e). Images are oriented with the medullary cavity (MC) towards the inferior part and outermost cortex (OC) towards the superior side unless specified. (a) Shift in the orientation of the tissue in the anterior part of the ID-3 / IPS-93664 femur separated by a partial LAG (white arrow). Number 1 written in white indicates reticular deposition; number 2 written in white indicates plexiform orientation deposited from the week 17 onwards. (b) LAG bordering the prenatal tissue (white asterisk) in the posterior part of the ID-3 / IPS-93664 tibia. (c) LAG (white arrow) in the medial part of ID-3 / IPS-93664 radius indicating the interruption of tissue deposition over six weeks. (d) LAG (white arrow) deposited at the age of 13 weeks in the antero-lateral sector of ID-24 / IPS-109291 radius. (e) Longitudinal canals at the beginning of postnatal deposition (white arrow) in the anterior sector of ID-3 / IPS-93664 metatarsus. The white asterisk marks the border of prenatal tissue. (f) Endosteal bone in the antero-lateral sector of ID-3 / IPS-93664 metatarsus; the cement line is marked with an asterisk. 3: label deposited at 13 weeks; 4: label deposited at 15 weeks; 5 label deposited at 17 weeks; 6: label deposited at 23 weeks. Black scale: 500 micrometres. Figure obtained from Calderón et al. (2021).

	Superimposition	Perinatal growth	Pre-weaning	Post-weaning
Femur				
Tibia				
Metatarsus				
Humerus				
Radius				
Metacarpus				
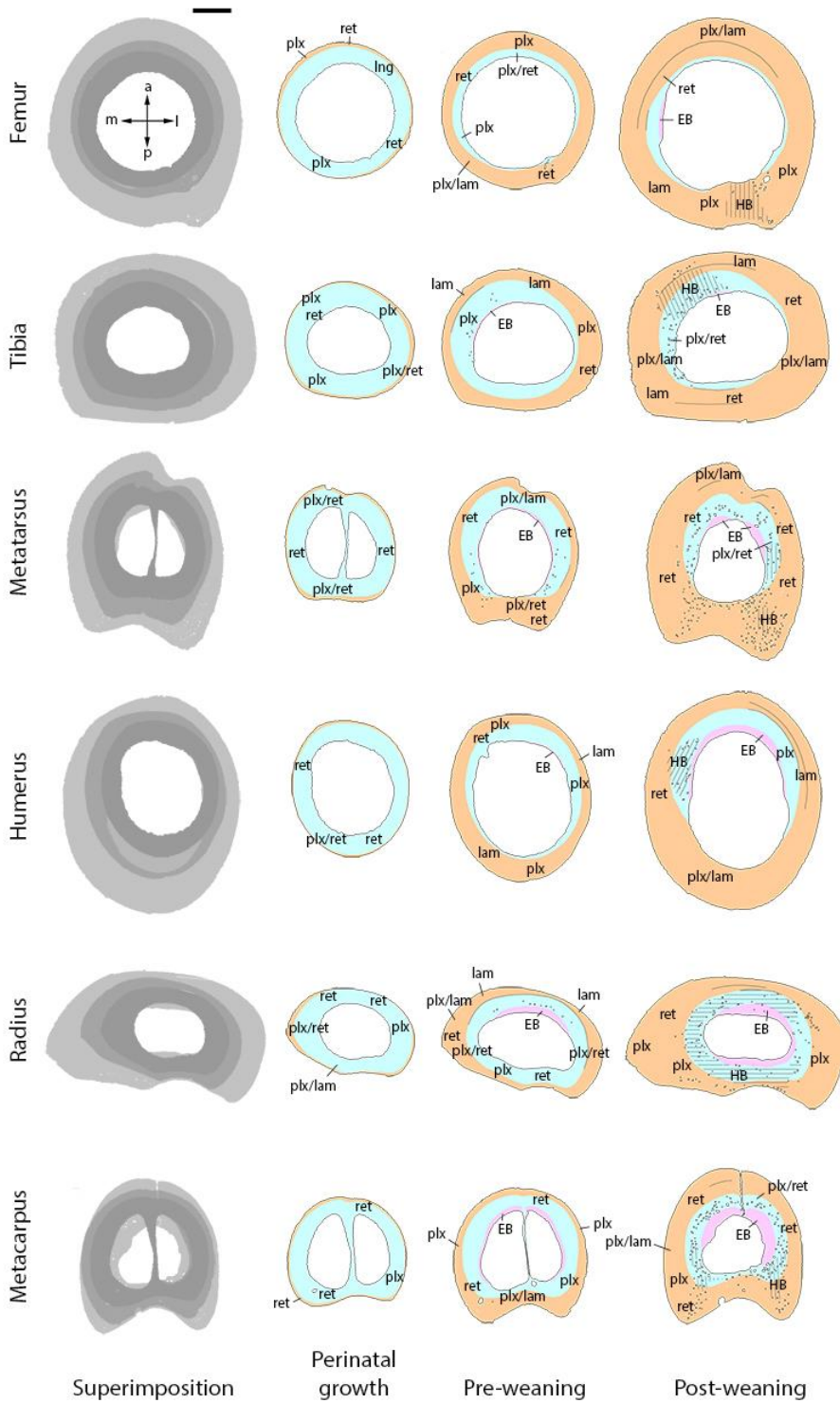
Figure S8.5. Superimposed outline of bone shaft sections and chronologically ordered by age to schematically illustrate perinatal growth (ID-1 / IPS-88714), growth during the pre-weaning period (ID-2 / IPS-88715) and growth after weaning (ID-3 / IPS-93664). Scale: 5mm. Dark grey: perinatal stage; Intermediate grey: pre-weaning stage; Light grey: post-weaning stage; Blue color: prenatal tissue (primary bone); orange color: postnatal tissue (primary bone); pink color: endosteal bone (secondary bone); dashed area: haversian bone (secondary bone); lam: laminar; plx: plexiform; ret: reticular; HB: Haversian bone; EB: Endosteal bone. A: anterior; P: posterior; M: medial; L: lateral. Figure obtained from Calderón et al. (2021).
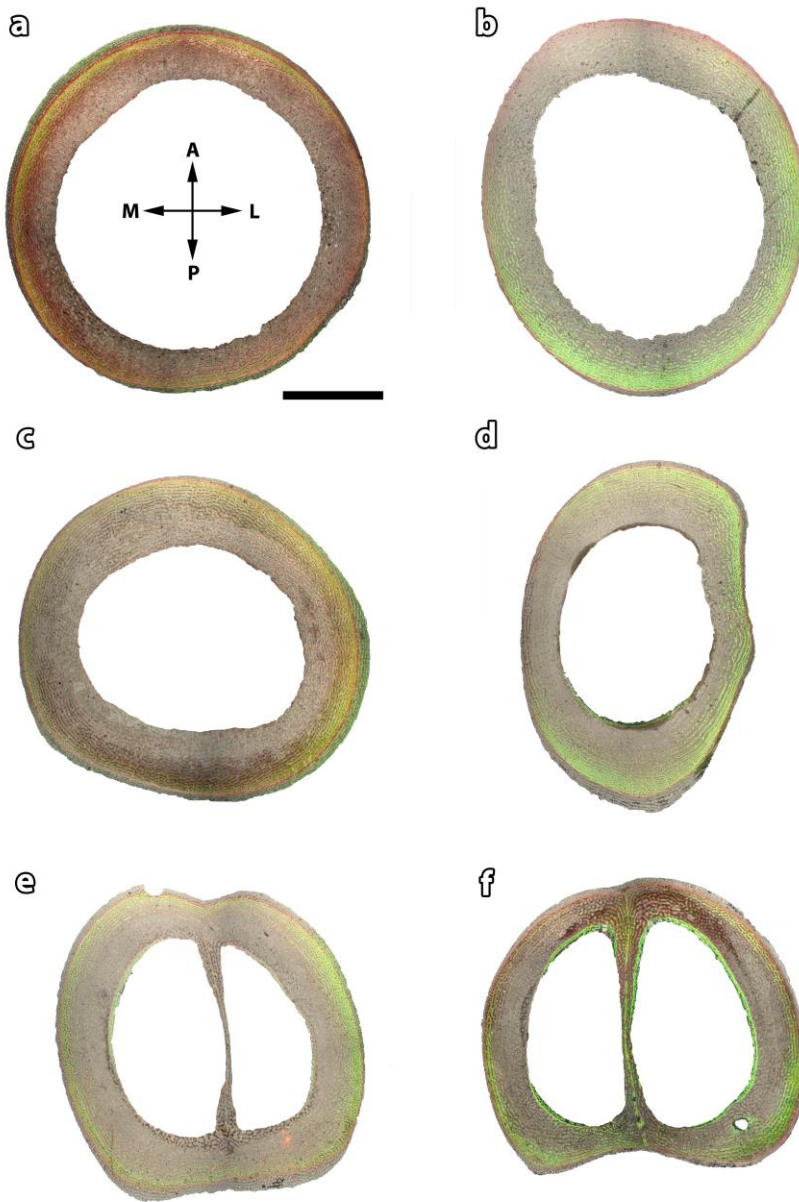
Figure S8.6. Histological compositions of the hindlimb (left) and forelimb (right) bones of the 15 days old individual ID-1 / IPS-8814 labelled at birth, and days 3 and 15. (a) femur. (b) humerus. (c) tibia. (d) radius. (e) metatarsus. (f) metacarpus. Scale: 5 milimetres. Figure obtained from Calderón et al. (2021).
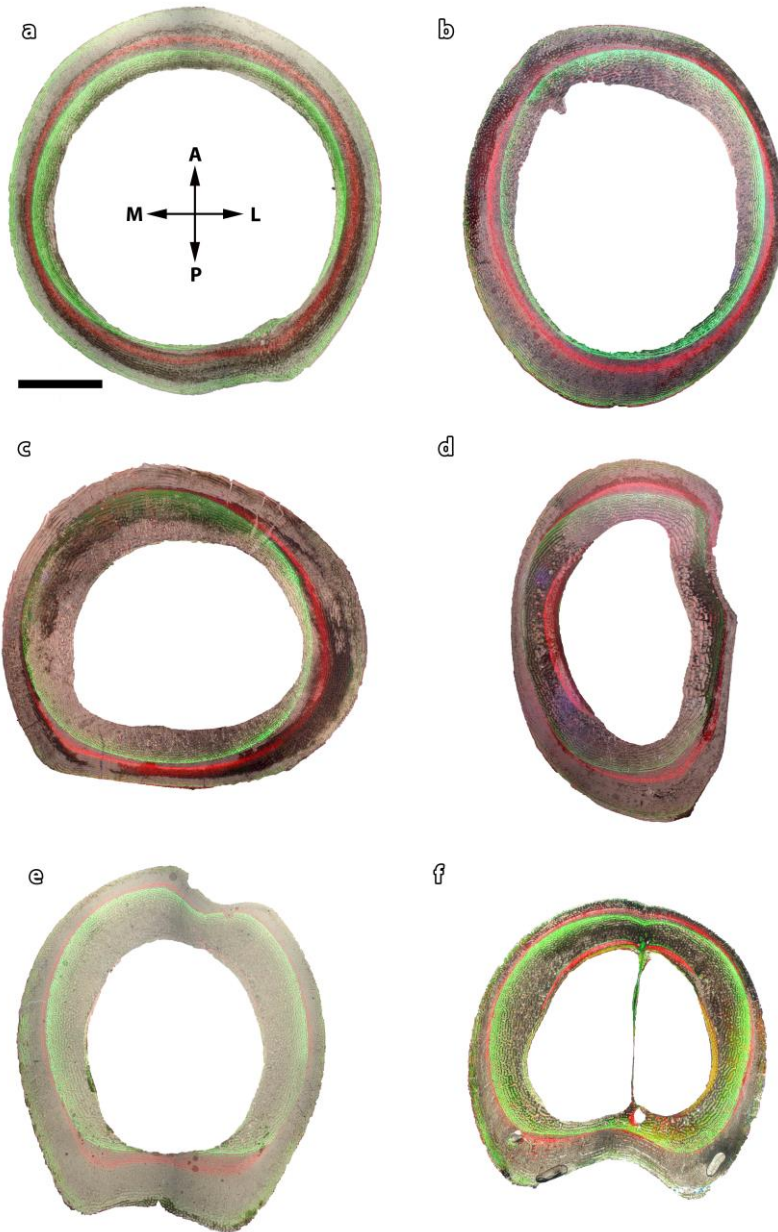
Figure S8.7. Histological compositions of the hindlimb (left) and forelimb (right) bones of the 15 weeks old individual ID-2 / IPS-8815 labelled at days 3 and 30, and weeks 13 and 15. (a) femur. (b) humerus. (c) tibia. (d) radius. (e) metatarsus. (f) metacarpus. Scale: 5 milimetres. Figure obtained from Calderón et al. (2021).
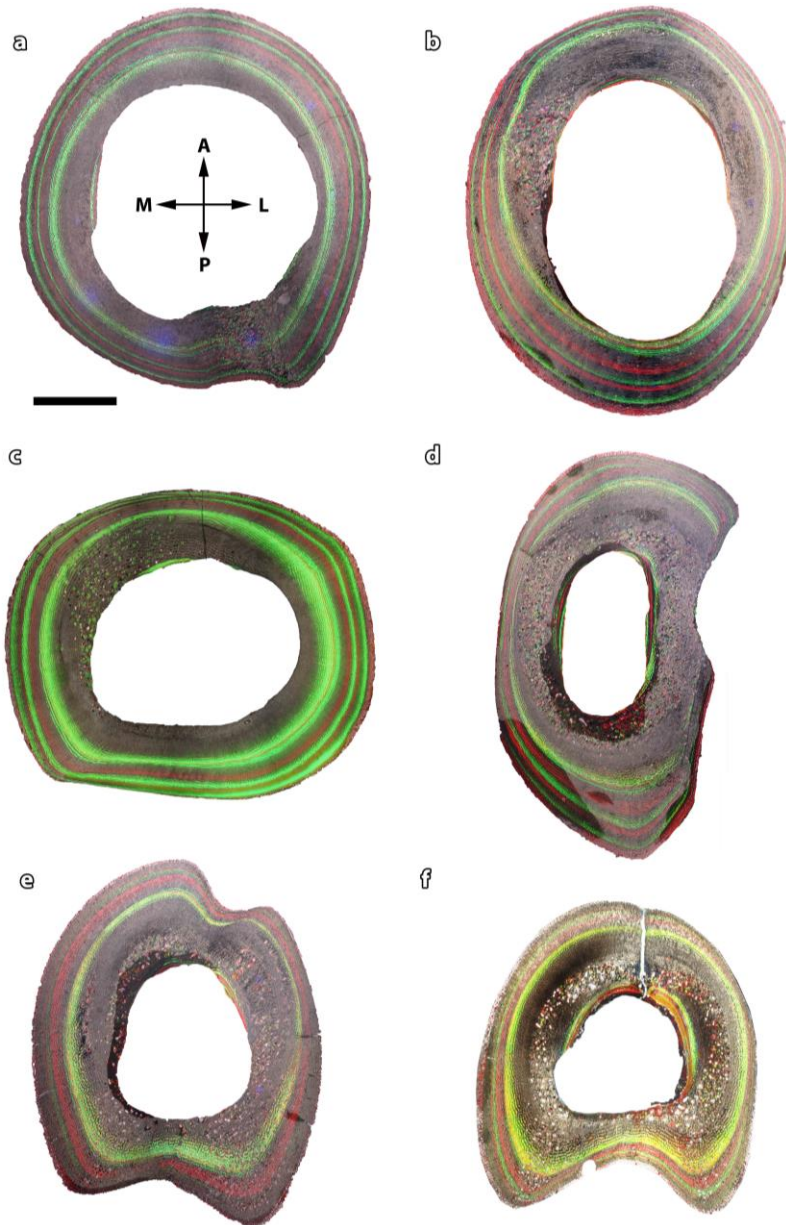
Figure S8.8. Histological compositions of the hindlimb (left) and forelimb (right) bones of the 43 weeks old individual ID-3 / IPS-93664 labelled at weeks 13, 15, 17 and 23 (subsequent labels have not been used in this study) (a) femur. (b) humerus. (c) tibia. (d) radius. (e) metatarsus. (f) metacarpus. Scale: 5 milimetres. Figure obtained from Calderón et al. (2021).
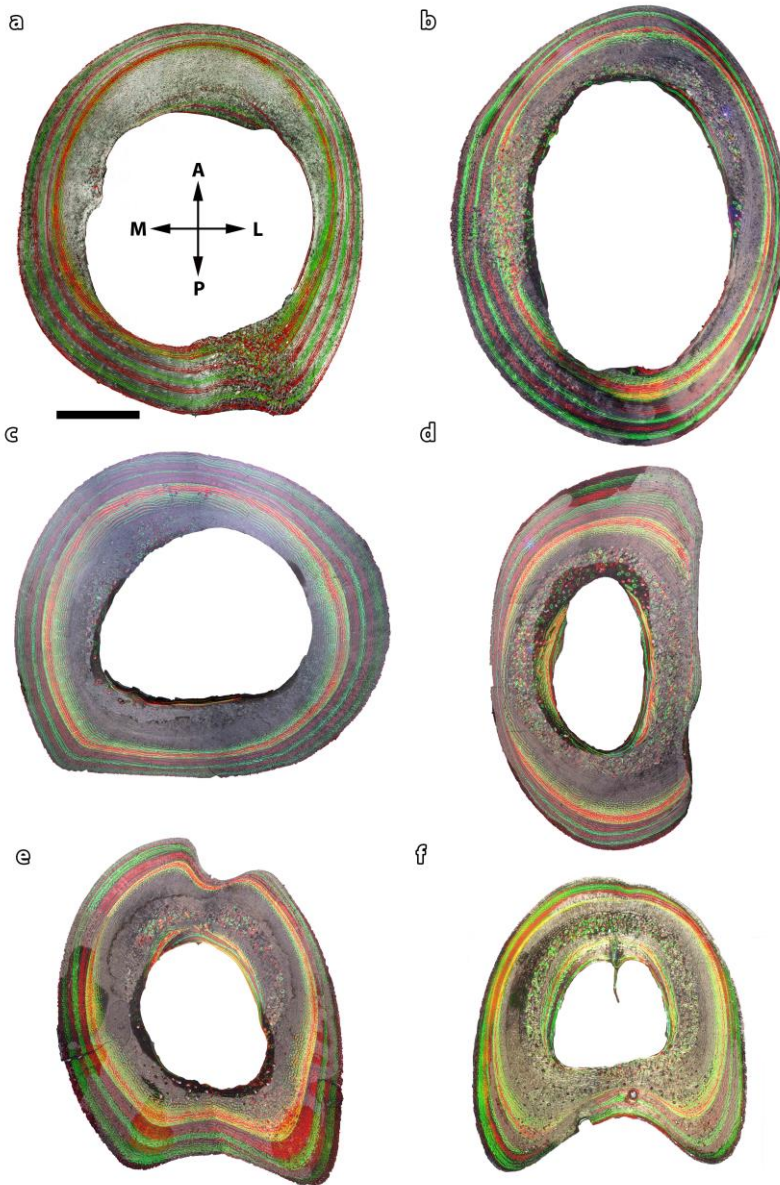
Figure S8.9. Histological compositions of the hindlimb (left) and forelimb (right) bones of the 43 weeks old individual ID-4 / IPS-88713 labelled at weeks 9, 11,13, 15, 17 and 23 (subsequent labels have not been used in this study) (a) femur. (b) humerus. (c) tibia. (d) radius. (e) metatarsus. (f) metacarpus. Scale: 5 milimetres. Figure obtained from Calderón et al. (2021).
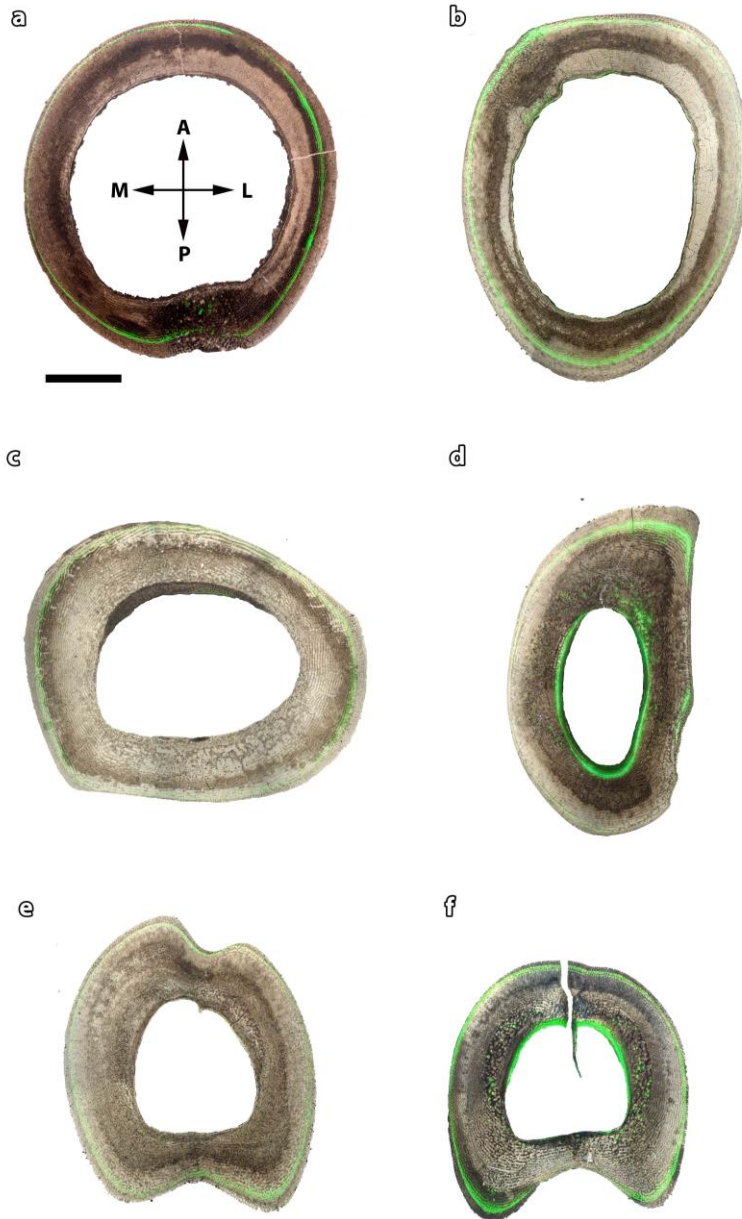
Figure S8.10. Histological compositions of the hindlimb (left) and forelimb (right) bones of the 24 weeks old individual ID-24 / IPS-190291 labelled at week 13. (a) femur. (b) humerus. (c) tibia. (d) radius. (e) metatarsus. (f) metacarpus. Scale: 5 milimetres. Figure obtained from Calderón et al. (2021).
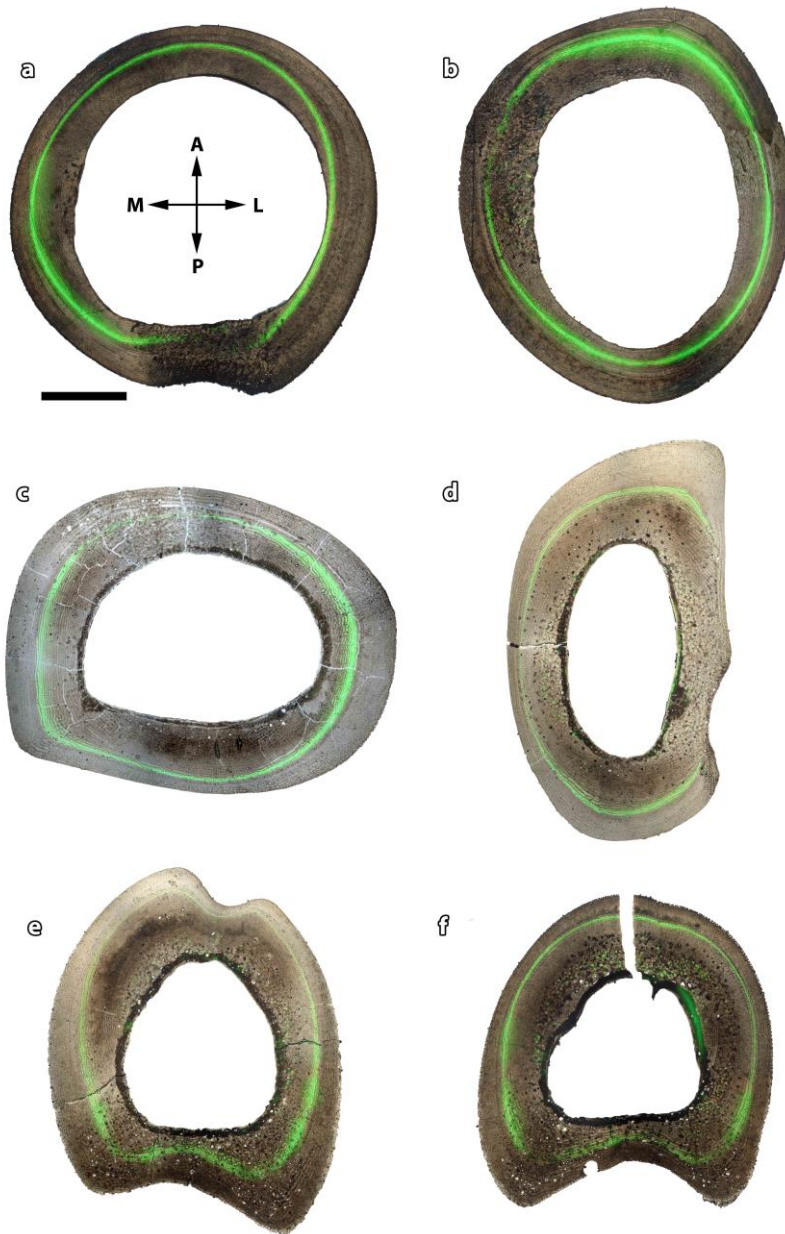
Figure S8.11. Histological compositions of the hindlimb (left) and forelimb (right) bones of the 64 weeks old individual ID-23/ IPS-109290 labelled at week 13 . (a) femur. (b) humerus. (c) tibia. (d) radius. (e) metatarsus. (f) metacarpus. Scale: 5 milimetres. Figure obtained from Calderón et al. (2021).
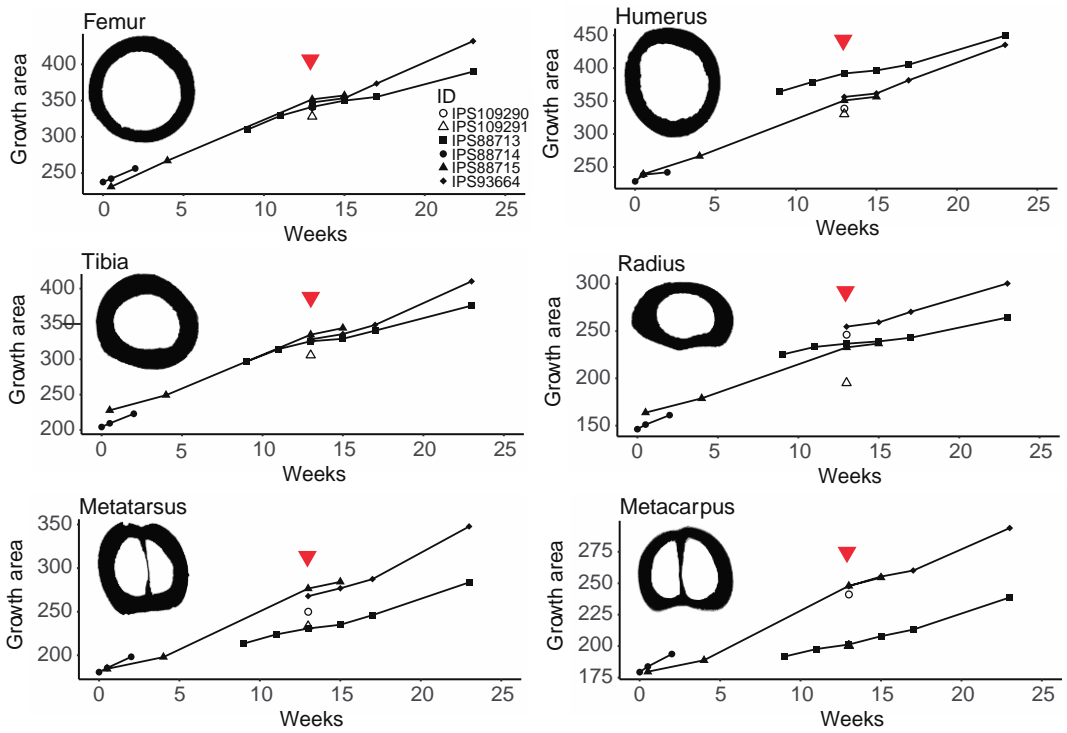
Figure S8.12. Amount of area between labels (in mm2) by bone. Red arrows indicate the day of weaning (week 13 label). Figure obtained from Calderón et al. (2021).
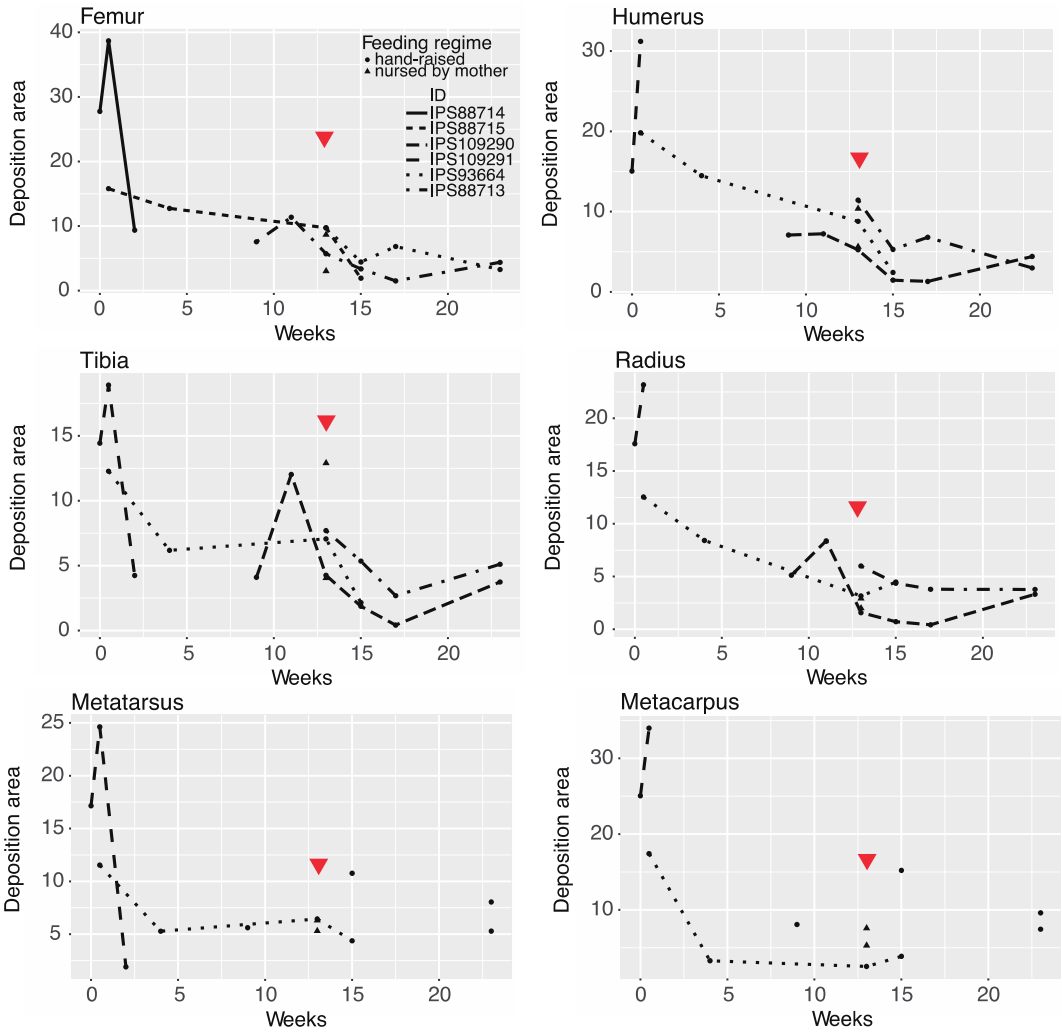
Figure S8.13. Labelled area (in mm2) in the different week intervals by bone. Triangular points represent specimens nursed by their mothers (C1); circular points represent hand-raised specimens (C2). Red arrows indicate the day of weaning (week 13 label). Figure obtained from Calderón et al. (2021).

ID	regime	bone	label	full area
ID-1	hand-raised	femur	1d	237.808
ID-1	hand-raised	femur	3d	242.405
ID-1	hand-raised	femur	15d	256.541
ID-1	hand-raised	tibia	1d	204.289
ID-1	hand-raised	tibia	3d	209.419
ID-1	hand-raised	tibia	15d	223.018
ID-1	hand-raised	humerus	1d	230.360
ID-1	hand-raised	humerus	3d	236.647
ID-1	hand-raised	humerus	15d	239.420
ID-1	hand-raised	radius	1d	146.271
ID-1	hand-raised	radius	3d	151.057
ID-1	hand-raised	radius	15d	161.037
ID-1	hand-raised	metatarsus	1d	180.775
ID-1	hand-raised	metatarsus	3d	185.499
ID-1	hand-raised	metatarsus	15d	198.244
ID-1	hand-raised	metacarpus	1d	179.301
ID-1	hand-raised	metacarpus	3d	183.754
ID-1	hand-raised	metacarpus	15d	193.687
ID-2	hand-raised	femur	3d	231.333
ID-2	hand-raised	femur	30d	267.172
ID-2	hand-raised	femur	13w	351.668
ID-2	hand-raised	femur	15w	357.089
ID-2	hand-raised	tibia	3d	227.845
ID-2	hand-raised	tibia	30d	249.279
ID-2	hand-raised	tibia	13w	334.795
ID-2	hand-raised	tibia	15w	344.183
ID-2	hand-raised	humerus	3d	239.020
ID-2	hand-raised	humerus	30d	266.452
ID-2	hand-raised	humerus	13w	350.922
ID-2	hand-raised	humerus	15w	356.527
ID-2	hand-raised	radius	3d	163.746
ID-2	hand-raised	radius	30d	178.842
ID-2	hand-raised	radius	13w	232.718
ID-2	hand-raised	radius	15w	236.742
ID-2	hand-raised	metatarsus	3d	184.430
ID-2	hand-raised	metatarsus	30d	198.002

ID-2	hand-raised	metatarsus	13w	276.604
ID-2	hand-raised	metatarsus	15w	284.293
ID-2	hand-raised	metacarpus	3d	179.629
ID-2	hand-raised	metacarpus	30d	188.713
ID-2	hand-raised	metacarpus	13w	247.853
ID-2	hand-raised	metacarpus	15w	254.540
ID-3	hand-raised	femur	13w	347.394
ID-3	hand-raised	femur	15w	353.204
ID-3	hand-raised	femur	17w	373.437
ID-3	hand-raised	femur	23w	431.909
ID-3	hand-raised	tibia	13w	328.269
ID-3	hand-raised	tibia	15w	335.684
ID-3	hand-raised	tibia	17w	348.687
ID-3	hand-raised	tibia	23w	410.311
ID-3	hand-raised	humerus	13w	356.304
ID-3	hand-raised	humerus	15w	361.591
ID-3	hand-raised	humerus	17w	381.539
ID-3	hand-raised	humerus	23w	435.301
ID-3	hand-raised	radius	13w	254.631
ID-3	hand-raised	radius	15w	259.261
ID-3	hand-raised	radius	17w	270.349
ID-3	hand-raised	radius	23w	300.305
ID-3	hand-raised	metatarsus	13w	267.904
ID-3	hand-raised	metatarsus	15w	276.853
ID-3	hand-raised	metatarsus	17w	287.444
ID-3	hand-raised	metatarsus	23w	347.812
ID-3	hand-raised	metacarpus	13w	247.637
ID-3	hand-raised	metacarpus	15w	255.261
ID-3	hand-raised	metacarpus	17w	260.107
ID-3	hand-raised	metacarpus	23w	293.885
ID-4	hand-raised	femur	9w	311.594
ID-4	hand-raised	femur	11w	335.874
ID-4	hand-raised	femur	13w	345.629
ID-4	hand-raised	femur	15w	347.996
ID-4	hand-raised	femur	17w	353.429
ID-4	hand-raised	femur	23w	389.875

ID-4	hand-raised	tibia	9w	296.621
ID-4	hand-raised	tibia	11w	314.435
ID-4	hand-raised	tibia	13w	325.529
ID-4	hand-raised	tibia	15w	329.074
ID-4	hand-raised	tibia	17w	340.563
ID-4	hand-raised	tibia	23w	376.034
ID-4	hand-raised	humerus	9w	364.467
ID-4	hand-raised	humerus	11w	378.948
ID-4	hand-raised	humerus	13w	391.944
ID-4	hand-raised	humerus	15w	396.563
ID-4	hand-raised	humerus	17w	405.130
ID-4	hand-raised	humerus	23w	449.214
ID-4	hand-raised	radius	9w	225.110
ID-4	hand-raised	radius	11w	233.181
ID-4	hand-raised	radius	13w	236.701
ID-4	hand-raised	radius	15w	239.066
ID-4	hand-raised	radius	17w	243.066
ID-4	hand-raised	radius	23w	264.374
ID-4	hand-raised	metatarsus	9w	213.554
ID-4	hand-raised	metatarsus	11w	223.786
ID-4	hand-raised	metatarsus	13w	230.701
ID-4	hand-raised	metatarsus	15w	235.060
ID-4	hand-raised	metatarsus	17w	245.944
ID-4	hand-raised	metatarsus	23w	283.655
ID-4	hand-raised	metacarpus	9w	191.704
ID-4	hand-raised	metacarpus	11w	197.688
ID-4	hand-raised	metacarpus	13w	201.220
ID-4	hand-raised	metacarpus	15w	207.829
ID-4	hand-raised	metacarpus	17w	213.111
ID-4	hand-raised	metacarpus	23w	238.677
ID-23	nursed by mother	femur	13w	341.141
ID-23	nursed by mother	tibia	13w	326.214
ID-23	nursed by mother	humerus	13w	338.718
ID-23	nursed by mother	radius	13w	246.142
ID-23	nursed by mother	metatarsus	13w	249.916
ID-23	nursed by mother	metacarpus	13w	241.059

ID-24	nursed by mother	femur	13w	328.146
ID-24	nursed by mother	tibia	13w	305.770
ID-24	nursed by mother	humerus	13w	330.281
ID-24	nursed by mother	radius	13w	195.157
ID-24	nursed by mother	metatarsus	13w	233.388
ID-24	nursed by mother	metacarpus	13w	200.248

Table S8.3. Size (in square millimetres) of tissue areas between two consecutive labels in cross-sections of various bones. Age at labelling is given in days (d) or weeks (w). Table obtained from Calderón et al. (2021).

ID	regime	bone	period	growth rate	canal density
ID-1	hand-raised	femur	prenatal	NA	10.992
ID-1	hand-raised	femur	1d-3d	1.532	NA
ID-1	hand-raised	femur	3d-15d	1.087	NA
ID-1	hand-raised	tibia	prenatal	NA	13.137
ID-1	hand-raised	tibia	1d-3d	1.71	NA
ID-1	hand-raised	tibia	3d-15d	1.046	NA
ID-1	hand-raised	humerus	prenatal	NA	17.158
ID-1	hand-raised	humerus	1d-3d	2.096	NA
ID-1	hand-raised	humerus	3d-15d	0.768	NA
ID-1	hand-raised	radius	prenatal	NA	12.601
ID-1	hand-raised	radius	1d-3d	1.595	NA
ID-1	hand-raised	radius	3d-15d	0.981	NA
ID-1	hand-raised	metatarsus	prenatal	NA	17.158
ID-1	hand-raised	metatarsus	1d-3d	1.575	NA
ID-1	hand-raised	metatarsus	3d-15d	0.28	NA
ID-1	hand-raised	metacarpus	prenatal	NA	9.383
ID-1	hand-raised	metacarpus	1d-3d	1.484	NA
ID-1	hand-raised	metacarpus	3d-15d	0.764	NA
ID-2	hand-raised	femur	prenatal	NA	14.745
ID-2	hand-raised	femur	3d-30d	1.327	8.311
ID-2	hand-raised	femur	30d-13w	1.457	8.300
ID-2	hand-raised	femur	13w-15w	0.387	NA
ID-2	hand-raised	tibia	prenatal	NA	11.260
ID-2	hand-raised	tibia	3d-30d	0.794	12.601
ID-2	hand-raised	tibia	30d-13w	1.474	11.000
ID-2	hand-raised	tibia	13w-15w	0.67	NA
ID-2	hand-raised	humerus	prenatal	NA	NA
ID-2	hand-raised	humerus	3d-30d	1.016	15.818
ID-2	hand-raised	humerus	30d-13w	1.456	18.499
ID-2	hand-raised	humerus	13w-15w	0.400	NA
ID-2	hand-raised	radius	prenatal	NA	16.086
ID-2	hand-raised	radius	3d-30d	0.559	11.796
ID-2	hand-raised	radius	30d-13w	0.929	14.700
ID-2	hand-raised	radius	13w-15w	0.287	NA
ID-2	hand-raised	metatarsus	prenatal	NA	13.673
ID-2	hand-raised	metatarsus	3d-30d	0.503	NA
ID-2	hand-raised	metatarsus	30d-13w	1.355	9.900

ID-2	hand-raised	metatarsus	13w-15w	0.549	NA
ID-2	hand-raised	metacarpus	prenatal	NA	13.405
ID-2	hand-raised	metacarpus	3d-30d	0.336	NA
ID-2	hand-raised	metacarpus	30d-13w	1.02	22.300
ID-2	hand-raised	metacarpus	13w-15w	0.477	NA
ID-3	hand-raised	femur	before 13w	NA	11.800
ID-3	hand-raised	femur	13w-15w	0.415	NA
ID-3	hand-raised	femur	15w-17w	1.445	7.500
ID-3	hand-raised	femur	17w-23w	1.271	7.500
ID-3	hand-raised	tibia	before 13w	NA	13.400
ID-3	hand-raised	tibia	13w-15w	0.53	NA
ID-3	hand-raised	tibia	15w-17w	0.929	7.200
ID-3	hand-raised	tibia	17w-23w	1.34	7.200
ID-3	hand-raised	humerus	before 13w	NA	18.500
ID-3	hand-raised	humerus	13w-15w	0.378	NA
ID-3	hand-raised	humerus	15w-17w	1.425	12.600
ID-3	hand-raised	humerus	17w-23w	1.169	12.600
ID-3	hand-raised	radius	prenatal	NA	NA
ID-3	hand-raised	radius	before 13w	NA	18.800
ID-3	hand-raised	radius	13w-15w	0.331	NA
ID-3	hand-raised	radius	15w-17w	0.792	11.300
ID-3	hand-raised	radius	17w-23w	0.651	11.300
ID-3	hand-raised	metatarsus	prenatal	NA	NA
ID-3	hand-raised	metatarsus	before 13w	NA	11.800
ID-3	hand-raised	metatarsus	13w-15w	0.639	NA
ID-3	hand-raised	metatarsus	15w-17w	0.757	6.700
ID-3	hand-raised	metatarsus	17w-23w	1.312	6.700
ID-3	hand-raised	metacarpus	prenatal	NA	NA
ID-3	hand-raised	metacarpus	before 13w	NA	13.100
ID-3	hand-raised	metacarpus	13w-15w	0.544	NA
ID-3	hand-raised	metacarpus	15w-17w	0.346	12.900
ID-3	hand-raised	metacarpus	17w-23w	0.734	12.900
ID-4	hand-raised	femur	before 9w	NA	NA
ID-4	hand-raised	femur	9w-11w	NA	10.700
ID-4	hand-raised	femur	11w-13w	NA	10.700
ID-4	hand-raised	femur	13w-15w	NA	NA

ID-4	hand-raised	femur	15w-17w	0.368	7.200
ID-4	hand-raised	femur	17w-23w	0.831	
ID-4	hand-raised	tibia	before 9w	NA	0.000
ID-4	hand-raised	tibia	9w-11w	NA	14.500
ID-4	hand-raised	tibia	11w-13w	NA	
ID-4	hand-raised	tibia	13w-15w	NA	NA
ID-4	hand-raised	tibia	15w-17w	0.821	9.900
ID-4	hand-raised	tibia	17w-23w	0.845	
ID-4	hand-raised	humerus	before 9w	NA	NA
ID-4	hand-raised	humerus	9w-11w	NA	13.100
ID-4	hand-raised	humerus	11w-13w	NA	
ID-4	hand-raised	humerus	13w-15w	NA	NA
ID-4	hand-raised	humerus	15w-17w	0.612	11.000
ID-4	hand-raised	humerus	17w-23w	1.050	
ID-4	hand-raised	radius	before 9w	NA	NA
ID-4	hand-raised	radius	9w-11w	NA	20.400
ID-4	hand-raised	radius	11w-13w	NA	
ID-4	hand-raised	radius	13w-15w	NA	NA
ID-4	hand-raised	radius	15w-17w	0.286	11.800
ID-4	hand-raised	radius	17w-23w	0.507	
ID-4	hand-raised	metatarsus	prenatal	NA	NA
ID-4	hand-raised	metatarsus	before 9w	NA	NA
ID-4	hand-raised	metatarsus	9w-11w	NA	24.100
ID-4	hand-raised	metatarsus	11w-13w	NA	
ID-4	hand-raised	metatarsus	13w-15w	NA	NA
ID-4	hand-raised	metatarsus	15w-17w	0.777	11.800
ID-4	hand-raised	metatarsus	17w-23w	0.898	
ID-4	hand-raised	metacarpus	before 9w	NA	0.000
ID-4	hand-raised	metacarpus	9w-11w	NA	8.300
ID-4	hand-raised	metacarpus	11w-13w	NA	
ID-4	hand-raised	metacarpus	13w-15w	NA	NA
ID-4	hand-raised	metacarpus	15w-17w	0.377	7.500
ID-4	hand-raised	metacarpus	17w-23w	0.609	
ID-23	nursed by mother	femur	before 13w	NA	13.100
ID-23	nursed by mother	femur	after 13w	NA	10.500
ID-23	nursed by mother	tibia	before 13w	NA	9.400
ID-23	nursed by mother	tibia	after 13w	NA	8.000

ID-23	nursed by mother	humerus	before 13w	NA	18.500
ID-23	nursed by mother	humerus	after 13w	NA	13.700
ID-23	nursed by mother	radius	before 13w	NA	14.200
ID-23	nursed by mother	radius	after 13w	NA	12.600
ID-23	nursed by mother	metatarsus	before 13w	NA	5.900
ID-23	nursed by mother	metatarsus	after 13w	NA	13.400
ID-23	nursed by mother	metacarpus	before 13w	NA	8.300
ID-23	nursed by mother	metacarpus	after 13w	NA	4.800
ID-24	nursed by mother	femur	before 13w	1.318	12.900
ID-24	nursed by mother	femur	after 13w	0.446	6.200
ID-24	nursed by mother	tibia	before 13w	1.736	7.000
ID-24	nursed by mother	tibia	after 13w	0.326	11.500
ID-24	nursed by mother	humerus	before 13w	0.850	8.600
ID-24	nursed by mother	humerus	after 13w	0.279	11.300
ID-24	nursed by mother	radius	before 13w	1.100	8.800
ID-24	nursed by mother	radius	after 13w	0.267	8.600
ID-24	nursed by mother	metatarsus	before 13w	1.264	7.500
ID-24	nursed by mother	metatarsus	after 13w	0.433	9.100
ID-24	nursed by mother	metacarpus	before 13w	0.838	9.700
ID-24	nursed by mother	metacarpus	after 13w	0.151	8.000

Table S8.4. Growth rate (mm2/day), canal density (%), tissue type and vascular orientation by period of each bone of the six individuals. w: week. d: days. FLC: fibro lamellar complex. Table obtained from Calderón et al. (2021).

ID	Day	Milk intake (ml)	Vegetal pellets (g/ml)	Bodymass (kg)
ID-1	1	-	0	11.5
ID-1	2	-	0	-
ID-1	3	1050	0	-
ID-1	4	1300	0	13.3
ID-1	5	900	0	14.0
ID-1	6	900	0	14.7
ID-1	7	1100	0	14.8
ID-1	8	1200	0	15.4
ID-1	9	1200	0	16.0
ID-1	10	1200	0	16.7
ID-1	11	1150	0	18.1
ID-1	12	1150	0	18.0
ID-1	13	1200	0	17.7
ID-1	14	800	0	18.0
ID-1	15	800	0	18.2
ID-1	16	1200	0	18.9
ID-1	17	1800	0	19.5
ID-2	1	-	0	-
ID-2	2	-	0	-
ID-2	3	850	0	10.5
ID-2	4	1000	0	11.1
ID-2	5	950	0	11.7
ID-2	6	1050	0	12.3
ID-2	7	1050	0	12.6
ID-2	8	1050	0	13.0
ID-2	9	1150	0	12.8
ID-2	10	900	0	13.4
ID-2	11	900	0	13.3
ID-2	12	900	0	13.9
ID-2	13	1100	0	13.9
ID-2	14	1200	0	14.4
ID-2	15	800	0	14.8
ID-2	16	1200	0	15.0
ID-2	17	1200	0	15.3
ID-2	18	1200	0	15.5

ID-2	19	800	0	16.1
ID-2	20	1200	0	16.0
ID-2	21	1200	0	16.4
ID-2	22	1200	0	17.1
ID-2	23	1200	0	17.4
ID-2	24	900	0	17.4
ID-2	25	700	0	17.9
ID-2	26	700	120	18.0
ID-2	27	700	-	18.7
ID-2	28	800	-	18.9
ID-2	29	800	100	18.9
ID-2	30	800	100	19.4
ID-2	31	1200	-	19.7
ID-2	32	500	100	19.3
ID-2	33	1100	100	19.7
ID-2	34	1000	100	20.2
ID-2	35	1000	140	20.6
ID-2	36	1200	140	20.8
ID-2	37	1200	140	21.2
ID-2	38	1200	140	21.4
ID-2	39	1200	160	21.4
ID-2	40	1200	160	21.8
ID-2	41	1200	160	22.0
ID-2	42	1400	160	22.8
ID-2	43	1400	160	23.0
ID-2	44	1400	160	23.4
ID-2	45	1400	160	23.6
ID-2	46	1400	160	23.6
ID-2	47	1400	200	24.2
ID-2	48	1400	200	24.8
ID-2	49	1400	200	25.2
ID-2	50	1400	200	25.4
ID-2	51	1400	200	25.8
ID-2	52	1400	220	26.8
ID-2	53	1400	240	26.6
ID-2	54	1400	240	27.4

ID-2	55	1400	240	28.0
ID-2	56	1400	260	28.6
ID-2	57	1400	300	28.6
ID-2	58	1400	300	29.0
ID-2	59	1400	300	29.0
ID-2	60	1400	300	29.6
ID-2	61	1400	300	29.6
ID-2	62	1400	300	29.6
ID-2	63	1400	300	30.0
ID-2	64	1400	340	31.0
ID-2	65	1400	400	31.2
ID-2	66	1400	400	31.6
ID-2	67	1400	400	31.6
ID-2	68	1400	400	32.0
ID-2	69	1400	400	32.2
ID-2	70	1400	400	33.0
ID-2	71	1400	400	33.2
ID-2	72	1400	400	33.0
ID-2	73	1400	400	33.8
ID-2	74	1400	400	34.0
ID-2	75	1400	400	34.0
ID-2	76	1400	400	35.0
ID-2	77	1400	400	35.2
ID-2	78	1400	400	35.4
ID-2	79	1400	400	35.6
ID-2	80	1400	400	35.6
ID-2	81	1400	400	35.6
ID-2	82	1400	400	36.4
ID-2	83	1400	400	36.6
ID-2	84	700	400	37.0
ID-2	85	1400	400	37.2
ID-2	86	1400	400	-
ID-2	87	1400	400	-
ID-2	88	1400	400	38.0
ID-2	89	0	400	38.0
ID-2	90	0	400	-

ID-2	91	0	350	-
ID-2	92	0	150	-
ID-2	93	0	150	-
ID-2	94	0	150	-
ID-2	95	0	150	-
ID-2	96	0	150	-
ID-2	97	0	150	-
ID-2	98	0	100	-
ID-2	99	0	100	-
ID-2	100	0	100	-
ID-2	101	0	-	-
ID-2	102	0	-	-
ID-2	103	0	-	-
ID-2	104	0	-	-
ID-2	105	0	-	42.0
ID-3	1	-	0	-
ID-3	2	-	0	-
ID-3	3	850	0	10.5
ID-3	4	1000	0	10.7
ID-3	5	1000	0	11.0
ID-3	6	1050	0	11.3
ID-3	7	1050	0	11.7
ID-3	8	1100	0	12.6
ID-3	9	1150	0	13.0
ID-3	10	900	0	13.2
ID-3	11	900	0	13.0
ID-3	12	900	0	13.2
ID-3	13	1100	0	13.6
ID-3	14	1200	0	13.9
ID-3	15	800	0	14.7
ID-3	16	1200	0	14.7
ID-3	17	1200	0	15.3
ID-3	18	1200	0	15.6
ID-3	19	1200	0	15.9
ID-3	20	1200	0	16.4
ID-3	21	1200	0	16.7

ID-3	22	1200	0	17.3
ID-3	23	1200	0	17.4
ID-3	24	1200	0	17.8
ID-3	25	1100	0	18.0
ID-3	26	800	200	18.5
ID-3	27	700	60	18.5
ID-3	28	800	85	18.5
ID-3	29	800	100	19.1
ID-3	30	800	100	19.0
ID-3	31	1800	-	19.5
ID-3	32	1800	-	19.5
ID-3	33	1800	100	20.0
ID-3	34	1200	100	20.2
ID-3	35	1000	140	20.8
ID-3	36	1200	140	20.8
ID-3	37	1200	140	21.4
ID-3	38	1200	140	21.4
ID-3	39	1200	160	21.6
ID-3	40	1200	160	21.8
ID-3	41	1200	160	22.4
ID-3	42	1400	160	22.6
ID-3	43	1400	160	23.0
ID-3	44	1400	160	23.6
ID-3	45	1400	160	23.4
ID-3	46	1400	160	23.6
ID-3	47	1400	200	24.4
ID-3	48	1400	200	24.6
ID-3	49	1400	200	25.2
ID-3	50	1400	200	25.2
ID-3	51	1400	200	25.6
ID-3	52	1400	200	26.2
ID-3	53	1400	240	26.4
ID-3	54	1400	240	27.2
ID-3	55	1400	240	27.6
ID-3	56	1400	260	28.2
ID-3	57	1400	300	28.2

ID-3	58	1300	280	27.8
ID-3	59	1400	260	28.6
ID-3	60	1400	260	29.2
ID-3	61	1400	260	29.8
ID-3	62	1400	260	30.0
ID-3	63	1400	260	30.6
ID-3	64	1400	280	31.0
ID-3	65	1400	300	31.6
ID-3	66	1400	300	31.6
ID-3	67	1400	300	31.8
ID-3	68	1400	300	32.2
ID-3	69	1400	300	33.0
ID-3	70	1400	300	33.2
ID-3	71	1400	300	33.8
ID-3	72	1400	300	33.6
ID-3	73	1400	300	33.8
ID-3	74	1400	300	34.2
ID-3	75	1400	300	34.2
ID-3	76	1400	300	35.0
ID-3	77	1400	300	35.4
ID-3	78	1400	300	35.8
ID-3	79	1400	300	36.5
ID-3	80	1400	300	37.6
ID-3	81	1400	300	37.4
ID-3	82	1400	300	38.2
ID-3	83	1400	300	38.6
ID-3	84	700	300	38.8
ID-3	85	1400	340	39.2
ID-3	86	1400	400	-
ID-3	87	1400	400	-
ID-3	88	1400	400	-
ID-3	89	0	400	41.0
ID-3	90	0	400	-
ID-3	91	0	350	-
ID-3	92	0	150	-
ID-3	93	0	150	-

ID-3	94	0	150	-
ID-3	95	0	150	-
ID-3	96	0	150	-
ID-3	97	0	150	-
ID-3	98	0	100	-
ID-3	99	0	100	-
ID-3	100	0	100	-
ID-3	101	0	-	44.0
ID-3	102-114	0	-	-
ID-3	115	0	-	52
ID-3	116-160	0	-	-
ID-3	161	0	-	70
ID-3	161-203	0	-	-
ID-3	204	0	-	72
ID-3	205-240	0	-	-
ID-3	241	0	-	75
ID-3	242-289	0	-	-
ID-3	290	0	-	80
ID-3	291-328	0	-	-
ID-3	329	0	-	92.5
ID-3	330-331	0	-	-
ID-3	332	0	-	-
ID-4	1	-	0	10.0
ID-4	2	-	0	-
ID-4	3	1150	0	-
ID-4	4	1100	0	-
ID-4	5	1000	0	-
ID-4	6	1000	0	11.2
ID-4	7	550	0	11.3
ID-4	8	600	0	11.5
ID-4	9	1150	0	11.6
ID-4	10	1200	0	11.7
ID-4	11	550	0	12.4
ID-4	12	1000	0	12.0
ID-4	13	850	0	12.8
ID-4	14	600	0	13.1

ID-4	15	600	0	13.7
ID-4	16	850	0	13.8
ID-4	17	900	0	14.1
ID-4	18	900	0	14.2
ID-4	19	900	0	14.5
ID-4	20	900	0	14.7
ID-4	21	700	0	15.2
ID-4	22	1200	0	15.4
ID-4	23	1050	0	16.2
ID-4	24	1100	0	16.3
ID-4	25	1050	0	16.9
ID-4	26	1200	0	16.7
ID-4	27	1200	0	-
ID-4	28	1200	0	17.5
ID-4	29	1250	0	18.0
ID-4	30	1350	0	18.5
ID-4	31	1350	0	19.4
ID-4	32	950	0	19.7
ID-4	33	1000	0	19.8
ID-4	34	1000	0	20.0
ID-4	35	1000	0	21.0
ID-4	36	1200	0	21.4
ID-4	37	1100	0	21.6
ID-4	38	950	0	21.9
ID-4	39	1000	0	22.5
ID-4	40	1000	0	22.8
ID-4	41	1000	0	23.2
ID-4	42	1000	0	23.7
ID-4	43	1200	0	23.8
ID-4	44	1100	0	24.8
ID-4	45	1100	0	25.0
ID-4	46	1100	0	25.4
ID-4	47	1100	0	26.0
ID-4	48	1000	0	26.0
ID-4	49	1000	0	26.4
ID-4	50	1000	0	26.8

ID-4	51	1000	0	27.0
ID-4	52	1000	0	27.4
ID-4	53	1000	0	28.2
ID-4	54	1000	0	28.6
ID-4	55	1100	0	28.8
ID-4	56	1200	0	29.6
ID-4	57	1200	0	30.2
ID-4	58	1200	0	30.4
ID-4	59	1200	0	31.2
ID-4	60	1200	0	31.4
ID-4	61	1200	0	31.6
ID-4	62	1200	0	32.4
ID-4	63	1200	0	33.0
ID-4	64	1200	0	33.4
ID-4	65	1200	0	33.4
ID-4	66	1200	0	33.8
ID-4	67	1200	0	-
ID-4	68	1200	0	34.2
ID-4	69	1200	0	34.6
ID-4	70	1200	0	35.0
ID-4	71	1200	0	35.4
ID-4	72	1200	0	35.8
ID-4	73	1200	0	36.4
ID-4	74	600	0	36.8
ID-4	75	1200	0	34.0
ID-4	76	1200	0	37.2
ID-4	77	1200	0	37.8
ID-4	78	1200	0	38.0
ID-4	79	600	0	38.2
ID-4	80	1200	0	38.2
ID-4	81	1200	0	-
ID-4	82	1200	0	38.6
ID-4	83	1200	0	39.2
ID-4	84	1200	0	39.4
ID-4	85	600	0	40.0
ID-4	86	1200	0	39.2

ID-4	87	1200	0	40.4
ID-4	88	1200	200	40.2
ID-4	89	1200	20	41.0
ID-4	90	1200	200	41.6
ID-4	91	1200	200	41.6
ID-4	92	1200	200	42.4
ID-4	93	1200	200	42.4
ID-4	94	1000	300	42.6
ID-4	95	0	300	-
ID-4	96	0	300	42.6
ID-4	97	0	300	42.6
ID-4	98	0	300	42.6
ID-4	99	0	300	43.0
ID-4	100	0	300	42.8
ID-4	101	0	300	43.0
ID-4	102	0	300	42.2
ID-4	103	0	300	42.4
ID-4	104	0	300	42.2
ID-4	105	0	150	42.4
ID-4	106	0	150	42.4
ID-4	107	0	150	42.8
ID-4	108	0	150	43.0
ID-4	109	0	150	43.2
ID-4	110	0	150	-
ID-4	111	0	150	42.6
ID-4	112	0	150	42.2
ID-4	113	0	150	42.4
ID-4	114	0	150	42.8
ID-4	115	0	150	43.8
ID-4	116	0	150	45.0
ID-4	117	0	150	44.0
ID-4	118	0	100	44.0
ID-4	119	0	100	44.8
ID-4	120	0	100	44.8
ID-4	121	0	100	45.0
ID-4	122	0	100	46.0

ID-4	123	0	100	46.4
ID-4	124	0	100	-
ID-4	125	0	100	46.8
ID-4	126	0	100	47.2
ID-4	127	0	100	47.8
ID-4	128	0	100	48.0
ID-4	129	0	100	47.8
ID-4	130	0	100	48.4
ID-4	131	0	100	48.8
ID-4	132	0	100	49.0
ID-4	133	0	100	49.4
ID-4	134	0	100	50.6
ID-4	135	0	100	50.5
ID-4	136	0	50	50.5
ID-4	137	0	50	51.5
ID-4	138	0	50	51.5
ID-4	139	0	50	51.0
ID-4	140	0	50	-
ID-4	141-164	0	-	-
ID-4	165	0	-	58.5
ID-4	166-206	0	-	-
ID-4	207	0	-	64
ID-4	208-248	0	-	-
ID-4	249	0	-	72.5
ID-4	250-290	0	-	-
ID-4	291	0	-	83
ID-4	292-330	0	-	-
ID-4	331	0	-	92
ID-4	332	0	-	-
ID-4	333	0	-	92

Table S8.5. Feed regime information based on the quantity of milk intake (i.e. artificial milk) and vegetal pellets (in grams per millilitre) together to the daily body mass (in kilograms) for the hand-raised individuals (C2 group). Table obtained from Calderón et al. (2021).

173

ID	regime	bone	period	measured area	correction factor	standarized area
ID-1	hand	femur	Birth	19.258	1.441	27.760
ID-1	hand	femur	3 d	27.356	1.414	38.685
ID-1	hand	femur	15 d	7.003	1.336	9.358
ID-2	hand	femur	3 d	10.662	1.482	15.799
ID-2	hand	femur	30 d	9.930	1.283	12.741
ID-2	hand	femur	13 w	9.741	1.000	9.741
ID-2	hand	femur	15 w	2.006	0.960	1.926
ID-3	hand	femur	13 w	9.727	1.000	9.727
ID-3	hand	femur	15 w	4.570	0.971	4.435
ID-3	hand	femur	17 w	7.438	0.918	6.828
ID-3	hand	femur	23 w	4.125	0.794	3.274
ID-4	hand	femur	9 w	6.874	1.100	7.562
ID-4	hand	femur	11 w	11.132	1.021	11.361
ID-4	hand	femur	13 w	5.708	1.000	5.708
ID-4	hand	femur	15 w	3.425	0.985	3.374
ID-4	hand	femur	17 w	1.561	0.970	1.514
ID-4	hand	femur	23 w	4.978	0.879	4.377
ID-24	nursed	femur	13 w	8.683	1.000	8.683
ID-23	nursed	femur	13 w	3.035	1.000	3.035
ID-1	hand	tibia	Birth	12.951	1.114	14.429
ID-1	hand	tibia	3 d	17.396	1.087	18.907
ID-1	hand	tibia	15 d	4.152	1.021	4.237
ID-2	hand	tibia	3 d	12.290	0.999	12.277
ID-2	hand	tibia	30 d	6.764	0.913	6.176
ID-2	hand	tibia	13 w	7.059	1.000	7.059
ID-2	hand	tibia	15 w	3.240	0.661	2.143
ID-3	hand	tibia	13 w	7.701	1.000	7.701
ID-3	hand	tibia	15 w	7.886	0.678	5.347
ID-3	hand	tibia	17 w	4.107	0.653	2.681
ID-3	hand	tibia	23 w	9.200	0.555	5.103
ID-4	hand	tibia	9 w	5.340	0.767	4.097
ID-4	hand	tibia	11 w	16.607	0.724	12.021
ID-4	hand	tibia	13 w	4.251	1.000	4.251
ID-4	hand	tibia	15 w	2.699	0.692	1.867

ID-4	hand	tibia	17 w	0.628	0.668	0.420
ID-4	hand	tibia	23 w	6.177	0.605	3.739
ID-24	nursed	tibia	13 w	12.8987	1.000	12.899
ID-23	nursed	tibia	13 w	4.046	1.000	4.046
ID-1	hand	humerus	Birth	10.692	1.407	15.044
ID-1	hand	humerus	3 d	22.773	1.370	31.190
ID-1	hand	humerus	15 d	NA	1.354	NA
ID-2	hand	humerus	3 d	14.617	1.356	19.821
ID-2	hand	humerus	30 d	11.895	1.216	14.469
ID-2	hand	humerus	13 w	8.784	1.000	8.784
ID-2	hand	humerus	15 w	2.665	0.909	2.423
ID-3	hand	humerus	13 w	11.424	1.000	11.424
ID-3	hand	humerus	15 w	5.904	0.896	5.292
ID-3	hand	humerus	17 w	8.006	0.849	6.801
ID-3	hand	humerus	23 w	4.009	0.745	2.985
ID-4	hand	humerus	9 w	7.975	0.889	7.092
ID-4	hand	humerus	11 w	8.466	0.855	7.241
ID-4	hand	humerus	13 w	5.253	1.000	5.253
ID-4	hand	humerus	15 w	1.791	0.817	1.464
ID-4	hand	humerus	17 w	1.642	0.800	1.314
ID-4	hand	humerus	23 w	6.114	0.722	4.411
ID-24	nursed	humerus	13 w	10.377	1.000	10.377
ID-23	nursed	humerus	13 w	5.624	1.000	5.624
ID-1	hand	radius	Birth	10.223	1.721	17.592
ID-1	hand	radius	3 d	13.908	1.666	23.175
ID-1	hand	radius	15 d	NA	1.563	NA
ID-2	hand	radius	3 d	8.156	1.537	12.537
ID-2	hand	radius	30 d	5.985	1.407	8.423
ID-2	hand	radius	13 w	3.158	1.000	3.158
ID-2	hand	radius	15 w	4.202	1.063	4.468
ID-3	hand	radius	13 w	5.996	1.000	5.996
ID-3	hand	radius	15 w	4.503	0.971	4.372
ID-3	hand	radius	17 w	4.075	0.931	3.794
ID-3	hand	radius	23 w	4.503	0.838	3.774
ID-4	hand	radius	9 w	4.580	1.118	5.121
ID-4	hand	radius	11 w	7.772	1.079	8.389

ID-4	hand	radius	13 w	1.581	1.000	1.581
ID-4	hand	radius	15 w	0.684	1.053	0.720
ID-4	hand	radius	17 w	0.411	1.036	0.426
ID-4	hand	radius	23 w	3.492	0.952	3.325
ID-24	nursed	radius	13 w	2.922	1.000	2.922
ID-23	nursed	radius	13 w	1.999	1.000	1.999
ID-1	hand	metatarsus	Birth	13.307	1.289	17.156
ID-1	hand	metatarsus	3 d	19.602	1.256	24.629
ID-1	hand	metatarsus	15 d	1.622	1.176	1.907
ID-2	hand	metatarsus	3 d	9.129	1.264	11.537
ID-2	hand	metatarsus	30 d	4.484	1.177	5.278
ID-2	hand	metatarsus	13 w	6.439	1.000	6.439
ID-2	hand	metatarsus	15 w	5.337	0.820	4.375
ID-3	hand	metatarsus	13 w	NA	1.000	NA
ID-3	hand	metatarsus	15 w	12.791	0.842	10.768
ID-3	hand	metatarsus	17 w	NA	0.811	NA
ID-3	hand	metatarsus	23 w	12.008	0.670	8.047
ID-4	hand	metatarsus	9 w	5.144	1.091	5.614
ID-4	hand	metatarsus	11 w	NA	1.041	NA
ID-4	hand	metatarsus	13 w	NA	1.000	NA
ID-4	hand	metatarsus	15 w	NA	0.992	NA
ID-4	hand	metatarsus	17 w	NA	0.948	NA
ID-4	hand	metatarsus	23 w	6.434	0.822	5.287
ID-24	nursed	metatarsus	13 w	6.31	1.000	6.310
ID-23	nursed	metatarsus	13 w	5.310	1.000	5.310
ID-1	hand	metacarpus	Birth	12.702	1.972	25.052
ID-1	hand	metacarpus	3 d	17.669	1.924	34.004
ID-1	hand	metacarpus	15 d	NA	1.826	NA
ID-2	hand	metacarpus	3 d	8.848	1.969	17.419
ID-2	hand	metacarpus	30 d	1.745	1.874	3.270
ID-2	hand	metacarpus	13 w	2.516	1.000	2.516
ID-2	hand	metacarpus	15 w	2.772	1.389	3.851
ID-3	hand	metacarpus	13 w	NA	1.000	NA
ID-3	hand	metacarpus	15 w	10.977	1.385	15.207
ID-3	hand	metacarpus	17 w	NA	1.360	NA
ID-3	hand	metacarpus	23 w	6.176	1.203	7.432

ID-4	hand	metacarpus	9 w	4.367	1.845	8.056
ID-4	hand	metacarpus	11 w	NA	1.789	NA
ID-4	hand	metacarpus	13 w	NA	1.000	NA
ID-4	hand	metacarpus	15 w	NA	1.702	NA
ID-4	hand	metacarpus	17 w	NA	1.659	NA
ID-4	hand	metacarpus	23 w	6.474	1.482	9.592
ID-24	nursed	metacarpus	13 w	7.571	1.000	7.571
ID-23	nursed	metacarpus	13 w	5.290	1.000	5.290

Table S8.6. Standardization of the fluorochrome-stained (labelled) areas (in square millimetres) by applying the correction factor based on the common label (i.e. 13weeks) on the measured labelled areas (also in square millimetres). hand: hand-raised regime; nursed: individuals that remained with their mothers; w: weeks; d: days. Table obtained from Calderón et al. (2021).

CHAPTER 9. REFERENCES

A

Ahnlund, H., 1976. Age determination in the european badger, *Meles meles* L. Zeitschrift fur Säugetierkd. 41, 119–125.

Albon, S.D., Clutton-Brock, T.H., Guinness, F.E., 1987. Early development and population dynamics in red deer II. Density-independent effects and cohort variation. J. Anim. Ecol. 56, 69–81.

Amprino, R., 1947. La structure du tissu osseux envisagée comme expression de différences dans la vitesse de l'accroisement. Arch. Biol. (Liege). 58, 315–330.

Amson, E., Kolb, C., Scheyer, T.M., Sánchez-Villagra, M.R., 2015. Growth and life history of Middle Miocene deer (Mammalia, Cervidae) based on bone histology. Comptes Rendus - Palevol 14, 637–645. https://doi.org/10.1016/j.crpv.2015.07.001

Anders, U., von Koenigswald, W., Ruf, I., Smith, B.H., 2011. Generalized individual dental age stages for fossil and extant placental mammals. Palaontologische Zeitschrift 85, 321–339. https://doi.org/10.1007/s12542-011-0098-9

Andrews, A.H., 1973. A survey of the relationship between age and the development of the anterior teeth in cattle. Vet. Rec. 92, 275–282. https://doi.org/10.1136/vr.92.11.275

Arendt, J.D., 1997. Adaptive Intrinsic Growth Rates : An Integration Across Taxa. Q. Rev. Biol. 72, 149–177.

Azanza, B., DeMiguel, D., DeMiguel, D., Andrés, M., Andrés, M., 2011. The antler-like appendages of the primitive deer *Dicrocerus elegans*: morphology, growth cycle, ontogeny, and sexual dimorphism. Estud.

Geológicos 67, 579–602. https://doi.org/10.3989/egeol.40559.207

Azanza, B., Ginsburg, L., 1997. A revision of the large lagomerycid artiodactyls of Europe. Palaeontology 40, 461–485.

Azanza, B., Rössner, G.E., Ortiz-Jaureguizar, E., 2013. The early Turolian (late Miocene) Cervidae (Artiodactyla, Mammalia) from the fossil site of Dorn-Dürkheim 1 (Germany) and implications on the origin of crown cervids. Palaeobiodiversity and Palaeoenvironments 93, 217–258. https://doi.org/10.1007/s12549-013-0118-8

Azorit, C., 2011. Guía para la determinación de la edad del ciervo ibérico (*Cervus elaphus hispanicus*) a través de su dentición: Revisión metodológica y técnicas de elección. An. Real Acad. ciencias Vet. Andalucía Orient. 24, 235–264.

Azorit, C., Analla, M., Carrasco, R., Calvo, J.A., Muñoz-Cobo, J., 2002. Teeth eruption pattern in red deer (*Cervus elaphus hispanicus*) in southern Spain. An. Biol. 24, 107–114.

Azorit, C., Muñoz-Cobo, J., Hervás, J., Analla, M., 2004. Aging through Growth Marks in Teeth of Spanish Red Deer. Wildl. Soc. Bull. 32, 702–710. https://doi.org/10.2193/0091-7648(2004)032[0702:ATGMIT]2.0.CO;2

B

Barker, J.M., Boonstra, R., Schulte-Hostedde, A.I., 2003. Age determination in yellow-pine chipmunks (*Tamias amoenus*): A comparison of eye lens masses and bone sections. Can. J. Zool. 81, 1774–1779. https://doi.org/10.1139/z03-173

Becker, M., Witzel, C., Kierdorf, U., Frölich, K., Kierdorf, H., 2020. Ontogenetic changes of tissue compartmentalization and bone type distribution in the humerus of Soay sheep. J. Anat. 237, 334–354. https://doi.org/10.1111/joa.13194

Botha, J., Chinsamy, A., 2005. Growth patterns of Thrinaxodon liorhinus, a non-mammalian cynodont from the Lower Triassic of South Africa. Palaeontology 48, 385–394. https://doi.org/10.1111/j.1475-4983.2005.00447.x

Braendle, C., Heyland, A., Flatt, T., 2011. Integrating mechanistic and evolutionary analysis of life history variation, in: Flatt, T., Hayland, A. (Eds.), Mechanisms of Life History Evolution. The Genetics and Physiology of Life History Traits and Trade- Offs. Oxford University Press, Oxford, pp. 3–10.

Bromage, T.G., Dirks, W., Erdjument-Bromage, H., Huck, M., Kullmer, O., Öner, R., Sandrock, O., Schrenk, F., 2002. A life history and climate change solution to the evolution and extinction of insular dwarfs: a Cypriot experience, in: Waldren, W.H., Ensenyat, J.A. (Eds.), World Islands in Prehistory: International Insular Investigations, V Deia International Conference of Prehistory. pp. 420–427.

Bromage, T.G., Goldman, H.M., McFarlin, S.C., Warshaw, J., Boyde, A., Riggs, C.M., 2003. Circularly polarized light standards for investigations of collagen fiber orientation in bone. Anat. Rec. - Part B New Anat. 274, 157–168. https://doi.org/10.1002/ar.b.10031

Bromage, T.G., Lacruz, R.S., Hogg, R., Goldman, H.M., McFarlin, S.C., Warshaw, J., Dirks, W., Perez-Ochoa, A., Smolyar, I., Enlow, D.H., Boyde, A., 2009. Lamellar bone is an incremental tissue reconciling enamel rhythms, body size, and organismal life history. Calcif. Tissue Int. 84, 388–404. https://doi.org/10.1007/s00223-009-9221-2

Bromage, T.G., Werning, S., 2013. Image standarization in paleohistology, in: Bone Histology of Fossil Tetrapods. pp. 161–176.

Brooke, V., 1878. On the Classification of the Cervidœ, with a Synopsis of the existing Species. Proc. Zool. Soc. 883–928.

Brown, J.H., Gillooly, J.F., Allen, P.A., Savage, V.M., Geoffrey, B.W., 2004. Toward a metabolic theory of ecology. Ecology 85, 1771–1789.

Brown, W.A.B., Chapman, N.G., 1991. The dentition of red deer (*Cervus elaphus*): a scoring scheme to assess age from wear of the permanent molariform teeth. J. Zool. 224, 519–536. https://doi.org/10.1111/j.1469-7998.1991.tb03783.x

Bubenik, A.B., 1990. Epigenetical, morphological, physiological, and behavioral aspects of evolution of horns, pronghorns, and antlers, in: Bubenik, G.A., Bubenik, A.B. (Eds.), Horns, Pronghorns, and Antlers: Evolution, Morphology, Physiology, and Social Significance. Springer, New York, p. 113. https://doi.org/10.2307/3809535

Buffrénil, V. de, Pascal, M., 1984. Croissance et morphogénèse postnatales de la mandibule du vison (*Mustela vison* Schreiber): données sur la dynamique et l'interprétation fonctionnelle des dépôts osseux mandibulaires. Can. J. Zool. 62, 2026–2037. https://doi.org/10.1139/z84-297

C

Calderón, T., Arnold, W., Stalder, G., Painer, J., Köhler, M., 2021. Labelling experiments in red deer provide a general model for early bone growth dynamics in ruminants. Sci. Rep. 11, 1–14. https://doi.org/10.1038/s41598-021-93547-4

Calderón, T., DeMiguel, D., Arnold, W., Stalder, G., Köhler, M., 2019. Calibration of life history traits with epiphyseal closure, dental eruption and bone histology in captive and wild red deer. J. Anat. 205–216. https://doi.org/10.1111/joa.13016

Cambra-Moo, O., Nacarino-Meneses, C., Díaz-Güemes, I., Enciso, S., García Gil, O., Llorente Rodríguez, L., Rodríguez Barbero, M.Á., de Aza, A.H., González Martín, A., 2015. Multidisciplinary characterization of the long-

bone cortex growth patterns through sheep's ontogeny. J. Struct. Biol. 191, 1–9. https://doi.org/10.1016/j.jsb.2015.06.013

Cantalapiedra, J.L., Hernández Fernández, M., Azanza, B., Morales, J., 2015. Congruent phylogenetic and fossil signatures of mammalian diversification dynamics driven by Tertiary abiotic change. Evolution (N. Y). 69, 2941–2953. https://doi.org/10.1111/evo.12787

Carden, R.F., Hayden, T.J., 2002. Epiphyseal fusion in the postcranial skeleton as an indicator of age at death of European Fallow Deer (*Dama dama dama*, Linnaeus, 1758), in: Ruscillo, D. (Ed.), Recent Advances in Ageing and Sexing Animal Bones. Oxbow Books, Park End Place, Oxford OX1 1HN, pp. 227–236.

Carranza, J., 2017. Ciervo – *Cervus elaphus* Linnaeus, 1758, in: Salvador, A., Barja, I. (Eds.), Enciclopedia Virtual de Los Vertebrados Españoles. Museo Nacional de Ciencias Naturales, Madrid, p. 34.

Carranza, J., 2007. *Cervus elaphus* Linnaeus, 1758. Ciervo rojo. Atlas y Libr. Rojo los Mamíferos Terr. España 352–355.

Carranza, J., Salinas, M., de Andrés, D., Pérez-González, J., 2016. Iberian red deer: Paraphyletic nature at mtDNA but nuclear markers support its genetic identity. Ecol. Evol. 6, 905–922. https://doi.org/10.1002/ece3.1836

Castanet, Croci, S., Aujard, F., Perret, M., Cubo, J., De Margerie, E., 2004. Lines of arrested growth in bone and age estimation in a small primate: *Microcebus murinus*. J. Zool. 263, 31–39. https://doi.org/10.1017/S0952836904004844

Castanet, J., 2006. Time recording in bone microstructures of endothermic animals; functional relationships. Comptes Rendus Palevol 5, 629–636. https://doi.org/10.1016/j.crpv.2005.10.006

Castanet, J., Curry Rogers, K., Cubo, J., Jacques-Boisard, J., 2000. Periosteal bone growth rates in extant ratites (ostriche and emu). Implications for

assessing growth in dinosaurs. Comptes Rendus l'Académie des Sci. - Ser. III - Sci. la Vie 323, 543–550. https://doi.org/10.1016/s0764-4469(00)00181-5

Castanet, J., Francillon-Vieillot, H., Meunier, F.J., de Ricqlès, A., 1993. Bone and individual aging, in: Bone Veolume 7 Bone Growth. CRC Press, Boca Raton, pp. 245–283.

Castanet, J., Grandin, A., Abourachid, A., de Ricqlès, A., 1996. Expression de la dynamique de croissance dans la structure de I'os periostique chez Anas platyrhynchos. Comptes Rendus, Académie des Sci. Paris, Sci. la Vie 319, 301–308.

Cederlund, G., Kjellander, P., Stålfelt., F., 1991. Age determination of roe deer by tooth wear and cementum layers-tests with known age material, in: 20th Congress of the International Union of Game Biologists. pp. 540–545. https://doi.org/10.2331/suisan.33.788

Cerrito, P., Cerrito, L., Hu, B., Bailey, S.E., Kalisher, R., Bromage, T.G., 2021. Weaning, parturitions and illnesses are recorded in rhesus macaque (*Macaca mulatta*) dental cementum microstructure. Am. J. Primatol. 83. https://doi.org/10.1002/ajp.23235

Chinsamy-Turan, A., 2005. The microstructure of dinosaur bone. Baltimore: The Johns Hopkins University Press.

Chinsamy, A., 1994. Dinosaur Bone Histology: Implications and Inferences. Paleontol. Soc. Spec. Publ. 7, 213–228. https://doi.org/10.1017/s2475262200009539

Chinsamy, A., Hurum, J.H., 2006. Bone microstructure and growth patterns of early mammals. Acta Palaeontol. Pol. 51, 325–338.

Chinsamy, A., Marugán-Lobón, J., Serrano, F.J., Chiappe, L., 2020. Osteohistology and Life History of the Basal Pygostylian, *Confuciusornis sanctus*. Anat. Rec. 303, 949–962. https://doi.org/10.1002/ar.24282

Chinsamy, A., Warburton, N.M., 2021. Ontogenetic growth and the development of a unique fibrocartilage entheses in *Macropus fuliginosus*. Zoology 144, 125860. https://doi.org/10.1016/j.zool.2020.125860

Clauss, M., Rössner, G.E., 2014. Old world ruminant morphophysiology, life history, and fossil record: Exploring key innovations of a diversification sequence. Ann. Zool. Fennici 51, 80–94. https://doi.org/10.5735/086.051.0210

Clutton-Brock, T., Guinness, F.E., Albon, S.D., 1983. The Costs of Reproduction to Red Deer Hinds. J. Anim. Ecol. 52, 367–383.

Clutton-Brock, T.H., Albon, S.D., Guinness, F.E., 1989. Fitness costs of gestation and lactation in wild mammals. Nature 337, 260–262.

Clutton-Brock, T.H., Guiness, F.E., Albon, S.D., 1982. Red deer: behaviour and ecology of two sexes. The University of Chicago Press, Chicago. https://doi.org/10.1016/0006-3207(83)90010-1

Clutton-Brock, T.H., Major, M., Albon, S.D., Guinness, F.E., 1987. Early Development and Population Dynamics in Red Deer. I. Density-Dependent Effects on Juvenile Survival. J. Anim. Ecol. 56, 53–67.

Cody, M.L., 1966. A General Theory of Clutch Size. Evolution (N. Y). 20, 174–184. https://doi.org/10.2307/2406571

Cook, J.G., Johnson, B.K., Cook, R.C., Riggs, R.A., Delcurto, T., Bryant, L.D., Irwin, L.L., 2004. Effects of Summer-Autumn Nutrition and Parturition Date on Reproduction and Survival of Elk. Wildl. Monogr. 1–61.

Cooper, S.M., Sieckenius, S.S., Silva, A.L., 2013. Dentine method: Aging white-tailed deer by tooth measurements. Wildl. Soc. Bull. 37, 451–457. https://doi.org/10.1002/wsb.275

Croitor, R., 2018. Plio-Pleistocene Deer of Western Palearctic: Taxonomy , Systematics, Phylogeny.

Croitor, R., 2014. Deer from Late Miocene to Pleistocene of Western Palearctic: Matching fossil record and molecular phylogeny data. Zitteliana R. B Abhandlungen der Bayer. Staatssammlung fur Palaontologie und Geol. 115–153. https://doi.org/10.5282/ubm/epub.22391

Cubo, J., Roy, N. Le, Martinez-maza, C., Montes, L., 2012. Paleohistological estimation of bone growth rate in extinct archosaurs. Paleobiology 38, 335–349. https://doi.org/10.5061/dryad.j2m25n82

Currey, J.D., 2003. The many adaptations of bone. J. Biomech. 36, 1487–1495. https://doi.org/10.1016/S0021-9290(03)00124-6

Curtin, A.J., Macdowell, A.A., Schaible, E.G., Curtin, A.J., Macdowell, A.A., Schaible, E.G., Carolina, N., 2012. Noninvasive histological comparison of bone growth patterns among fossil and extant neonatal elephantids using synchrotron radiation x- ray microtomography. J. Vertebr. Paleontol. 32, 939–955.

D

Davis, S.J.M., 2000. The effect of castration and age on the development of the Shetland sheep skeleton and a metric comparison between bones of males, females and castrates. J. Archaeol. Sci. 27, 373–390. https://doi.org/10.1006/jasc.1999.0452

de Buffrénil, V., de Ricqlès, A.J., Zylberberg, L., Padian, K., 2021. Vertebrate skeletal histology and paleohistology. CRC Press.

de Buffrenil, V., Mazin, J.-M., 1990. Bone Histology of the Ichtyosaurs Comparative Data and Functional Interpretation Paleontological Society Stable. Paleobiology 16, 435–447.

de Buffrénil, V., Quilhac, A., 2021. Bone tissue types: A brief account of currently used categories, in: de Buffrénil, V., de Riclès, J.A., Zylbeberg, L., Padian, K. (Eds.), Vertebrate Skeletal Histology and Paleohistology. CRC

Press, pp. 148–192.

de Margerie, E., Cubo, J., Castanet, J., 2002. Bone typology and growth rate: Testing and quantifying "Amprino's rule" in the mallard (*Anas platyrhynchos*). Comptes Rendus - Biol. 325, 221–230. https://doi.org/10.1016/S1631-0691(02)01429-4

de Margerie, E., Robin, J.-P., Verrier, D., Cubo, J., Griscikas, R., Castanet, J., 2004. Assessing a relationship between bone microstructure and growth rate: a fluorescent labelling study in the king penguin chick (*Aptenodytes patagonicus*). J. Exp. Biol. 207, 869–879. https://doi.org/10.1242/jeb.00841

DeMiguel, D., Azanza, B., Morales, J., 2014. Key innovations in ruminant evolution: A paleontological perspective. Integr. Zool. 9, 412–433. https://doi.org/10.1111/1749-4877.12080

Dirks, W., Bowman, J.E., 2007. Life history theory and dental development in four species of catarrhine primates. J. Hum. Evol. 53, 309–320. https://doi.org/10.1016/j.jhevol.2007.04.007

Dirks, W., Bromage, T.G., Agenbroad, L.D., 2012. The duration and rate of molar plate formation in *Palaeoloxodon cypriotes* and *Mammuthus columbi* from dental histology. Quat. Int. 255, 79–85. https://doi.org/10.1016/j.quaint.2011.11.002

Dmitriew, C.M., 2011. The evolution of growth trajectories : what limits growth rate? Biol. Rev. 86, 97–116. https://doi.org/10.1111/j.1469-185X.2010.00136.x

E

Engström, C., Engström, H., Sagne, S., 1983. Lower third molar development in relation to skeletal maturity and chronological age. Angle Orthod. 53.

Enlow, D.H., 1962a. A study of the post-natal growth and remodelling of bone.

Am. J. Anat. 110, 79–101.

Enlow, D.H., 1962b. Functions of the haversian system. Am. J. Anat. 110, 269–305. https://doi.org/10.1002/aja.1001100305

Enlow, D.H., Brown, S.O., 1958. A Comparative Histological Study of Fossil and Recent Bone Tissues, Part III. Texas J. Sci. 10, 187–230.

Enlow, D.H., Brown, S.O., 1957. A Comparative Histological Study of Fossil and Recent Bone Tissues, Part II. Texas J. Sci. 9, 186–204.

Enlow, D.H., Brown, S.O., 1956. A comparative histological study of fossil and recent tissues I. Texas J. Sci. 8.

Enríquez, D., Hötzel, M.J., Ungerfeld, R., 2011. Minimising the stress of weaning of beef calves: A review. Acta Vet. Scand. 53, 1–8. https://doi.org/10.1186/1751-0147-53-28

Erben, R.G., 2003. Bone-Labeling Techniques, in: Martin, Y.H.A. and K.L. (Ed.), Handbook of Histology Methods for Bone and Cartilague. Humana Press Inc., Totowa, NJ, pp. 99–100.

Erickson, G.M., 2005. Assessing dinosaur growth patterns: A microscopic revolution. Trends Ecol. Evol. 20, 677–684. https://doi.org/10.1016/j.tree.2005.08.012

F

Fernández, M.H., Vrba, E.S., 2005. A complete estimate of the phylogenetic relationships in Ruminantia: a dated species-level supertree of the extant ruminants. Biol. Rev. 80, 269–302. https://doi.org/10.1017/S1464793104006670

Ferré, P., Decaux, J.F., Issad, T., Girard, J., 1986. Changes in energy metabolism during the suckling and weaning period in the newborn. Reprod. Nutr. Dev. 26, 619–631. https://doi.org/10.1051/rnd:19860413

Festa-bianchet, M., Jorgenson, J.T., Réale, D., 2000. Early development, adult mass, and reproductive success in bighorn sheep. Behav. Ecol. 11, 633–639.

Flinn, E.B., Strickland, B.K., Demarais, S., Christiansen, D., 2013. Age and Gender Affect Epiphyseal Closure in White-tailed Deer. Southeast. Nat. 12, 297–306. https://doi.org/10.1656/058.012.0205

Francillon-Vieillot, H., de Buffrénil, V., Castanet, J., Géraudie, J., Meunier, F.J., Sire, J.Y., Zykververg, L., de Ricqlès, A., 1990. Microstructural and mineralization of vertebral skeletal tissues, in: Carter, J.G. (Ed.), Skeletal Biommineralization: Patterns, Processes and Evolutionary Trends. Van Nostrand Reinhold, New York.

G

Gadgil, M., Bossert, W.H., 1970. Life history consequences of natural selection. Am. Nat. 104, 1–24.

Gaillard, A.J., Pontier, D., Allainé, D., Lebreton, J.D., Trouvilliez, J., Clobert, J., 1989. An Analysis of Demographic Tactics in Birds and Mammals. Oikos 56, 59–76.

Gaillard, J.M., Pontier, D., Allaine, D., Loison, A., Herve, J.C., Heizmann, A., 1997. Variation in growth form and precocity at birth in eutherian mammals. Proc. R. Soc. B Biol. Sci. 264, 859–868. https://doi.org/10.1098/rspb.1997.0120

García-Martínez, R., Marín-Moratalla, N., Jordana, X., Köhler, M., 2011. The ontogeny of bone growth in two species of dormice: Reconstructing life history traits. Comptes Rendus - Palevol 10, 489–498. https://doi.org/10.1016/j.crpv.2011.03.011

Garde, J ., Fernández-Santos, M.R., Soler, A.J., Esteso, M.C., Maroto-Morales, A., García-Álvarez, O., García-Díaz, A.J., Ortiz, J.A., Ramón, M., 2010. Ciervo ibérico (*Cervus elaphus hispanicus*, Hilzheimer, 1909), in: INIA (Ed.),

Ungulados Silvestres de España : Biología y Tecnologías Reproductivas Para Su Conservación y Aprovechamiento Cinegético. pp. 157–178.

Geist, V., 1998. Deer of the World: Their Evolution, Behavior and Ecology. Mechanicsburg: Stackpole Books. https://doi.org/10.14430/arctic950

Gentry, A.W., 2000. The ruminant radiation, in: Vrba, E.S., Schaller, G.B. (Eds.), Antelopes, Deer, and Relatives: Fossil Record, Behavioral Ecology, Systematics and Conservation. Yale University Press, New Haven, Connecticut, pp. 11–25.

Gilbert, C., Ropiquet, A., Hassanin, A., 2006. Mitochondrial and nuclear phylogenies of Cervidae (Mammalia, Ruminantia): Systematics, morphology, and biogeography. Mol. Phylogenet. Evol. 40, 101–117. https://doi.org/10.1016/j.ympev.2006.02.017

Gillooly, J.F., Charnov, E.L., Geoffrey, B.W., Savage, V.M., James, H.B., 2002. Effects of size and temperature on developmental time. Nature 417, 70–73. https://doi.org/10.1038/417070a

Gotthard, K., Nylin, S., Wiklund, C., 1994. Adaptive variation in growth rate: life history costs and consequences in the speckled wood butterfly, *Pararge aegeria*. Oecologia 99, 281–289. https://doi.org/10.1007/BF00627740

Grooves, C.P., 2007. Family Cervidae, in: Prothero, D.R., Foss, S.E. (Eds.), The Evolution of Artiodactyls. John Hopkins University Press, Baltimore, Maryland, pp. 249–256.

H

Hamel, S., Gaillard, J.M., Yoccoz, N.G., Loison, A., Bonenfant, C., Descamps, S., 2010. Fitness costs of reproduction depend on life speed: Empirical evidence from mammalian populations. Ecol. Lett. 13, 915–935. https://doi.org/10.1111/j.1461-0248.2010.01478.x

Hassanin, A., Delsuc, F., Ropiquet, A., Hammer, C., Jansen Van Vuuren, B., Matthee, C., Ruiz-Garcia, M., Catzeflis, F., Areskoug, V., Nguyen, T.T., Couloux, A., 2012. Pattern and timing of diversification of Cetartiodactyla (Mammalia, Laurasiatheria), as revealed by a comprehensive analysis of mitochondrial genomes. Comptes Rendus - Biol. 335, 32–50. https://doi.org/10.1016/j.crvi.2011.11.002

Hayashi, S., Kubo, M.O., Sánchez-Villagra, M.R., Taruno, H., Izawa, M., Shiroma, T., Nakano, T., Fujita, M., 2020. Variation and mechanisms of life history evolution in insular dwarfism as revealed by a natural experiment. bioRxiv.

Heck, C.T., Varricchio, D.J., Gaudin, T.J., Woodward, H.N., Horner, J.R., 2019. Ontogenetic changes in the long bone microstructure in the nine-banded armadillo (*Dasypus novemcinctus*). PLoS One 14, 1–24. https://doi.org/10.1371/journal.pone.0215655

Heckeberg, N.S., 2020. The systematics of the Cervidae: A total evidence approach. PeerJ 2020, 1–76. https://doi.org/10.7717/peerj.8114

Hillson, S., 2005. Teeth. Cambridge University Press, Cambridge. https://doi.org/10.1016/B978-0-12-394619-5.00002-X

Holland, J.L., Kronfeld, D.S., Hoffman, R.M., Greiwe-Crandell, K.M., Boyd, T.L., Cooper, W.L., Harris, P.A., 1996. Weaning stress is affected by nutrition and weaning methods. Pferdeheilkunde 12, 257–260. https://doi.org/10.21836/pem19960319

Horner, J.R., De Ricqlès, A., Padian, K., 2000a. Long Bone Histology of the Hadrosaurid Dinosaur *Maiasaura peeblesorum*: Growth Dynamics and Physiology Based on an Ontogenetic Series of Skeletal Elements. J. Vertebr. Paleontol. 20, 115–129. https://doi.org/10.1671/0272-4634(2000)020[0115:LBHOTH]2.0.CO;2

Horner, J.R., De Ricqlès, A., Padian, K., 2000b. Long Bone Histology of the

Hadrosaurid Dinosaur Maiasaura peeblesorum: Growth Dynamics and Physiology Based on an Ontogenetic Series of Skeletal Elements. J. Vertebr. Paleontol. 20, 115–129. https://doi.org/10.1671/0272-4634(2000)020[0115:LBHOTH]2.0.CO;2

Horner, J.R., Ricqlès, A. de, Padian, K., 1999. Variation in Dinosaur Skeletochronology Indicators : Implications for Age Assessment and Physiology. Paleobiology 25, 295–304. https://doi.org/10.1666/0094-8373(1999)025<0295:VIDSII>2.3.CO;2

Hou, C., 2013. The energy trade-off between growth and longevity. Mech. Ageing Dev. 134, 373–380. https://doi.org/10.1016/j.mad.2013.07.001

Hugi, J., Sánchez-Villagra, M.R., 2012. Life history and skeletal adaptations in the galapagos marine iguana (*Amblyrhynchus cristatus*) as reconstructed with bone histological dataa comparative study of iguanines. J. Herpetol. 46, 312–324. https://doi.org/10.1670/11-071

Huttenlocker, A.K., Botha-Brink, J., 2014. Bone microstructure and the evolution of growth patterns in Permo-Triassic therocephalians (Amniota, Therapsida) of South Africa. PeerJ 2014, 1–31. https://doi.org/10.7717/peerj.325

Huttenlocker, A.K., Woodward, H., Hall, B.K., 2013. The biology of bone, in: Padian, K., Lamm, E.-T. (Eds.), Bone Histology Offossil Tetrapods. Berkeley: University of California Press, pp. 13–34.

I

Ibler, B., 2017. Costs of reproduction. A demographical approach to examine life-history trade-offs. Ernst-Moritz-Arndt-Universität Greifswald.

Ibler, B., Fischer, K., 2016. Costs of reproduction. A demographical approach to examine life-history trade-offs in two old-world deer species. Mamm. Biol. 81, 455–463.

J

Jordana, X., Marín-Moratalla, N., Moncunill-Solè, B., Nacarino-Meneses, C., Köhler, M., 2016. Ontogenetic changes in the histological features of zonal bone tissue of ruminants: A quantitative approach. Comptes Rendus - Palevol 15, 265–276. https://doi.org/10.1016/j.crpv.2015.03.008

K

Kahle, P., Witzel, C., Kierdorf, U., Frölich, K., Kierdorf, H., 2018. Mineral Apposition Rates in Coronal Dentine of Mandibular First Molars in Soay Sheep: Results of a Fluorochrome Labeling Study. Anat. Rec. 301, 902–912. https://doi.org/10.1002/ar.23753

Kierdorf, H., Hommelsheim, S., Kierdorf, U., 2012. Development of the permanent mandibular cheek teeth in fallow deer (*Dama dama*). J. Vet. Med. Ser. C Anat. Histol. Embryol. 41, 419–427. https://doi.org/10.1111/j.1439-0264.2012.01151.x

Kierdorf, H., Kierdorf, U., Frölich, K., Witzel, C., 2013. Lines of Evidence-Incremental Markings in Molar Enamel of Soay Sheep as Revealed by a Fluorochrome Labeling and Backscattered Electron Imaging Study. PLoS One 8. https://doi.org/10.1371/journal.pone.0074597

Klevezal, G.A., 1996. Recording Structures of Mammals. A. A. Balkema Publishers, Rotterdam.

Klevezal, G.A., Kleinenberg, S.E., 1967. Age determination of mammals by layered structures of teeth and bones.

Klevezal, G.A., Mina, M. V, 1984. Tetracycline labelling as a method of field studies of individual growth and population structure in rodents. Lynx (Praha), n.s. 22, 67–78.

Köhler, M., 2010. Fast or slow? The evolution of life history traits associated

with insular dwarfing. Recerca 19, 261–280.

Köhler, M., Marin-Moratalla, N., Jordana, X., Aanes, R., 2012. Seasonal bone growth and physiology in endotherms shed light on dinosaur physiology. Nature 487, 358–361. https://doi.org/10.1038/nature11264

Köhler, M., Moyà-Solà, S., 2009. Physiological and life history strategies of a fossil large mammal in a resource-limited environment. Proc. Natl. Acad. Sci. U. S. A. 106, 20354–8. https://doi.org/10.1073/pnas.0813385106

Kolb, C., Scheyer, T.M., Lister, A.M., Azorit, C., de Vos, J., Schlingemann, M., Rössner, G.E., Monaghan, N.T., Sánchez-Villagra, M.R., 2015a. Growth in fossil and extant deer and implications for body size and life history evolution. BMC Evol. Biol. 15, 19. https://doi.org/10.1186/s12862-015-0295-3

Kolb, C., Scheyer, T.M., Veitschegger, K., Forasiepi, A.M., Amson, E., Van der Geer, A.A.E., Van den Hoek Ostende, L.W., Hayashi, S., Sánchez-Villagra, M.R., 2015b. Mammalian bone palaeohistology: a survey and new data with emphasis on island forms. PeerJ 3, e1358. https://doi.org/10.7717/peerj.1358

L

Lamm, E.-T., 2013. Preparation and sectioning of specimens, in: Bone Histology of Fossil Tetrapods. pp. 55–160.

Landete-Castillejos, T., Garciá, A., Garde, J., Gallego, L., 2000. Milk intake and production curves and allosuckling in captive Iberian red deer, *Cervus elaphus hispanicus*. Anim. Behav. 60, 679–687. https://doi.org/10.1006/anbe.2000.1515

Landete-Castillejos, T, Garcia, A., Molina, P., Vergara, H., Garde, J., Gallego, L., 2000. Milk production and composition in captive Iberian red deer (*Cervus elaphus hispanicus*): effect of birth date . The online version of this

article , along with updated information and services , is located on the World Wide Web at : Milk production. J. Anim. Sci. 78, 2771–2777.

Lee, A. H., Huttenlocker, A. K., Padian, K. & Woodward, H.N., 2013. Analysis of growth rates, in: Padian, K., Lamm, E.-T. (Eds.), Bone Histology of Fossil Tetrapods. Berkeley: University of California Press, pp. 217–264.

Lesbre, F.-X., 1897. Contribution à l'étude de l'ossification du squelette des mammifères domestiques, principalement au point de vue de sa marche et de sa chronologie. Bull. la Société d'anthropologie Lyon 16, 239–333. https://doi.org/10.3406/linly.1897.16386

Lincoln, G.A., 1992. Biology of seasonal breeding in deer, in: Brown, R.D. (Ed.), The Biology of Deer. Springer, New York, pp. 565–576. https://doi.org/10.2307/4003028

Lincoln, G.A., 1971. Puberty in a seasonally breeding male, the red deer stag(Cervus elaphus L.). J. Reprod. Fertil. 25, 41–54.

Loe, L.E., Meisingset, E.L., Mysterud, A., Langvatn, R., Stenseth, N.C., 2004. Phenotypic and environmental correlates of tooth eruption in red deer (*Cervus elaphus*). J. Zool. 262, 83–89. https://doi.org/10.1017/S0952836903004436

Lorenzini, R., Garofalo, L., 2015. Insights into the evolutionary history of Cervus (Cervidae, tribe Cervini) based on Bayesian analysis of mitochondrial marker sequences, with first indications for a new species. J. Zool. Syst. Evol. Res. 53, 340–349. https://doi.org/10.1111/jzs.12104

Lovari, S., Lorenzini, R., Masseti, M., Pereladova, O., Carden, R.F., Brook, S.M., Mattioli, S., 2016. Cervus elaphus, Red Deer. IUCN Red List Threat. Species 2016 18.

Lowe, V.P.W., 1967. Teeth as indicators of age with special reference to Red deer (*Cervus elaphus*) of known age from Rhum. J. Zool. 152, 137–153. https://doi.org/10.1111/j.1469-7998.1967.tb01881.x

Ludt, C.J., Schroeder, W., Rottmann, O., Kuehn, R., 2004. Mitochondrial DNA phylogeography of red deer (Cervus elaphus). Mol. Phylogenet. Evol. 31, 1064–1083. https://doi.org/10.1016/j.ympev.2003.10.003

M

MacArthur, R.H., Wilson, E.O., 1967. The Theory of Island Biogeography. Princeton University Press, Princeton.

Malo, A.F., Roldan, E.R.S., Garde, J., Soler, A.J., Gomendio, M., 2005. Antlers honestly advertise sperm production and quality. Proc. R. Soc. B Biol. Sci. 272, 149–157. https://doi.org/10.1098/rspb.2004.2933

Mariezkurenna, K., 1983. Contribución al conocimiento del desarrollo de dentición y el esqueleto postcraneal de *Cervus elaphus*. Munibe 35, 149–202.

Marín-Moratalla, N., Cubo, J., Jordana, X., Moncunill-Solé, B., Köhler, M., 2014. Correlation of quantitative bone histology data with life history and climate: A phylogenetic approach. Biol. J. Linn. Soc. 112, 678–687. https://doi.org/10.1111/bij.12302

Marín-Moratalla, N., Cubo, J., Jordana, X., Moncunill-Solè, B., Köhler, M., 2013a. Correlates of bone histology quantitative data with life history traits and ecological parameters in bovids.

Marín-Moratalla, N., Jordana, X., García-Martínez, R., Köhler, M., 2011. Tracing the evolution of fitness components in fossil bovids under different selective regimes. Comptes Rendus - Palevol 10, 469–478. https://doi.org/10.1016/j.crpv.2011.03.007

Marín-Moratalla, N., Jordana, X., Köhler, M., 2013b. Bone histology as an approach to providing data on certain key life history traits in mammals: Implications for conservation biology. Mamm. Biol. 78, 422–429. https://doi.org/10.1016/j.mambio.2013.07.079

Martinez-Maza, C., Alberdi, M.T., Nieto-Diaz, M., Prado, J.L., 2014. Life-history traits of the miocene *Hipparion concudense* (Spain) inferred from bone histological structure. PLoS One 9. https://doi.org/10.1371/journal.pone.0103708

Mateos, C., Alarcos, S., Carranza, J., Sánchez-Prieto, C.B., Valencia, J., 2008. Fluctuating asymmetry of red deer antlers negatively relates to individual condition and proximity to prime age. Anim. Behav. 75, 1629–1640. https://doi.org/10.1016/j.anbehav.2007.10.016

Mayya, A., Banerjee, A., Rajesh, R., 2016. Haversian microstructure in bovine femoral cortices: An adaptation for improved compressive strength. Mater. Sci. Eng. C 59, 454–463. https://doi.org/10.1016/j.msec.2015.10.047

McNab, B.K., 2010. Geographic and temporal correlations of mammalian size reconsidered: A resource rule. Oecologia 164, 13–23. https://doi.org/10.1007/s00442-010-1621-5

Mennecart, B., DeMiguel, D., Bibi, F., Rössner, G.E., Métais, G., Neenan, J.M., Wang, S., Schulz, G., Müller, B., Costeur, L., 2017. Bony labyrinth morphology clarifies the origin and evolution of deer. Sci. Rep. 7, 1–11. https://doi.org/10.1038/s41598-017-12848-9

Miszkiewicz, J.J., Louys, J., O'Connor, S., 2019. Microanatomical Record of Cortical Bone Remodeling and High Vascularity in a Fossil Giant Rat Midshaft Femur. Anat. Rec. 302, 1934–1940. https://doi.org/10.1002/ar.24224

Mitchell, B., 1967. Growth layers in dental cement for determining the age of red deer (*Cervus Elaphus* L.). J. Anim. Ecol. 36, 279–293. https://doi.org/10.2307/2912

Mitchell, B., Staines, C.W., Welch, D., 1977. Ecology of Red Deer. A research review relavant to their management in Scotland. Institute of Terrestrial Ecology, Cambridge.

Moncunill-Solé, B., Orlandi-Oliveras, G., Jordana, X., Rook, L., Köhler, M., 2016. First approach of the life history of *Prolagus apricenicus* (Ochotonidae, Lagomorpha) from Terre Rosse sites (Gargano, Italy) using body mass estimation and paleohistological analysis. Comptes Rendus - Palevol 15, 235–245. https://doi.org/10.1016/j.crpv.2015.04.004

Montes, L., Le Roy, N., Perret, M., De Buffrenil, V., Castanet, J., Cubo, J., 2007. Relationships between bone growth rate, body mass and resting metabolic rate in growing amniotes: A phylogenetic approach. Biol. J. Linn. Soc. 92, 63–76. https://doi.org/10.1111/j.1095-8312.2007.00881.x

Montoya-Sanhueza, G., Bennett, N.C., Oosthuizen, M.K., Dengler-Crish, C.M., Chinsamy, A., 2021. Bone remodeling in the longest living rodent, the naked mole-rat: Interelement variation and the effects of reproduction. J. Anat. https://doi.org/10.1111/joa.13404

Montoya-Sanhueza, G., Bennett, N.C., Oosthuizen, M.K., Dengler-Crish, C.M., Chinsamy, A., 2020. Long bone histomorphogenesis of the naked mole-rat: Histodiversity and intraspecific variation. J. Anat. 238, 1259–1283. https://doi.org/10.1111/joa.13381

Montoya-Sanhueza, G., Chinsamy, A., 2017. Long bone histology of the subterranean rodent *Bathyergus suillus* (Bathyergidae): ontogenetic pattern of cortical bone thickening. J. Anat. 230, 203–233. https://doi.org/10.1111/joa.12547

Moore, G.H., Littlejohn, R.P., Cowie, G.M., 1988. Liveweights, growth rates, and mortality of farmed red deer at Invermay. New Zeal. J. Agric. Res. 31, 293–300. https://doi.org/10.1080/00288233.1988.10423418

Morris, P., 1972. A review of mammalian age determination methods. Mamm. Rev. 2, 69–104. https://doi.org/10.1111/j.1365-2907.1972.tb00160.x

Morris, P.A., 1970. A method for determining absolute age in the hedgehog. Notes from mammal Soc. 277–280.

Muggeo, V.M.R., 2017. Interval estimation for the breakpoint in segmented regression: a smoothed score-based approach. Aust. N. Z. J. Stat. 59, 311–322.

Munro, N.D., Bar-Oz, G., Stutz, A.J., 2009. Aging mountain gazelle (Gazella gazella): refining methods of tooth eruption and wear and bone fusion. J. Archaeol. Sci. 36, 752–763. https://doi.org/10.1016/j.jas.2008.10.020

N

Nacarino-Meneses, C., 2018. Life history inferences in extant and extinct Equus from the histological analysis of bone and enamel tissues. Universitat Autònoma de Barcelona.

Nacarino-Meneses, C., Jordana, X., Köhler, M., 2016a. Histological variability in the limb bones of the Asiatic wild ass and its significance for life history inferences. PeerJ 4, e2580. https://doi.org/10.7717/peerj.2580

Nacarino-Meneses, C., Jordana, X., Köhler, M., 2016b. First approach to bone histology and skeletochronology of *Equus hemionus*. Comptes Rendus - Palevol 15, 277–287. https://doi.org/10.1016/j.crpv.2015.02.005

Nacarino-Meneses, C., Köhler, M., 2018. Limb bone histology records birth in mammals. PLoS One 13. https://doi.org/10.1371/journal.pone.0198511

Nacarino-Meneses, C., Orlandi-Oliveras, G., 2019. The life history of European Middle Pleistocene equids: first insights from bone histology. Hist. Biol. 1–11. https://doi.org/10.1080/08912963.2019.1655011

Nussey, D.H., Wilson, A.J., Morris, A., Pemberton, J., Clutton-Brock, T., Kruuk, L.E.B., 2008. Testing for genetic trade-offs between early- and late-life reproduction in a wild red deer population. Proc. R. Soc. B Biol. Sci. 275, 745–750. https://doi.org/10.1098/rspb.2007.0986

O

O'Connor, T., 2000. The Archaeology of Animal Bones. Sutton Publishing.

Olea, L., Miguel-ayanz, A.S., 2006. The Spanish *dehesa*. A traditional Mediterranean silvopastoral system linking production and nature conservation. 21st Gen. Meet. Eur. Grassl. Fed. 11, 1–13. https://doi.org/10.1016/j.ndteint.2011.08.005

Orlandi-Oliveras, G., Jordana, X., Moncunill-Solé, B., Köhler, M., 2016. Bone histology of the giant fossil dormouse *Hypnomys onicensis* (Gliridae, Rodentia) from Balearic Islands. Comptes Rendus - Palevol 15, 247–253. https://doi.org/10.1016/j.crpv.2015.05.001

Orlandi-Oliveras, G., Nacarino-Meneses, C., Koufos, G.D., Köhler, M., 2018. Bone histology provides insights into the life history mechanisms underlying dwarfing in hipparionins. Sci. Rep. 8, 1–15. https://doi.org/10.1038/s41598-018-35347-x

Ozanne, S.E., Hales, C.N., 2005. Poor fetal growth followed by rapid postnatal catch-up growth leads to premature death. Mech. Ageing Dev. 126, 852–854. https://doi.org/10.1016/j.mad.2005.03.005

P

Padian, K., 2013. Why study the bone of fossil tetrapods?, in: Bone Histology of Fossil Tetrapods. pp. 1–12.

Padian, K., 2011. Vertebrate palaeohistology then and now: A retrospective in the light of the contributions of Armand de Ricqlès. Comptes Rendus - Palevol 10, 303–309. https://doi.org/10.1016/j.crpv.2011.02.001

Padian, Kevin, de Boef Miara, M., Larsson, H.C.E., Wilson, L., Bromage, T., 2013. Research applications and integration, in: Bone Histology of Fossil Tetrapods. pp. 265–285.

https://doi.org/10.1525/california/9780520273528.003.0003

Padian, K., De Ricqlès, A.J., Horner, J.R., 2001. Dinosaurian growth rates and bird-origins. Nature 412, 405–408. https://doi.org/10.1038/35086500

Padian, K., Horner, J.R., De Ricqlès, A., 2004. Growth in small dinosaurs and pterosaurs: The evolution of archosaurian growth strategies. J. Vertebr. Paleontol. 24, 555–571. https://doi.org/10.1671/0272-4634(2004)024[0555:GISDAP]2.0.CO;2

Padian, K., Lamm, E.-T., Werning, S., 2013. Selection of specimens, in: Padian, Kevin, Lamm, E.-T. (Eds.), Bone Histology of Fossil Tetrapods. Berkeley: University of California Press, pp. 35–54.

Payne, S., 1973. Kill-off Patterns in Sheep and Goats : The Mandibles from Aşvan Kale. Anatol. Stud. 23, 281–303.

Pianka, E.R., 1970. On r- and K-Selection. Amrican Soc. Nat. 104, 592–597.

Pitra, C., Fickel, J., Meijaard, E., Groves, C.P., 2004. Evolution and phylogeny of old world deer. Mol. Phylogenet. Evol. 33, 880–895. https://doi.org/10.1016/j.ympev.2004.07.013

Pluske, J.R., Dividich, J. Le, Verstegen, M.W.A., 2003. Weaning the pig. Concepts and consequences, Weaning the pig. Wageningen Academic Publishers, Wageningen. https://doi.org/10.3920/978-90-8686-513-0

Pollard, J.C., Asher, G.W., Littlejohn, R.P., 2002. Weaning date affects calf growth rates and hind conception dates in farmed red deer (*Cervus elaphus*). Anim. Sci. 74, 111–116. https://doi.org/10.1017/s1357729800052279

Pontier, D., Gaillard, J.M., Allainé, D., Trouvilliez, J., Gordon, I., Duncan, P., 1989. Postnatal growth rate and adult body weight in mammals: a new approach. Oecologia 80, 390–394. https://doi.org/10.1007/BF00379041

Popkin, P.R.W., Baker, P., Worley, F., Payne, S., Hammon, A., 2012. The Sheep

Project (1): Determining skeletal growth, timing of epiphyseal fusion and morphometric variation in unimproved Shetland sheep of known age, sex, castration status and nutrition. J. Archaeol. Sci. 39, 1775–1792. https://doi.org/10.1016/j.jas.2012.01.018

Pratt, I. V., Cooper, D.M.L., 2018. The effect of growth rate on the three-dimensional orientation of vascular canals in the cortical bone of broiler chickens. J. Anat. 233, 531–541. https://doi.org/10.1111/joa.12847

Prondvai, E., Stein, K.H.W., de Ricqlès, A., Cubo, J., 2014. Development-based revision of bone tissue classification: The importance of semantics for science. Biol. J. Linn. Soc. 112, 799–816. https://doi.org/10.1111/bij.12323

Purdue, J.R., 1983. Epiphyseal Closure in White-Tailed Deer. J. Wildl. Manage. 47, 1207–1213.

R

Raia, P., Barbera, C., Conte, M., 2003. The fast life of a dwarfed giant. Evol. Ecol. 17, 293–312. https://doi.org/10.1023/A:1025577414005

Randi, E., Mucci, N., Claro-Hergueta, F., Bonnet, A., Douzery, E.J.P., 2001. A mitochondrial DNA control region phylogeny of the Cervinae: Speciation in *Cervus* and implications for conservation. Anim. Conserv. 4, 1–11. https://doi.org/10.1017/S1367943001001019

Rauw, W.M., 2008. Resource allocation. Introduction, in: Rauw, W.M. (Ed.), Resource Allocation Theory Applied to Farm Animal Production. Department of Animal Biotechnology. Univerity of Nevada-Reno, pp. 1–22. https://doi.org/10.1079/9781845933944.0000

Ray, S., Botha, J., Chinsamy, A., 2004. Bone histology and growth patterns of some nonmammalian therapsids. J. Vertebr. Paleontol. 24, 634–648. https://doi.org/10.1671/0272-4634(2004)024[0634:BHAGPO]2.0.CO;2

Ray, S., Chinsamy, A., Bandyopadhyay, S., 2005. *Lystrosaurus murrayi* (therapsida, dicynodontia): Bone histology, growth and Lifestyle adaptations. Palaeontology 48, 1169–1185. https://doi.org/10.1111/j.1475-4983.2005.00513.x

Reiland, S., 1978. Growth and skeletal development of the pig. Acta Radiol. Suppl. 358, 15–22.

Reznick, D., Bryant, M.J., Bashey, F., 2002. r- and k-selection: the role of population regulation in life-history evolution. Ecol. Soc. Am. 83, 1509–1520.

Rockwood, L.L., 2006. Introduction to Population Ecology. Blackwell publishing, Oxford, UK.

Roff, D.A., 2002. Life history evolution. Sinauer Associates, Sunderland.

Roff, D.A., 1992. The Evolution of Life Histories: Theory and Analysis. Sinauer Associates, New York.

Rosvold, J., Herfindal, I., Andersen, R., Hufthammer, A.K., 2014. Long-term morphological changes in the skeleton of red deer (Artiodactyla, Cervidae) at its northern periphery. J. Mammal. 95, 626–637. https://doi.org/10.1644/13-MAMM-A-231

Ruddle, J.L., 1997. An investigation of bone histology as a potential age indicator in Roe Deer. PhD. University College London.

S

Sánchez, I.M., Cantalapiedra, J.L., Ríos, M., Quiralte, V., Morales, J., 2015. Systematics and evolution of the Miocene three-horned Palaeomerycid Ruminants (Mammalia, Cetartiodactyla). PLoS One 10, 1–31. https://doi.org/10.1371/journal.pone.0143034

Sánchez, I.M., Domingo, M.S., Morales, J., 2010. The genus *Hispanomeryx*

(Mammalia, Ruminantia, Moschidae) and its bearing on musk deer phylogeny and systematics. Palaeontology 53, 1023–1047. https://doi.org/10.1111/j.1475-4983.2010.00992.x

Sánchez, I.M., Quiralte, V., Cantalapiedra, J.L., Ríos, M., Morales, J., 2018. Historia evolutiva de Ruminantia, in: La Colina de Los Tigres Dientes de Sable. pp. 1–30.

Sander, P.M., 2000. Longbone histology of the Tendaguru sauropods: implications for growth and biology. Paleobiology 26, 466–488. https://doi.org/10.1666/0094-8373(2000)026<0466:lhotts>2.0.co;2

Schneider, C.A., Rasband, W.S., Eliceiri, K.W., 2012. NIH Image to ImageJ: 25 years of image analysis. Nat. Methods 9, 671–675. https://doi.org/10.1038/nmeth.2089

Schour, I., Hoffman, M.M., Sarnat, B.G., Engel, M.B., 1941. Vital staining of growing bones and teeth with alizarine red S. J. Dent. Reseach 20, 411–418.

Shim, M.-J., 2016. Bone Changes in Femoral Bone of Mice Using Calcein Labeling. Korean J. Clin. Lab. Sci. 48, 114–117. https://doi.org/10.15324/kjcls.2016.48.2.114

Sinsch, U., 2015. Review: Skeletochronological assessment of demographic life-History traits in amphibians. Herpetol. J. 25, 5–13.

Skog, A., Zachos, F.E., Rueness, E.K., Feulner, P.G.D., Mysterud, A., Langvatn, R., Lorenzini, R., Hmwe, S.S., Lehoczky, I., Hartl, G.B., Stenseth, N.C., Jakobsen, K.S., 2009a. Phylogeography of red deer (Cervus elaphus) in Europe. J. Biogeogr. 36, 66–77. https://doi.org/10.1111/j.1365-2699.2008.01986.x

Skog, A., Zachos, F.E., Rueness, E.K., Feulner, P.G.D., Mysterud, A., Langvatn, R., Lorenzini, R., Hmwe, S.S., Lehoczky, I., Hartl, G.B., Stenseth, N.C., Jakobsen, K.S., 2009b. Phylogeography of red deer (*Cervus elaphus*) in Europe. J. Biogeogr. 36, 66–77. https://doi.org/10.1111/j.1365-

2699.2008.01986.x

Smith, B.H., 2000. 'Schultz's Rule' and the evolution of tooth emergence and replacement patterns in primates and ungulates, in: Teaford, M.F., Smith, M.M., Ferguson, M. (Eds.), Development, Function and Evolution of Teeth. Cambridge University Press, New York, pp. 212–228. https://doi.org/10.1017/cbo9780511542626.015

Smith, B.H., 1991. Dental development and the evolution of life history in Hominidae. Am. J. Phys. Anthropol. 86, 157–174. https://doi.org/10.1002/ajpa.1330860206

Smith, C.C.D., 2020. *Giraffa camelopardalis*: Limb bone histology through ontogeny. University of Cape Town.

Smith, T.M., 2006. Experimental determination of the periodicity of incremental features in enamel. J. Anat. 208, 99–113. https://doi.org/10.1111/j.1469-7580.2006.00499.x

Smith, T.M., Reid, D.J., Sirianni, J.E., 2006. The accuracy of histological assessments of dental development and age at death. J. Anat. 208, 125–138. https://doi.org/10.1111/j.1469-7580.2006.00500.x

Sommer, R.S., Zachos, F.E., Street, M., Jöris, O., Skog, A., Benecke, N., 2008. Late Quaternary distribution dynamics and phylogeography of the red deer (Cervus elaphus) in Europe. Quat. Sci. Rev. 27, 714–733. https://doi.org/10.1016/j.quascirev.2007.11.016

Stankovic, A., Doan, K., Mackiewicz, P., Ridush, B., Baca, M., Gromadka, R., Socha, P., Weglenski, P., Nadachowski, A., Stefaniak, K., 2011. First ancient DNA sequences of the Late Pleistocene red deer (Cervus elaphus) from the Crimea, Ukraine. Quat. Int. 245, 262–267. https://doi.org/10.1016/j.quaint.2011.05.023

Starck, J.M., Chinsamy, A., 2002. Bone microstructure and developmental plasticity in birds and other dinosaurs. J. Morphol. 254, 232–246.

https://doi.org/10.1002/jmor.10029

Stearns, S.C., 2000. Life history evolution: Successes, limitations, and prospects. Naturwissenschaften 87, 476–486. https://doi.org/10.1007/s001140050763

Stearns, S.C., 1992. The Evolution of Life Histories. Oxford University Press.

Stearns, S.C., 1989. Trade-Offs in Life-History Evolution. Funct. Ecol. 3, 259–268. https://doi.org/10.2307/2389364

Stearns, S.C., 1983. The Influence of size and phylogeny on patterns of covariation among life-History traits in the mammals 41, 173–187.

Stein, K., Prondvai, E., 2014. Rethinking the nature of fibrolamellar bone: An integrative biological revision of sauropod plexiform bone formation. Biol. Rev. 89, 24–47. https://doi.org/10.1111/brv.12041

Suzuki, H.K., Mathews, A., 1966. Two-color fluorescent labeling of mineralizing tissues with tetracycline and 2,4-bis[n,n'-di-(carbomethyl)aminomethyl] fluorescein. Biotech. Histochem. 41, 57–60. https://doi.org/10.3109/10520296609116280

T

Teagasc, 2017. Development of the Calf Digestive System, in: Teagasc Calf Rearing Manual: Best Practice from Birth to Three Months. pp. 59–76.

Team, Rs., 2019. RStudio: Integrated Development for R.

Trut, L., 1999. Early Canid Domestication: The Farm-Fox Experiment. Am. Sci. 87, 160. https://doi.org/10.1511/1999.20.813

Turner, T.R., Cramer, J.D., Nisbett, A., Gray, J.P., 2016. A comparison of adult body size between captive and wild vervet monkeys (*Chlorocebus aethiops sabaeus*) on the island of St. Kitts 57, 211–220. https://doi.org/10.1111/cdoe.12200.Factors

Turvey, S.T., Holdaway, R.N., 2005. Postnatal ontogeny, population structure, and extinction of the giant moa Dinornis. J. Morphol. 265, 70–86. https://doi.org/10.1002/jmor.10341

V

Van Eetvelde, M., Opsomer, G., 2017. Innovative look at dairy heifer rearing: Effect of prenatal and post-natal environment on later performance. Reprod. Domest. Anim. 52, 30–36. https://doi.org/10.1111/rda.13019

van Gaalen, S.M., Kruyt, M.C., Geuze, R.E., de Bruijn, J.D., Alblas, J., Dhert, W.J. a, 2010. Use of fluorochrome labels in in vivo bone tissue engineering research. Tissue Eng. Part B. Rev. 16, 209–217. https://doi.org/10.1089/ten.TEB.2009.0503

Vaughan, T.A., Ryan, J.M., Czaplewski, N.J., 2013. Mammalogy. Jones & Barlett Publishers.

Veiberg, V., Loe, L.E., Mysterud, A., Solberg, E.J., Langvatn, R., Stenseth, N.C., 2007. The ecology and evolution of tooth wear in red deer and moose. Oikos 116, 1805–1818. https://doi.org/10.1111/j.0030-1299.2007.16159.x

Veitschegger, K., Sánchez-Villagra, M.R., 2015. Tooth Eruption Sequences in Cervids and the Effect of Morphology, Life History, and Phylogeny. J. Mamm. Evol. 23, 251–263. https://doi.org/10.1007/s10914-015-9315-8

Von Bertallanffy, L., 1957. Quantitative laws in metabolism and growth. Q. Rev. Biol. 32, 217–231.

W

Wang, Y., Bekhit, A.E.D.A., Morton, J.D., Mason, S., 2017. Nutritional value of deer milk, in: Nutrients in Dairy and Their Implications for Health and Disease. pp. 363–375. https://doi.org/10.1016/B978-0-12-809762-5.00028-0

Warren, L.K., Lawrence, L.M., Parker, A.L., Barnes, T., Griffin, A.S., 1998. The effect of weaning age on foal growth and radiographic bone density. J. Equine Vet. Sci. 18, 335–340. https://doi.org/10.1016/S0737-0806(98)80548-0

Webb, S.D., Taylor, E.B., 1980. The phylogeny of hornless ruminants and a description of the cranium of Archaeomeryx. Bull. Am. Museum Nat. Hist. 167, 117–158.

Witzel, C., Kierdorf, U., Frölich, K., Kierdorf, H., 2018. The pay-off of hypsodonty - Timing and dynamics of crown growth and wear in molars of Soay sheep. BMC Evol. Biol. 18, 1–14. https://doi.org/10.1186/s12862-018-1332-9

Wolter, B.F., Ellis, M., 2001. The effects of weaning weight and rate of growth immediately after weaning on subsequent pig growth performance and carcass characteristics. Can. J. Anim. Sci. 81, 363–369. https://doi.org/10.4141/A00-100

Woodward, H.N., Padian, K., Lee, A.H., 2013. Skeletochronology, in: Padian, K., Lamm, E.-T. (Eds.), Bone Histology of Fossil Tetrapods. Berkeley: University of California Press, pp. 195–216.

Z

Zachos, F.E., Hartl, G.B., 2011. Phylogeography, population genetics and conservation of the European red deer *Cervus elaphus*. Mamm. Rev. 41, 138–150. https://doi.org/10.1111/j.1365-2907.2010.00177.x

Zedda, M., Lepore, G., Biggio, G.P., Gadau, S., Mura, E., Farina, V., 2015. Morphology, Morphometry and Spatial Distribution of Secondary Osteons in Equine Femur. J. Vet. Med. Ser. C Anat. Histol. Embryol. 44, 328–332. https://doi.org/10.1111/ahe.12141

Zuck, T.T., 1938. Age order of epiphyseal union in the guinea pig. Anat. Rec.

70, 389–399.